Optimal Control Energy Management Strategy for Hybrid Propulsion and Power Supply Vessels using Data-Driven Load Forecasting

S. Slagter

Optimal Control Energy Management Strategy for Hybrid Propulsion and Power Supply Vessels using Data-Driven Load Forecasting

Master Thesis Project

by

S. Slagter

Master thesis

in partial fulfilment of the requirements for the degree of
Master of Science
in mechanical engineering

at the Department Maritime and Transport Technology of Faculty Mechanical, Maritime and Materials Engineering of Delft University of Technology to be defended publicly on Monday February 20, 2023 at 14:00.

Student number:	5405459
MSc track:	Multi-Machine Engineering
Report number:	2023.MME.8764
Project duration:	June 16, 2022 – February 20, 2023
TU Delft Supervisor:	Dr. A. Coraddu
Damen Naval Supervisor:	M. Kalikatzarakis
TU Delft Committee Chair:	Dr. Ir. H. Polinder
TU Delft Committee Member:	T. Kopka

An electronic version of this thesis is available at `http://repository.tudelft.nl/`.

Cover Image: Holland-class offshore patrol vessel 2022, digital photograph, Dutch Ministry of Defence, accessed 14 January 2023.

TU Delft

Abstract

Hybrid propulsion is a promising technology to reduce the environmental footprint of the vessel. It combines the use of mechanical and electrical propulsion, as such, it is able to operate efficiently at a multitude of operational setpoints. Hybrid power supply uses two or more types of power sources to provide electrical power to the propulsive system. For instance, power supply combinations such a battery and diesel generator-sets are quite common. The combination of the hybrid power supply allows for the efficient use of the diesel generator-sets. An energy management system is required to effectively operate the complex systems of hybrid propulsion and hybrid power supply systems. For that reason, in this research an energy management system is developed for a hybrid propulsion and hybrid power supply vessel. The EMS is developed through a case study of the Holland-class offshore patrol vessel. The EMS consists of three main pillars, namely, the powertrain model, shaft power forecasting model, and the controller. The forecasting model predicts the shaft power, and provides reference values for the controller over a control horizon.

Four shaft power forecasting models were developed in the course of this research. The methodologies of linear regression, moving average, ARIMA and RNN were applied. The linear regression model is able to predict accurately for up to 18 seconds, showing a MAPE of 4.25%. The moving average improved on the performance of the linear regression model and is able to accurately predict 27 seconds in the future, with a MAPE of 4.67%. In order to capture the variance of the shaft power an ARIMA model was applied also. However, due to occasional divergence of the ARIMA model it proved an unreliable prediction tool for the purpose of shaft power prediction. It was only able to accurately predict the shaft power for 3 seconds in the future with a MAPE of 3.28%. The RNN is able to predict the shaft power 48 seconds in the future while maintaining a MAPE of 4.78%. Unfortunately, a prediction horizon of 48 seconds is not enough for the purpose of an energy management system. To effectively make use of the hybrid power supply, medium to long-term predictions are required; in the order of minutes to hours.

The energy management system is optimization-based using an equivalent consumption minimization strategy (ECMS). The designed controller is able to incorporate the use of the battery as an equivalent fuel consumption (ESFC) in the optimization problem. The controller correctly provides the system with an optimal power split between induction machine and diesel engines (Hybrid propulsion). It is also able to find an optimal split for the hybrid power supply; between the battery and the diesel generator-sets. Additionally, through constraints on the SOC between 20% and 80% the battery is operating at a favourable setpoint, which could prolong battery life. Four simulation studies were performed in the research to test and compare the effectiveness of the EMS. (1) Optimization at every timestep. (2) Triggered optimization, when a significant change (5%) occurs in SOC or shaft power demand. (3) Non-causal optimization for a prediction horizon of 48 seconds with 3 timesteps in the prediction horizon. (4) Optimization for a prediction horizon of 48 seconds with 3 timesteps in the prediction horizon, using RNN predicted shaft power reference values. The total fuel consumption and SOC trajectories of the 4 simulations are almost identical. Energy fuel reduction could not be proven. Given the parameters of the case study this is not surprising: (a) There is limited data availability leading to short-term predictions, and (b) a small battery capacity, leading to limited usefulness of the hybrid power supply system. With a simulation, reduction of 0.77% of total energy consumption was achieved with the implementation of a 400 kW battery compared to a no-battery scenario.

Keywords Energy management system · Propulsion control · Hybrid vehicles · Marine systems · Hybrid energy supply

Contents

List of Figures

List of Tables

1

Introduction

1.1. Background

At present, ocean shipping facilitates 80% of the transportation of global trade [1]. The shipping industry is only expected to grow, and this development is naturally paired by a multitude of environmental problems. The increased carbon and nitrogen oxides (NO_x) emissions resulting from the increased shipping demand is one of these problems [2]. In fact, the shipping industry is one of the fastest growing industries with regard to greenhouse gas emissions [3]. To combat the ever-increasing emissions, regulations have been put in place and are expected to become more stringent over time. Currently, there are restrictions on the weighted cycle NO_x emissions for diesel engines with an output of more than 130 kW [4]. In future, it is expected that there will not only be restrictions on engine specific NO_x emissions but on NO_x emissions per mile also [5]. Additionally, new ships are expected to adhere to a specific Energy Efficiency Design Index (EEDI) [4]. This index is a measure of CO2 emissions of a cargo vessel per mile or per tonne of goods. Given these restrictions as well as the increasing price of energy, it is imperative that the propulsion and power generation plants of ships have ways of reducing fuel consumption and emissions.

Hybrid propulsion is a promising technology to reduce the environmental footprint of a vessel. It involves the combined use of mechanical and electrical propulsion, such as the combination of diesel engines and induction machines [4]. It is primarily used in ships with operating profiles that present power demand peaks followed by periods of low loading [6]. The benefit of such a system is that the two types of propulsion can compensate for each other's respective weaknesses. For instance, mechanical propulsion is particularly efficient when operating close to rated speed. Moreover, it consists of only three power conversion stages, the main engine, the gearbox (torque and speed conversion) and the propeller, leading to low conversion losses. However, at lower operating speeds mechanical propulsion is far less efficient. Additionally, during increased accelerations there is a high NO_x emission profile [5]. Also, dynamic loading can effect the required maintenance frequency of the engine. Electric propulsion, on the other hand, is particularly effective for vessels with diverse operating loads. However, the power conversion of electric propulsion is less efficient due to the increased number of conversion stages [4]. So in a hybrid propulsion system, a direct mechanical drive can provide propulsion at high speeds and high efficiencies. And at lower speeds and part load, the electric drive takes over. Typical propulsion layouts are depicted below in Figure 1.1. In these layouts the variable speed motors that are not in-line with a propeller serve other mission-critical purposes and can be considered an auxiliary load.

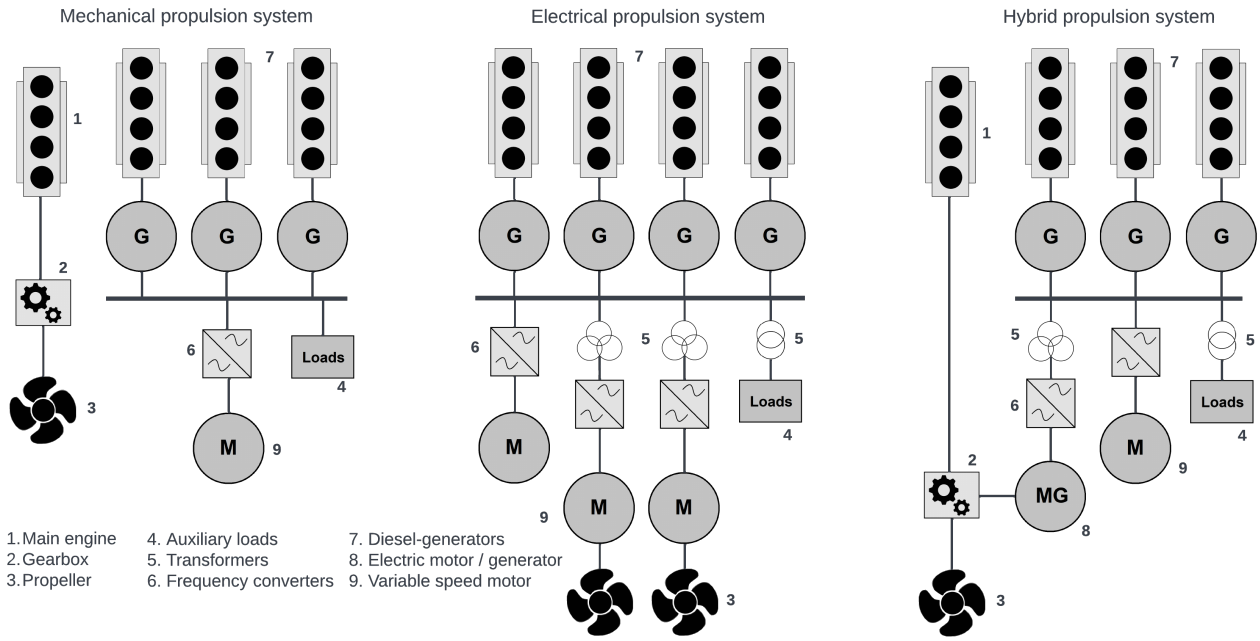

Figure 1.1: Overview of typical propulsion system layouts: (a) Mechanical propulsion system, (b) Electrical propulsion system, and (c) Hybrid propulsion system. Images retrieved from [4].

Besides hybrid propulsion there is also hybrid power supply. With a hybrid power supply a combination of two types of power sources can provide electrical power to the propulsive system. Most commonly a combination of diesel generators and energy storage systems such as a battery is used. The battery is charged and discharged in a manner that allows the diesel generator to operate at a more efficient operating point. Generally this means that (a) the battery is charged when a diesel generator has low load, in order to push it to higher loads which are generally more efficient. Or (b) the battery is discharged when it allows the idling of the diesel generator. Consequently, this lowers specific fuel consumption (sfc), as well as emissions [7]. Additionally, the battery can enable load levelling and peak shaving, by taking over the power fluctuations and delivering power during high power demand periods. This results in a more levelled loading of the engines, while maintaining a more efficient operating point. The challenges of a hybrid power supply lie in the complexity of the control strategies and recovering investments costs of the batteries [4]. Typical propulsion layouts with hybrid power supply are depicted below in Figure 1.2.

To effectively operate the complex system of a combined hybrid propulsion and hybrid power supply system, an energy management system (EMS) is required. An EMS finds favourable setpoints for the diesel engines, diesel generators, electric drives and battery in order to reduce fuel consumption and emissions. The complexity originates from the number of degrees of freedom that the system has: the diesel generators set points, main engines set points, induction machines set points and battery set point. These components are also linked directly and indirectly, which is described mathematically in detail in section 7.2. The objective of the EMS is to find an optimal split between the mechanical and electric drive, to find an optimal power split between power sources, and to minimize fuel consumption. Closely related to the EMS are the power management system (PMS) and the battery management system (BMS). The PMS has the job of ensuring power availability, as well as load levelling of the engines, and peak shaving. The goal of the BMS is to keep the battery within a safe operating region in terms of voltage, current, and temperature during charging, and discharging [1]. As will be evident later, in section 7.2, some goals of the PMS and BMS can also be partially performed by the controller of the EMS. Currently, few energy management systems have been developed for a system of hybrid propulsion & hybrid power supply (HPHPS) for the maritime domain, of which an overview is given in chapter 2.

More advanced EMSs also take into account receding horizon control. A receding horizon control problem takes into account setpoints in the future, over a prediction horizon, and additionally how each

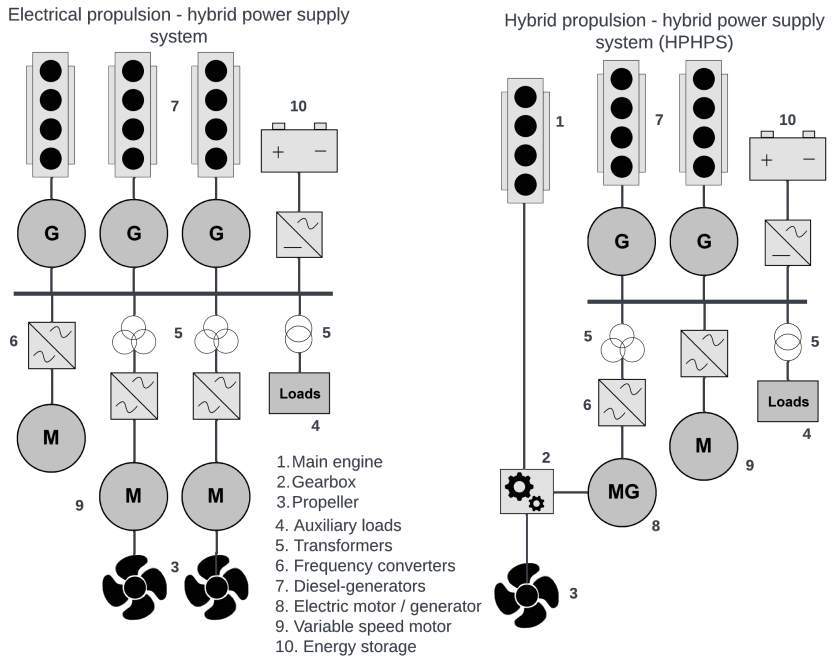

Figure 1.2: Overview of two typical propulsion system layouts with hybrid power supply: (a) Electrical propulsion system, (b) Hybrid propulsion system. Images retrieved from [4].

set point in each timestep effects the overall outcome. In order to further improve EMSs that optimize over a receding horizon, one can employ load forecasting. Load forecasting schemes anticipate future load demand, based on historical data of the load demand. By anticipating the load over a receding horizon, leveraging data driven load predictions, a controller can find optimal solutions accordingly. An overview of data driven load forecasting methods is given in chapter 2.

The focus of this master thesis project is to develop a novel energy management system leveraging a receding horizon principle and with load forecasting. As well as to implement this system to a case study in a simulated environment, and evaluate the outcome to a benchmark performance. The case study in this project is the Holland-class offshore patrol vessel (HCOPV). Damen naval, one of the stakeholders of the project, has supplied data on this vessel, as well as powertrain models. It is also in their interest to study this particular case. The case study details are elaborated in chapter 3. It should be noted that the HCOPV is not a ship with hybrid power supply. However, for the purpose of this project the ship model of the HCOPV will be augmented with a battery, to make the model have a hybrid power supply system. In this manner, an EMS can be developed for a HPHPS system.

1.2. Research goal and research questions

The research goal of this project is to prescribe an efficient energy management system for vessels with hybrid propulsion and hybrid power supply, applied to a case study of the Holland-class offshore patrol vessel.

In order to achieve this energy management system, first the overall strategy of the EMS should be determined. The strategies are discussed in the literature review in chapter 2, where an overview of available strategies is given such as heuristic, optimization-based and learning based strategies. Secondly, more specific design features of the EMS can be developed such as a controller. To achieve the research goal, the following research questions, noted below, have been composed.

1. What is an effective energy management strategy for a hybrid propulsion & hybrid energy supply marine vessel, that is able to reduce energy consumption & emissions and prescribe power allocation in real-time?

   (a) What are the state-of-the-art energy management strategies that have been developed for electric or hybrid propulsion & hybrid energy supply marine or ground vessels?
   (b) What are suitable key performance indicators (KPIs) for the evaluation of an energy management strategy?

2. What is an appropriate powertrain description of the Holland-class offshore patrol vessel that is augmented with a battery?
   (a) What are the components of the powertrain of the Holland-class offshore patrol vessel, how are they connected, and how would a battery be connected to the powertrain?
   (b) What features of the components should be modelled in order to obtain an accurate numerical description of the complete powertrain behaviour, while also providing enough information for the KPIs?

3. What is an effective data driven model for power load forecasting with a prediction horizon of two minutes while maintaining high levels of accuracy, given the data set of the Holland-class offshore patrol vessel?
   (a) What are the state-of-the-art data-driven methods currently employed for power load forecasting, and which is the most effective in terms of accuracy and prediction horizon?
   (b) Which data attributes should be included in input space X, and which data cleaning and preparation steps are required for the provided data set?
   (c) What are the relevant hyperparameters for the selected data-driven method, and what are their optimal settings, evaluated with model selection criteria of k-fold cross-validation and MSE?
   (d) What is the performance of the model evaluated with MAE, MSE, R^2, and sMAPE, and their respective confidence intervals? How does the model performance compare to state-of-the-art data driven methods for power load prediction?*

4. What is an effective controller design given the selected energy management strategy (RQ1), powertrain model (RQ2), and data-driven power load forecasting model (RQ3), that is able to reduce energy consumption & emissions and prescribe power allocation in real-time?
   (a) What should be the input vector $\vec{x}$, output vector $\vec{y}$, control vector $\vec{u}$ and disturbance vector $\vec{d}$ of the system?
   (b) What is an objective function for the controller that is able to a) find an optimal power split between mechanical and electric drive, b) find an optimal split between diesel generators and battery, and c) reduce energy consumption?
   (c) What are appropriate constraints for the states, outputs, control variables, and disturbances of the system, with respect to accomplishing EMS goals and KPI performance?
   (d) What is the performance of the model evaluated with selected KPI (RQ1.3)?

* The metrics mentioned here are discussed in detail in chapter 6. The metrics have been selected based on common practise for forecasting problems.

1.3. Contributions

This report presents an overview of the state-of-the-art of energy management strategies for hybrid power supply marine vessel systems. Additionally, the research provides a novel energy management approach for the application of hybrid propulsion and hybrid power supply systems; Namely the combination of an optimal control-based controller and data-driven load forecasting. An overview of currently available methods compared to the novelty of this research is shown in chapter 2. The main contributions of this report, summarized, are:

- A state-of-the-art overview of energy management strategies for HPHPS systems, in chapter 2.
- Implementation and evaluation of various load prediction methods, in chapter 6.
- A novel optimization-based controller with a receding horizon principle leveraging predicted load demand, in chapter 7.

1.4. Outline

This paper is organised as follows: chapter 2 shows the findings of the literature review. Case related information about the Holland-class offshore patrol vessel, and the data provided by Damen are discussed in chapter 3. An overview of the methodology is provided in chapter 4. A complete account of the methodology is given in subsequent chapters for the powertrain model, power load forecasting model and the controller respectively. Powertrain model is described in chapter 5, the power load forecasting models in chapter 6, and the energy management system & controller description, in chapter 7. The results of implementation of the EMS are presented in chapter 8. Finally, chapter 9 summarises the conclusions of the report and provides suggestions for future work. A graphical representation of the structure of the report is presented below in Figure 1.3.

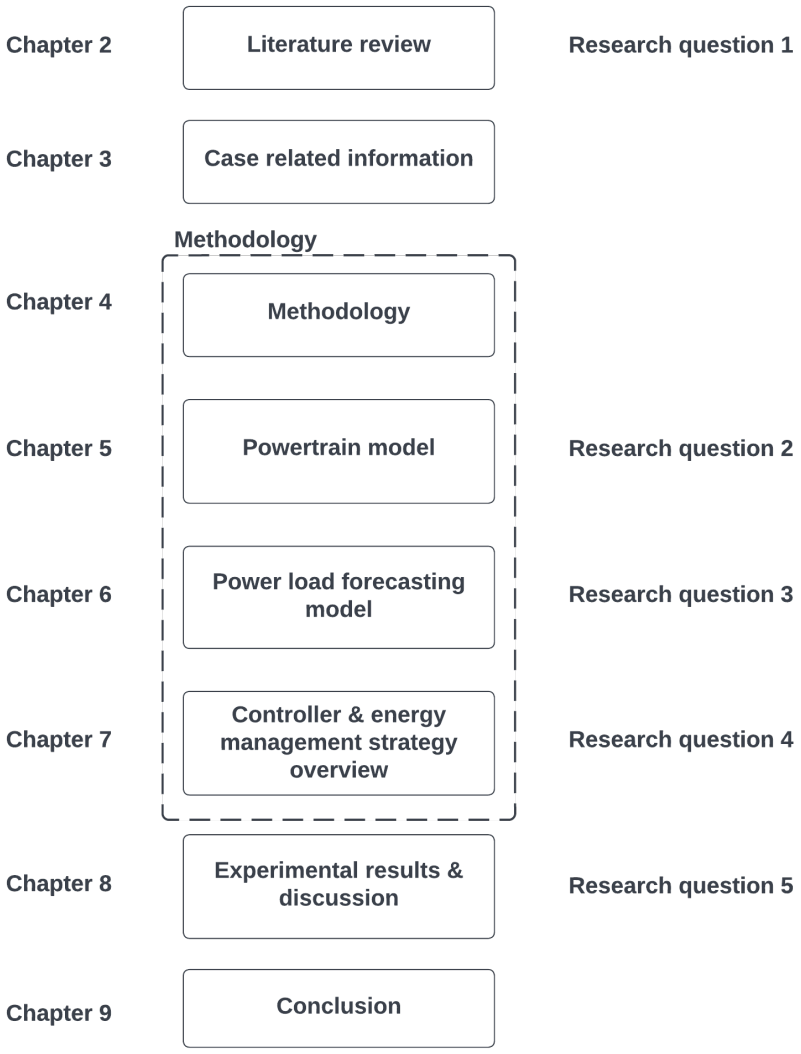

Figure 1.3: Graphical representation of the structure of the report.

2

Literature review

In this chapter the results to research question 1 are presented. A literature review is given that shows the state-of-the-art in energy management systems that have been developed for electric or hybrid propulsion & hybrid energy supply vehicles. Secondly, suitable key performance indicators are identified for the evaluation of an energy management strategy. For convenience the research question is restated here.

Research question 1: "What is an effective energy management strategy for a hybrid propulsion & hybrid energy supply marine vessel, that is able to reduce energy consumption & emissions and prescribe power allocation in real-time?"

(a) What are the state-of-the-art energy management strategies that have been developed for electric or hybrid propulsion & hybrid energy supply marine or ground vessels?

(b) What are suitable key performance indicators (KPIs) for the evaluation of an energy management strategy?

Research question 2a is answered below, in the related work sections. Question 2b is answered in the subsequent section. As a conclusion to the chapter the main research question is answered.

2.1. Related works

In this section the state-of-the-art methods for energy management systems are discussed as well as the strengths and limitations of more prominent methods. In [4] the various powertrain topologies of ships are classified, as well as the control strategies employed for these respective topologies. These different topologies are all the combinations between mechanical and electric drive, coupled with various types of power supply. Some of these topologies have already been shown in Figure 1.1 and Figure 1.2. The control strategies of relevance to this project are the EMSs that have been developed for topologies with hybrid power supplies. These developed control strategies can be classified as heuristic control strategies or optimization-based control strategy [8]. Among the more popular optimization-based control strategies in the maritime sector are equivalent consumption minimization strategy (ECMS), and power management through operating load estimation [4, 9–11]. Within optimization-based control strategies there is online and offline optimization. Online optimization involves a controller that is causal and is often computationally fast enough to facilitate real-time optimization outputs. Causality implies the controller only uses information that is available at each time step. Offline optimization, or global optimization, are controllers that are not operated in real-time [12]. Within offline optimization there are also non-causal control strategies that require the detailed knowledge of the future driving conditions. These controllers are not considered here, as they require specific knowledge on operational conditions and in practise that is rarily the case [12]. Non-causal controllers can serve as a good benchmark for online controllers however, since the non-causality ensures that an optimal solution can be found over the whole period of an operational profile. Other relevant control strategies discussed in this section are learning-based energy management strategies.

2.1.1. Heuristic control

Heuristic control uses logical rules to determine the operating modes of the vessel and energy system. Heuristic control often uses two guiding principles [12]. The first principle of heuristic strategies is that in hybrid vehicles the main engine should only be used when its efficiency is relatively high; For less favorable situations the electric motors should take over and the main engine should be turned off. Often, also the engines are running at a higher load than operator demanded power, in order to run the engine at a more favorable set point. The additional power is used to charge the battery. The second principle of heuristic control of an EMS is that the state of charge of the battery stays within a predefined bound. Therefore, when the state of charge is relatively high, the EMS will aim to discharge the battery, and when the state of charge is relatively low, the EMS will aim to charge the battery. Note that there are more facets to heuristic control and energy management systems, but only the ones relevant to the project are mentioned here.

Two common implementation approaches for heuristic control are the map-based and rule-based approaches. In the map-based approach [13–15], the output setpoints of the EMS are determined by mapped control set points for different speeds and torque request points by the operator. In this map different regions are established that will warrant different behaviours. In Figure 2.1, an example of a map is shown. In this example for a region of $u = 0$ corresponds to the use of the main engine alone, $u = 1$ is electric mode. The other regions are combined use of the main engine and electric motor to charge or discharge to battery. Different maps can be established for a high and low state of charge as well. In some other methods [16–18], these map regions are not rigid and can instead be defined using other methodology such as fuzzy logic.

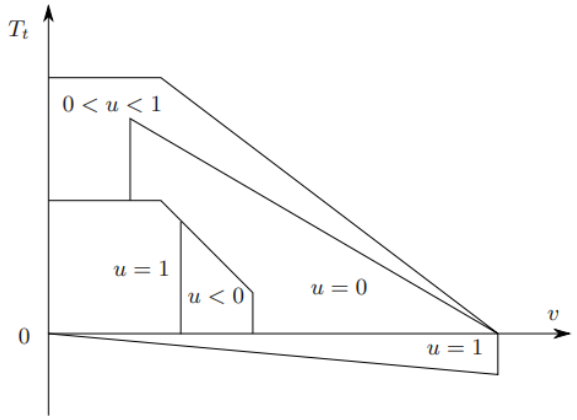

Figure 2.1: Typical map-based heuristic energy-management strategy for a hybrid electric vehicle. Image retrieved from [12].

Various articles have presented implementation of rule-based controllers. For instance, [19] presents a control strategy that uses the batteries at low speeds for propulsion rather than the engine, and at higher speeds the battery can electrically assist the engine. The article shows that the strategy is able to reduce fuel consumption, and that these savings are proportional to the battery capacity. In [20], ECMS, rule-based logic and reinforcement learning are compared in terms of appropriateness for real-time implementation in an automotive setting. The rule-based controller outperformed the other methods in computational time. However, higher fuel saving were achieved by the other methods when the operational profile of the vehicle is not known.

2.1.2. Online optimization-based control

Optimization-based control uses a performance index J, that is either minimized or maximised. The most common an simplest performance index is the fuel mass consumed over a period of time:

$$min\, J = \int_0^{t_f} \dot{m}_f(u(t))dt, \tag{2.1}$$

where $\dot{m}_f(u(t))$ is the fuel mass, as a function of the control output $u(t)$. Rather than just taking into account the fuel mass consumption in the performance index, pollutants can also be incorporated [21, 22].

More advanced optimization-based control allow for the incorporation of a battery in the performance index. In the Equivalent Consumption Minimisation Strategy (ECMS), an optimal control problem is formulated that minimises the fuel consumption of the engine and the equivalent fuel consumption of the battery. This means that an equivalent fuel consumption cost function has to be designed for the use of the battery. [9] proves the effectiveness of ECMS as an EMS in automotive industry, as it outperformed heuristic control. This control method performs particularly well compared to other strategies when the operating profile is not known beforehand. Fuel savings of up to 10% were shown in [10] while using the ECMS strategy compared to rule-based logic. In [11], 6% fuel savings were achieved in a simulation study of a tugboat, with unknown load demand. ECMS methods do not necessarily operate in real-time, it is partially dependant on the solvers, and complexity of the problem whether it is possible to apply the method online. The relative simplicity of a ground vehicle with only a single generator and motor, has made some of these approaches more feasible in the automotive industry in real-time. Whereas the maritime applications often involve more engines and more complex inter-relations between them, leading to more difficult control problems.

In order to further improve the performance of an optimization-based controller, for unknown operating profiles, is to incorporate load predictions. Load predictions are methods that anticipate future load demand based on historical load demand data. For instance [23], shows that a 9% improvement on the cost function performance compared to the rule-based control of [19] can be achieved by predicting the load. In [24], power load prediction is implemented in conjunction with a multi-level model predictive control (MPC) scheme. First a wavelet transform splits the signal in low and high frequencies. Secondly, separately for the low and high frequencies, and consequently short- and long-term, an MPC controller minimizes fuel consumption and ensures power availability. The reference values of the MPCs are obtained by prediction. Unfortunately, the article does not disclose the exact method of prediction. It does, however, show an improved performance with the load prediction compared to classic MPC without load prediction.

At this point it is important to be aware of the effect of time scales in predictions. There are short-term predictions in the order of a few seconds. Medium-term predictions in the order of minutes and long-term in the order of an hour or longer. The farther predictions can be made in the future, the more the optimizer can leverage future knowledge to obtain reduced fuel use over a prediction horizon. Short-term trends can often be identified and predicted reasonable accurate, where-as long-term trends are difficult. For this reason [24] designed the two-level MPC; To have accurate short-term predictions and control, combined with capturing a less accurate but broader trend of power consumption in the long-term. [25] also uses MPC to account for future power demand, while also taking into account environmental disturbances and uncertainties. Various machine learning prediction methodologies have not yet been applied in an EMS framework for the application of a ship. Depending of the methodology of prediction and control, load forecasting schemes are not necessarily real-time methods.

2.1.3. Offline optimization-based control

Offline optimization-based control methods are often global optimization (GO) methods that are not fast enough to be implemented in real-time, or they utilize future knowledge in the present (non-causal). One such method is presented in [26], where the fuel consumption of the engines is predicted rather than the load demand, using a neural network. Based on the predicted fuel consumption an appropriate course of action over the prediction horizon can be computed. In [27] a combination of fuzzy logic and optimal control is used. The fuzzy logic provides a set of operational constraint to which the energy management system is to adhere. The optimal control minimizes for fuel consumption using quantum particle swarm optimization (QPSO). This method proved more efficient than classic heuristic control. Other GO control methods include particle swarm optimization (PSO) [28], simulated annealing algorithm (SAA) [29], genetic algorithm (GA) [30], differential evolution algorithm (DEA) [31], and ant colony optimization algorithm (ACOA) [32]. The ACOA method was combined with ECMS, and showed a reduction of fuel usage of 12.1% compared to a reduction of 6.9% achieved by rule-based control in the same simulation.

2.1.4. Learning based EMS

In [33], a combination of ECMS and rule-based logic is used in order to generate data and train a neural network. The paper proved the methodology is feasible but does not compare the performance to a benchmark. The employment of a neural network is an attempt to perform the lengthy optimization

of optimal control offline, in order to operate a more computationally cheap trained machine learning model in real-time. [34] and [35] apply this idea to hybrid vehicle power control and diesel engine air path control. They successfully show that computationally heavy non-linear MPC and dynamic programming (DP), can be replaced by training machine learning models such as neural networks.

2.2. Key performance indicators

Research question 1b: ”What are suitable key performance indicators (KPIs) for the evaluation of an energy management strategy?” will be answered here. In [4] a list of performance criteria is given for powertrains, namely:

1. **Fuel consumption**;
2. **Emissions**;
3. Radiated noise;
4. **Propulsion availability**;
5. Maneuverability;
6. Comfort due to minimal noise, vibrations, and smell
7. maintenance cost due to engine thermal and mechanical loading; and
8. Purchase cost.

The criteria purchase cost, maintenance cost, comfort, and maneuverability are design- and operation-related considerations and will therefore not be selected as KPIs for the energy management system. Radiated noise is a relevant EMS KPI as the controller could opt for the electric drive when low noise operations are required. However, given the scope of the project they will not be selected as a KPI. Propulsion availability can be guaranteed through constraints that ensure the required power will be delivered by the main engines and induction machines. Propulsion availability is therefore a KPI that is selected. Note, that theoretical availability does not represent accurate reliability of propulsion availability. The main KPIs that are selected for this project is fuel consumption and emissions. The controller in this project will minimize for fuel consumption. It is assumed that with reduced fuel consumption comes reduced emissions. More specific performance indexes to reduce pollutants are not considered.

2.3. Conclusion

Of all the methods mentioned in this literature review very few have been specifically applied for hybrid propulsion & hybrid energy supply (HPHPS) systems [1, 11, 19]. [1] presents an EMS for a hybrid energy supply leveraging power load forecasting, however, hybrid propulsion was not considered.[19] does consider a HPHPS system but only for optimal powertrain design purposes, and not for an energy management system. [11] considers an optimization-based controller for a HPHPS system using ECMS. However, the method did not leverage power load forecasting to further enhance the performance of the EMS. Therefore, what is currently missing is the implementation and evaluation of a state-of-the-art energy management systems for HPHPS systems leveraging power load forecasting; More specifically, an online optimization-based control method. Given the excellent performance of these load predicting optimization-based control algorithms, it is worth exploring their effectiveness for HPHPS systems.

Finally, to answer research question 1: Optimization-based control has proven to outperform heuristic methods in the reduction of energy consumption and emissions. Additionally, the method is more adaptive when operating profiles are unknown or not well-defined. This makes the method more widely useful, and prevents the need to redefine sets of rules in heuristic control for ship specific behaviour. Whether optimization-based control can be used in real-time depends on the optimizer and the complexity of the internal models of the controller. The optimization-based method that stands out is the ECMS. The ECMS methods have proven to handle the complexity of the models well and can provide real-time optimization with reducing the fuel consumption. Finally, the ECMS also allows for the incorporation of the battery through a equivalent specific fuel consumption (ESFC), which is very useful in

the HPHPS system. This ESFC describes the battery as a resource with a particular cost depending of the amount of power consumed or discharged. Therefore, because of its strong performance as well as the capability to incorporate the battery in the fuel minimization problem, the ECMS is selected as the energy management strategy. The addition of power load forecasting can further increase the performance of the controller, as more accurate predicted future states, lead to better control outputs by the controller when optimizing over a control horizon. Therefore, the energy management strategy used in this project will be an optimization-based controller leveraging the ECMS scheme, as well as a load prediction model, evaluated with the following KPIs: fuel consumption, emissions, and propulsion availability. The details of the controller will be discussed in chapter 7, and the load predictions in chapter 6.

3

Case related information

In this chapter the information relating to the case to be studied is discussed. First, the Holland-class offshore patrol vessel (HCOPV) is described and its powertrain. The engines and battery specifications are mentioned also. Secondly, the data shared by Damen naval is described, processed and evaluated for predictive value. Because the case-specific information directly effects the selection of methods of the research, it is discussed prior to the methodology.

3.1. Holland-class offshore patrol vessel

The Holland-class offshore patrol vessel is a sea-going patrol vessel constructed for the Royal Netherlands Navy. ”They are designed to fulfill patrol and intervention tasks against lightly armed opponents, such as pirates and smugglers, but have much higher level electronic and radar surveillance capabilities which are used for military stabilization and security roles, short of outright war” [36]. The vessel can viewed below in Figure 3.1.

Figure 3.1: Holland-class offshore patrol vessel of the Royal Netherlands Navy. Image retrieved from [37].

The propulsion system is made up of two diesel engines and two electric motors. The diesel engines

are 4-stroke diesel engines with a power of 5400 kW each, with a rated speed of 1000 rpm. The electric motors have a power of 400 kW each. The gears combine a diesel engine and a electric motor to drive a controllable pitch propeller on each of the two shafts. The vessel has 3 generator sets of 968 kW each and one emergency generator set of 255 kW, combining for a total of 4 [38]. The system has various hotel loads such as air-conditioning, lights, and water-cooling systems, these auxiliary loads are assumed to be constant. The size of the auxiliary loads are not described in the public domain, and will therefore not be states here. The selected battery pack has a capacity of 400 kWh, and allows 1c charging and discharging, therefore, the maximum power the battery can deliver is 400 kW. An overview of the power ratings of the components is given in Table 3.1

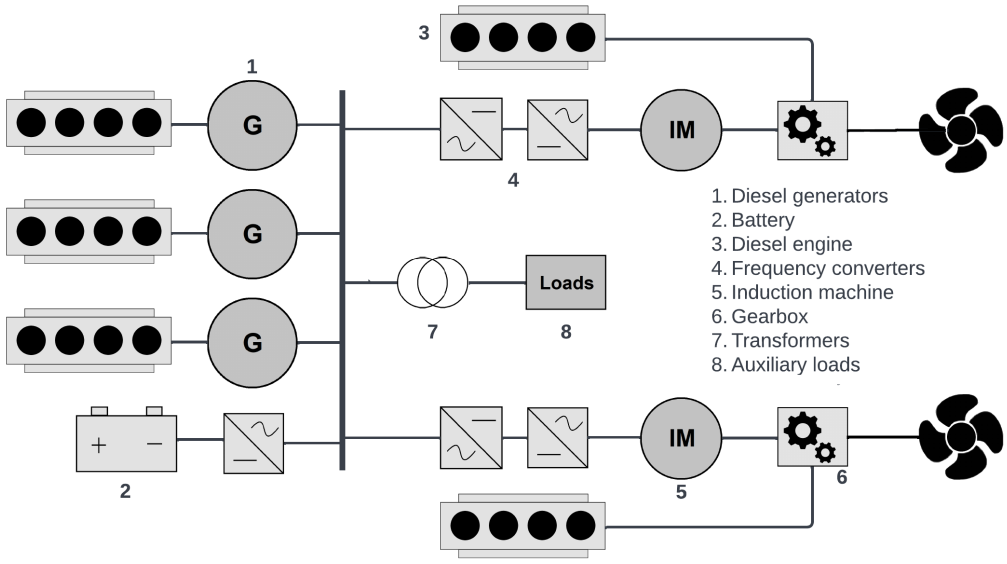

Figure 3.2: Powertrain of the Holland-class offshore patrol vessel, augmented with a battery.

Given the description above of the powertrain components the powertrain can be visualized as presented in Figure 3.2. The emergency generator set has been excluded, as in the energy management system it is not to be relied on as a readily available resource. The battery supplies energy to the bus, and conversely, can receive energy as well. A transformer is used to connect the electric circuit to the electric network of auxiliary load.

Component	Power rating [kW]	Amount
Main engine	5400	2
Diesel-generator set	968	3
Induction machine	400	2
Battery pack	400	1
Emergency generator-set	255	1

Table 3.1: Overview of power ratings of powertrain components

3.2. Data description

Data is provided for four different offshore patrol vessels (OPVs). There are 6 data features in the time series data set, shown below in Table 3.2.

X	Data description
x_1	Percentage available power main engine starboard
x_2	Percentage available power main engine portside
x_3	Power of induction machine starboard in [kW]
x_4	Power of induction machine portside in [kW]
x_5	Main engine shaft speed starboard in [rpm]
x_6	Main engine shaft speed portside in [rpm]

Table 3.2: Data features of the shared data set.

The total shaft power demand, and predicted total shaft power demand is the data feature that the controller needs in order to allocate set points for the engines effectively. However, as is evident from the table above this data is not directly available; It can be computed with the available data features though. Data features x_1 and x_2 can be used in conjunction with the main engine fuel efficiency map, example shown in Figure 7.1. This provides the main engine power, x_7 and x_8 for starboard and portside respectively as a time series. The total shaft power for starboard and portside are respectively $x_9 = x_7 + x_3$ and $x_{10} = x_8 + x_4$.

Data features x_9 and x_{10} are additive compositions of x_1, x_2, x_3 and x_4. The individual power of induction machines and main engines are not interesting to the controller, since the power split is one of the decisions to be made by the controller and therefore should not be provided through data. These four data features also do not capture trends that aren't already captured by x_9 and x_{10}. Therefore, the data features x_1, x_2, x_3 and x_4 do not hold additional predictive power compared to x_9 and x_{10}, and for that reason they are not included in the prediction models in this project.

The operational profile of the vessel speed x_{11}, which is an operator set point, can be deduced based on main engines shaft speed x_5 and x_6. Therefore, x_{11} is the scaled version of x_5 and x_6 between 0-100%. The extrapolated data features are presented in Table 3.3. How these data features are used will be discussed in chapter 6.

X	Data description
x_7	Main engine power starboard in [kW]
x_8	Main engine power portside in [kW]
x_9	Total shaft power starboard in [kW]
x_{10}	Total shaft power portside in [kW]
x_{11}	Vessel speed set point in [%]

Table 3.3: Extrapolated data features.

3.3. Operational profiles

From the available data 8 operational profiles are composed, shown in Figure 3.3. Note that the numbers have been removed from the axes since the data is confidential. There are 2 operational profiles per offshore patrol vessel. The operational profiles have been selected at random days, and are all around 2 hours in length. These operational profiles should sufficiently represent the power profiles, and power needs of the Holland-class offshore patrol vessels for the purposes of this project. These profiles are selected to show a variety in vessel, season of operation and electric- or hybrid operating modes. To smooth out some of the erratic variances in the data, which is due to disturbances like measurement noise, a moving average of order 15 has been applied. The order was selected with to smooth out the profile, while retaining significant power changes in the operational profiles. These operational profiles will be used in the forecasting methods in chapter 6, as well as showing the behaviour of the controller in chapter 7.

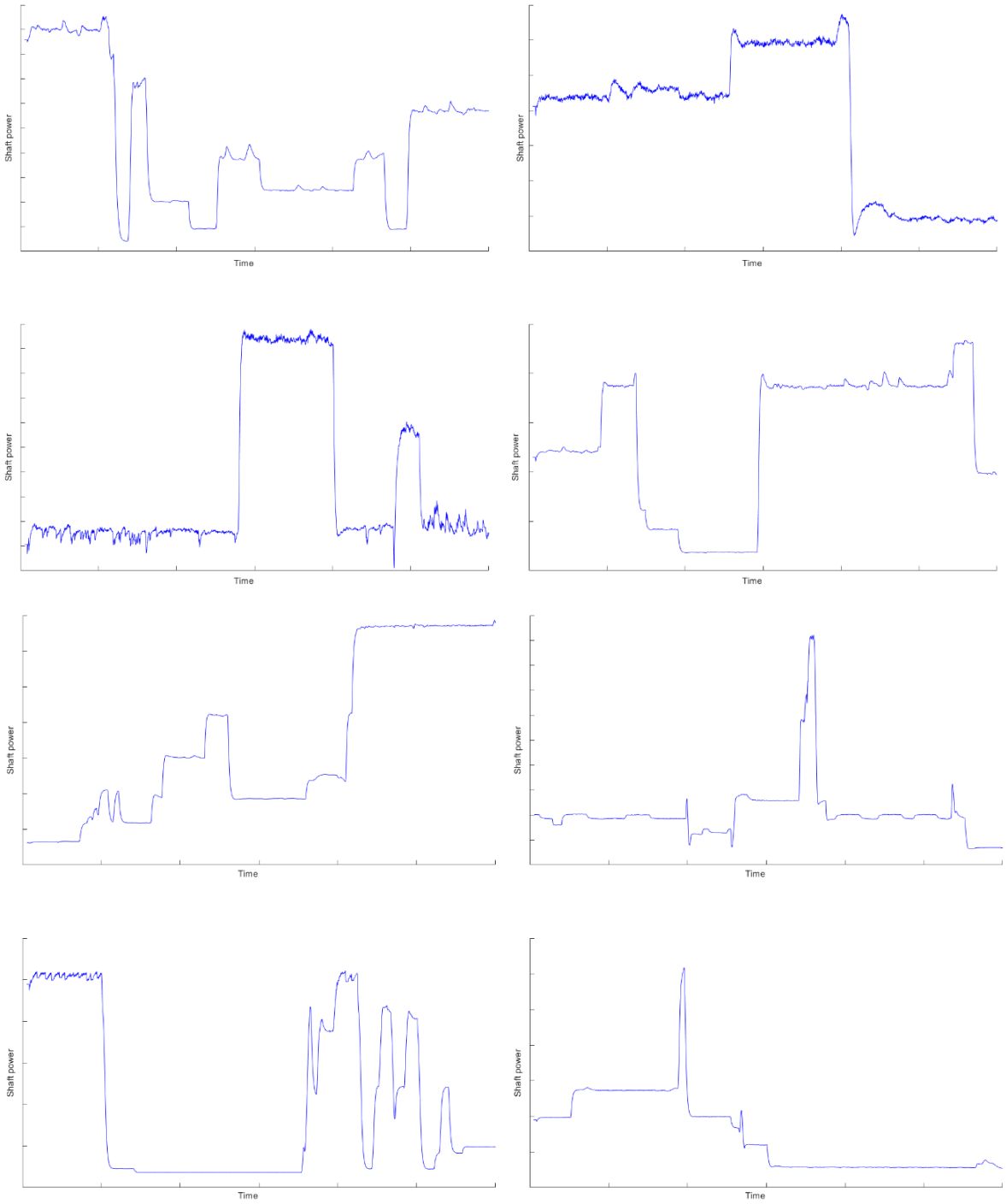

Figure 3.3: Operational profiles

It can be noted that the profiles show many flat spots, indication a stable shaft power demand. These flat spots are followed up by sudden shifts in power demand.

4

Methodology

The summarized methodology of the research is described in this chapter, for reader convenience. A complete description of the methodology is described in subsequent chapters. The methodology of the research can be represented by the three pillars that make up the energy management strategy: the powertrain model, power load forecasting model, and the optimization based controller. The relationship between these respective components is graphically shown in Figure 4.1.

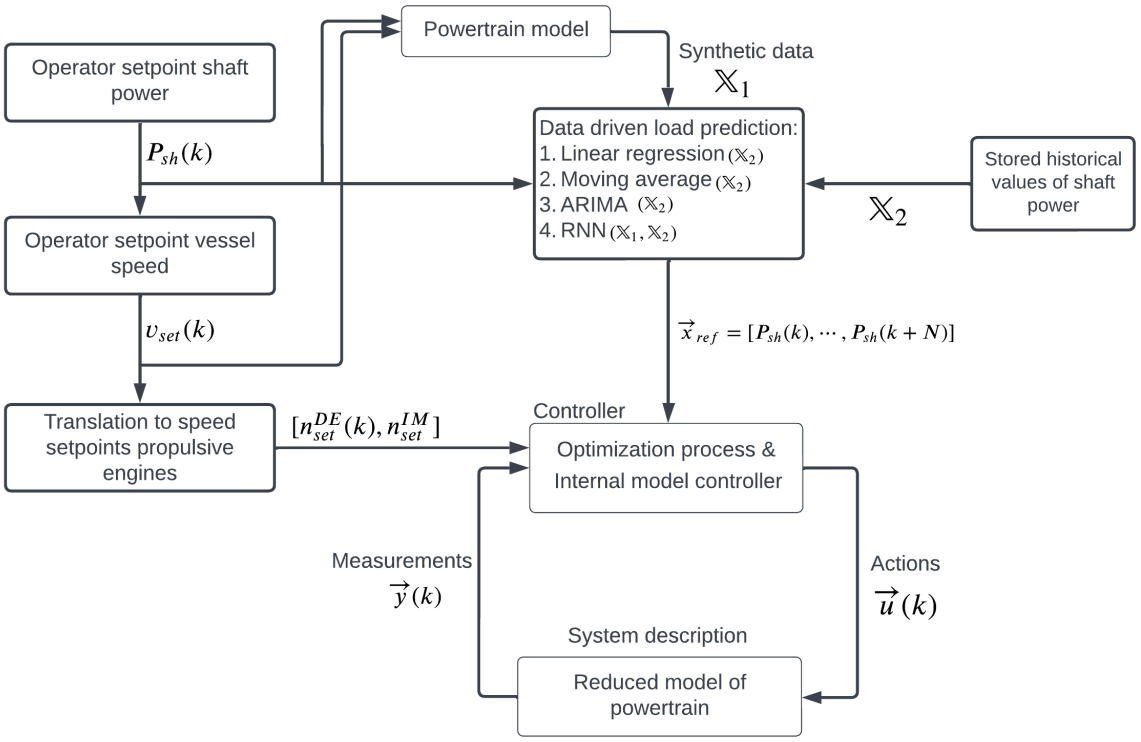

Figure 4.1: Overview of relationship between the controller, power prediction model and powertrain model.

The information that is known at the start of an iteration is the operator setpoint for the shaft power, $P_{sh}(k)$. This shaft power is used as a starting point since it is one of the few data features available. This data is shown graphically in Figure 3.3. Based on the shaft power setpoint the operator setpoint for the vessel speed, $v_{set}(k)$, is assumed. It is assumed that the setpoints of shaft power and vessel speed are proportional. For instance, when 100% of the available shaft power is demanded, the vessel speed setpoint is also assumed at 100%. Based on the vessel speed setpoint the speed setpoints for the diesel engines, $n_{set}^{DE}(k)$, and induction machines, n_{set}^{IM}, are inferred.

For the diesel engines the speed setpoint is assumed proportional to the vessel speed and shaft power. For the induction machine the speed setpoint is assumed stationary at rated speed. Rated speed is assumed here, since not enough information is available to make a more informed assumption. The assumption of proportionality of the speed setpoint for the induction machine to the vessel speed, leads to limited power availability by the induction machine, and is therefore not preferred here. This occurs because the power of the induction machine is speed dependant, as shown in Equation 7.2. The available efficiency map of the induction machine shows that for induction machine speed in range [0, n_{rated}] the available torque is equal for all speeds. Additionally, the efficiency curves obtained for different speed settings are similar. Therefore, although not optimal, the lack of a variable induction machine setpoint should not have a diminishing effect on the results of the energy management system.

The physical system is described by a powertrain model of the Holland-class offshore patrol vessel. The full description is given in chapter 5. This powertrain model is a mathematical representation that shows the dynamics of the components of the powertrain of the ship. The models chosen are selected based on availability, and accuracy. The models are made available in an adaptive pitch control framework, the framework is presented in [11, 39]. To operate this framework multiple controllers are required to maintain setpoints for the engines and motors and propeller pitch. It is outside the time limits and scope of this project to use this full model to evaluate the novel energy management strategy developed in this research as it would involve re-tuning multiple controllers. Instead, in this project the powertrain model is used in order generate synthetic data. The set of synthetic data features, $\mathbb{X}_1$, is used by data driven load prediction methods. These will be described later.

The controller is an optimization-based control tool. It uses reduced models of the powertrain in order to evaluate which set of decision variables will work best in order to minimize fuel consumption. The simplified models that represent the powertrain dynamics within the controller will from now on be referred to as the internal model of the controller. The internal model of the controller has the purpose of modelling the relationship between power, torque and and specific fuel consumption of diesel engines, diesel generators and induction machines. Additionally, an artificial fuel consumption model is established for the battery. Based on the internal model of the controller, the optimizer is able to find a set point for the engines and battery. Based on defined constraints, these are feasible set points, that fall within the operating envelopes of the engines. The internal model of the controller is defined in detail in section 7.1. The speed setpoints for the induction machines and diesel engines, as well as the measurement variables, $\vec{y}(k)$, are used as input by the controller. The output is a set of decision variables , $\vec{u}(k)$, that minimizes fuel consumption of a prediction horizon with N steps.

To evaluate the output of the controller a reduced model of the powertrain model is used. In fact this model is the same as the internal model of the controller. The full powertrain model could not be used here, since in order to operate this full model multiple extra controllers for pitch control, engine control and induction machine control are required. Due to time constraints and the scope of the project, this is not possible to implement. Therefore, the reduced model is used to evaluate the output and recorded the measurement variables $\vec{y}(k)$.

The data-driven load prediction tool uses historical data on the shaft power, $\mathbb{X}_2$, to predict future shaft power demand. In this research project, unfortunately, very few data features are available. Consequently, univariate prediction methods are used. These methods use a single data feature to predict a single data feature in the future. In this case past shaft power is used to predict future shaft power. In order to improve on the performance of these univariate prediction methods, synthetic data is also computed, using the full powertrain model, and used to train a recurrent neural network (RNN). This RNN uses as input not only the historical data on the shaft power, $\mathbb{X}_2$, but also measurement variables provided by the powertrain model $\mathbb{X}_1$. The total input space for the RNN is $\mathbb{X} = \mathbb{X}_1 \cup \mathbb{X}_2$. The output to the prediction tools are reference values for the expected shaft power demand over a prediction horizon with N steps. The reference values are denoted by $\vec{x}_{ref}$. The reference values are used by the controller to make decisions over the prediction horizon.

For each of the three components of the energy management system, (1) Powertrain model, (2) Load forecasting tool, and (3) Controller, a brief description is given on the methods used, and the reasoning behind using these methods. The details on the implementation of the methods is discussed in subsequent chapters, as well as the results.

4.1. Powertrain model

The powertrain model is an extensive model that aims to represent the behaviour of the ships powertrain accurately. It is outside the scope of this project, to model this powertrain, since the purpose of the project is to design a controller and a load forecasting model. Thankfully, TU Delft and Damen Naval have an accurate powertrain model available. An overview of the powertrain component models are listed in Table 4.1. Descriptions of the models can be found in chapter 5. The model calibration and validation can be found in [11], and will not be restated here.

Component	Model
Diesel Engine	Mean value first principle model
Induction Machine	Dq equivalent circuit
Frequency converter	Modelled as a power loss
Battery	2nd order RC equivalent circuit
Auxiliary loads	Constant power load
Diesel generator set	Synchronous generator per-phase equivalent circuit
Propeller	4-quadrant open water diagram
Gearbox & shaft	Modelled as torque loss
Hull dynamics	Single DoF surge model
Wave model	Wave model at propeller centre

Table 4.1: Overview of selected powertrain component models.

4.2. Power load forecasting model

As mentioned before, the shared data set of the Holland-class patrol vessel has very few data features. The scarcity of data features implies that many state-of-the-art forecasting models will not be feasible. Therefore, first some univariate forecasting methods will be used, namely: Linear regression, moving averaging, and ARIMA. Linear regression and moving average methods are easy to implement, and have a short computation time. Given the shape of the operational profiles - which show many flat spots, followed by sudden large shifts in power - these methods can be a good prediction tool for short-term predictions; in the order of seconds. In order to implement a bit more advanced methods and to capture short-term variance the Auto-Regressive Integrated Moving Average (ARIMA) model is also used. ARIMA models are one of the most widely used approaches to time series forecasting [40]. ARIMA models aim to describe the auto-correlations in the data. Therefore, it is an appropriate choice for univariate load predictions. ARIMA models combine the use of an auto-regression model with a moving average model. The ARIMA model can still only predict the load demand in the short-term.

Using the powertrain model, some synthetic data is generated for a selection of data features, described in Table 4.2. The procedure of establishing the synthetic data is explained in section 6.5. Using the synthetic data, the state-of-the-art method recurrent neural network (RNN) with long-short-term-memory(LSTM) can be applied. The RNN model is selected since it has proven to have excellent predictive capabilities in a multitude of fields. In the maritime domain the method is used for instance, for ship position estimations [41, 42], non-parametric modeling of ship maneuvering motion [43], as well as pitch, heave and roll motion predictions [44, 45].

RNN can predict in the short- and medium-term; order of seconds and minutes. However, it is greatly dependant on the quality of the data that is used for training the neural network. Since the shaft power data is real data containing measurement noise and uncertainty, as well as large and inconsistent variances, it can be deduced that RNN will only produce accurate prediction results for short-term predictions. Since the synthetic data is a product of the real data, the synthetic data will also contain these variances.

$\mathbb{X}_1$	Data description
x_{12}	Main engine shaft speed in [rpm]
x_{13}	Pitch ratio
x_{14}	Propeller torque M_p in [Nm]
x_{15}	Propeller thrust T_p in [N]
x_{16}	Vessel speed v_s in [knots]

Table 4.2: Generated data features, and input space $\mathbb{X}_1$.

Figure 4.1 shows that the output of the data driven load prediction model should be a set of reference values for the total shaft power demand over prediction horizon with N steps. In order to achieve these predictions the load prediction model is provided with input space $\mathbb{X} = \mathbb{X}_1 \cup \mathbb{X}_2$. The stored shaft power values are represented by $\mathbb{X}_2$ and the synthetic data features are represented by $\mathbb{X}_1$. This implies only the RNN will be using the output of the powertrain model as input to make predictions on the shaft power. The other methods are univariate regression methods that only use $\mathbb{X}_2$.

4.3. Controller

The controller uses an internal model, which describes the relationship between torque, power and specific fuel consumption of the main engines, diesel-generator sets and induction machines using fuel efficiency maps. The battery is described using an equivalent fuel consumption map, which is constructed based on the diesel-generator fuel curve, and then fine-tuned based on simulations and control parameters. This fine-tuning is required in order to get the desired optimization behaviour, and battery usage; by incentivizing and disincentivizing battery charging and discharging at the right moments. A full account of the procedure is given in section 6.5 and section 7.3.

Since the controller uses an equivalent fuel consumption for the battery the optimization problem is an equivalent consumption minimization strategy (ECMS). The objective function of an ECMS is simply the summation of the sources of fuel consumption, as can be seen below. The objective function is subject to system dynamics, constraints, and boundary conditions. The operating envelopes of the engines maps are also constraints. The objective function is:

$$\min_{\vec{u}(k)} \; J = \sum_{k=1}^{N} \left(\sum_{i=1}^{2} \dot{m}_{f,DE_i}(k) + \sum_{i=1}^{3} \dot{m}_{f,DG_i}(k) + \dot{m}_{f,BAT}(k) \right) \tag{4.1}$$

with N the prediction horizon, k the discrete step-size, $\dot{m}_{f,DE_i}(k)$ the fuel consumption rate of the diesel engine i, $\dot{m}_{f,DG_i}(k)$ the fuel consumption rate of the diesel-generator set i and $\dot{m}_{f,BAT}(k)$ the equivalent fuel consumption rate of the battery. The summation of the fuel consumption rates is taken at each timestep until the maximum prediction horizon step N is reached. A full account of constraints, system dynamics described, and internal model of the controller is presented in chapter 7.

5

Powertrain Model

In this chapter the results to research question 2 are presented, regarding the powertrain model. For convenience the research question is restated here.

Research question 2: What is an appropriate powertrain description of the Holland-class offshore patrol vessel that is augmented with a battery?

(a) What are the components of the powertrain of the Holland-class offshore patrol vessel, how are they connected, and how would a battery be connected to the powertrain?

(b) What features of the components should be modelled in order to obtain an accurate numerical description of the complete powertrain behaviour, while also providing enough information for the KPIs?

The answer to research question 2a is the powertrain overview given in section 3.1. Question 2b is answered in the following section.

5.1. Powertrain models

The powertrain model is an extensive model that aims to represent the behaviour of the ships powertrain accurately. It is outside the scope of this project, to model this powertrain, since the purpose of the project is to design a controller and a load forecasting model. Thankfully, TU Delft and Damen Naval have an accurate powertrain model available. An overview of the powertrain component models are listed in Table 5.1. Descriptions of the models can be found in subsequent sections. The model calibration and validation can be found in [11], and will not be restated here.

Component	**Model**
Diesel Engine	Mean value first principle model
Induction Machine	Dq equivalent circuit
Frequency converter	Modelled as a power loss
Battery	2nd order RC equivalent circuit
Auxiliary loads	Constant power load
Diesel generator set	Synchronous generator per-phase equivalent circuit
Propeller	4-quadrant open water diagram
Gearbox & shaft	Modelled as torque loss
Hull dynamics	Single DoF surge model
Wave model	Wave model at propeller centre

Table 5.1: Overview of selected powertrain component models.

5.1.1. Main diesel engine

For the main diesel engines a mean value first principle model is used. The method is proposed and validated with Factory Acceptance Test (FAT) and Sea Acceptance Trial (SAT) data in [39]. The diesel engine model is graphically presented in Figure 5.1. The model is directly taken from [39], it consists of the following sub-models: fuel pump, air swallow, heat release, Seiliger cycle, exhaust receiver and turbocharger, and mechanical conversion. The interested reader may refer to [39], for the mathematical description of the model. For the purpose of this project, the model provides more information than is required on the dynamic behaviour of the engine. However, due to the availability of the model it has been selected.

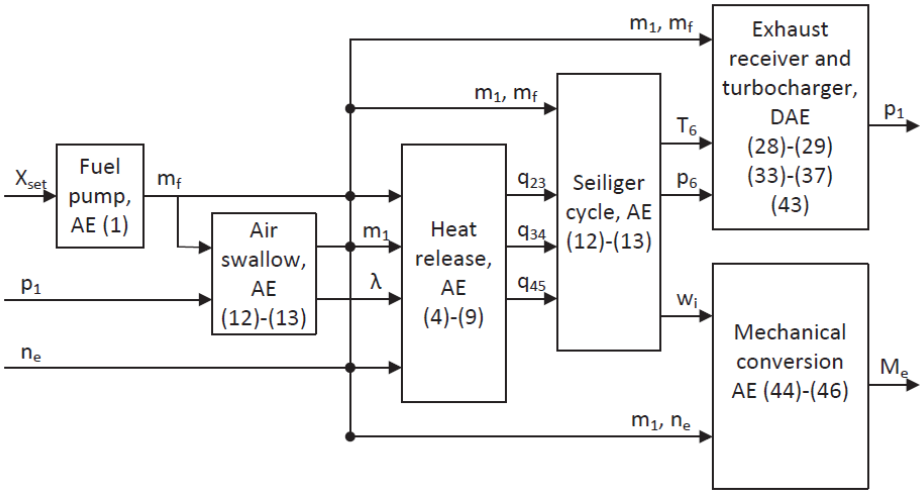

Figure 5.1: Schematic presentation of the diesel engine model and the interaction between its subsystems. Image retrieved from [39].

5.1.2. Induction machine

For the induction machines, a state space model based on [46] is used, which is a dq equivalent circuit of an induction machine with an arbritrary rotating reference frame, shown in Figure 5.2. The interested reader may refer to [11], for the implementation and mathematical description of the model. The model has been selected for its accurate representation of the induction machine behaviour as well as the availability of the model. Just as the diesel engine model, the induction machine model provides more information than is required on the dynamic behaviour of the engine, for the purposes of this project.

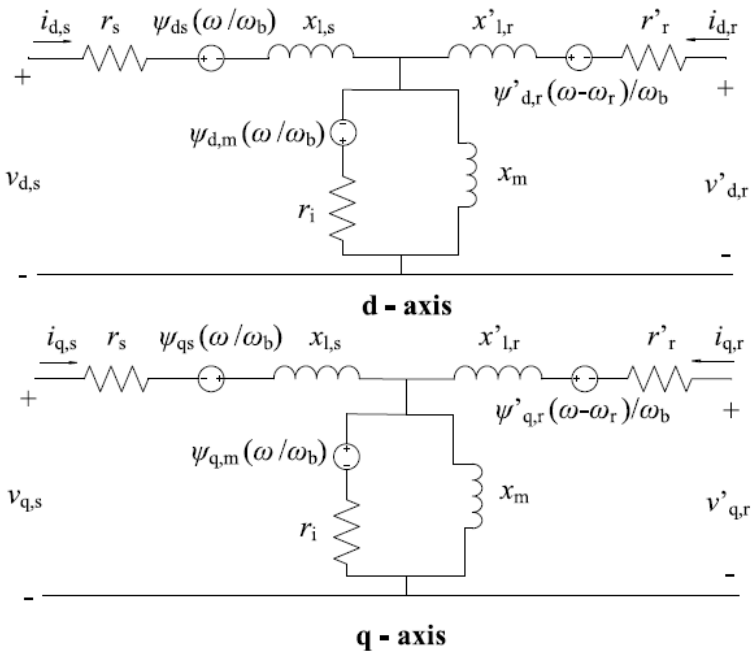

Figure 5.2: Dq equivalent circuit of an induction machine in an arbitrary rotating reference frame. Image retrieved from [11].

5.1.3. Diesel generator set

The electrical network dynamics are not considered in this study as they do not effect the fuel consumption [47]. Therefore, simplified diesel generator set models are used, namely, a steady-state model based on the synchronous generator per-phase equivalent circuit. In [11], the mathematical description of the model can be found, for the interested reader.

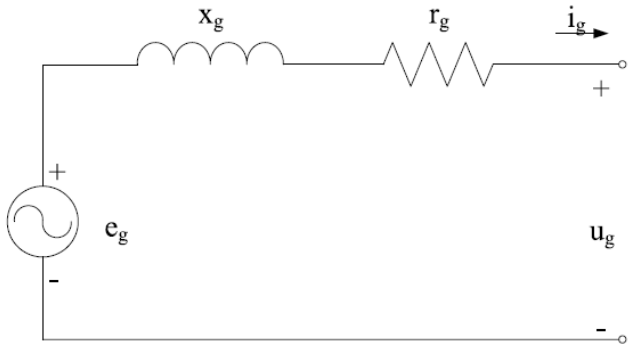

Figure 5.3: Synchronous generator per-phase equivalent circuit. Image retrieved from [11].

5.1.4. Frequency converter model

The power losses of the frequency converters can be estimated using an empirical relationship, the method is proposed in [48]. The polynomial loss equation $P_{\text{fc, loss}}(t)$ with fitted parameters a,b and c is as follows:

$$P_{\text{fc, loss}}(t) = P_{\text{fc,nom}}\left(1-\eta_{\text{fc,nom}}\right)\left(a + bi^*_{\text{fc}}(t) + ci^{*2}_{\text{fc}}(t)\right) \tag{5.1}$$

$$P_{\text{fc}}(t) = P_{\text{im,el}} + P_{\text{fc, loss}}\,, \tag{5.2}$$

where $\eta_{\text{fc,nom}}$ is an efficiency measure of the frequency converter and $P_{\text{im,el}}$ is the electrical power of the induction machine.

5.1.5. Battery model

The battery is modelled as a second-order RC equivalent circuit. This model provides a good trade-off between accuracy and model complexity [49]. In the model the parameters are all functions of the state of charge, as can be seen from Equation 5.3, Equation 5.4, and Equation 5.5. u_{OC}, is the open circuit voltage in V, c_i the capacitors in F, r_i the resistors in Ohm. $\vec{\mathbf{v}} = (v_1 \ldots v_6)$, $\alpha_{i,j} \in \mathbb{R}^{3x2}$, and $\beta_{i,j} \in \mathbb{R}^{2x2}$, are the model's parameters that are constant.

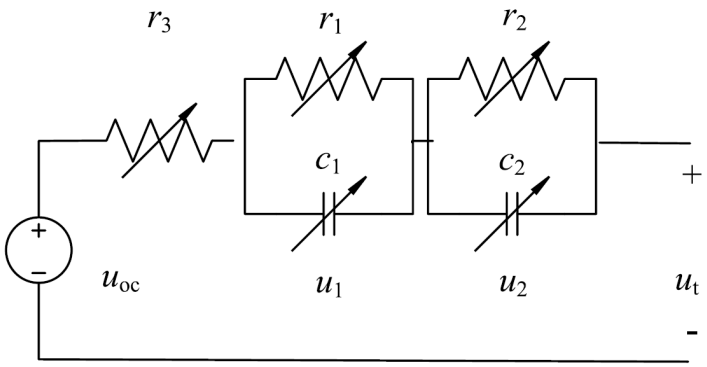

Figure 5.4: 2nd order RC equivalent circuit of a battery. Image retrieved from [11].

The model description is as follows [50, 51]:

$$u_{\mathrm{OC}}\left(SOC(\mathrm{t})\right) = v_1 e^{-v_2 SOC(\mathrm{t})} + v_3 + v_4 SOC(\mathrm{t}) + v_5 SOC^2(\mathrm{t}) + v_6 SOC^3(\mathrm{t}) \tag{5.3}$$

$$r_i\left(SOC(\mathrm{t})\right) = \alpha_{i,1} e^{-\alpha_{i,2} SOC(\mathrm{t})} + \alpha_{i,2}, \quad i = 1,2,3 \tag{5.4}$$

$$c_i\left(SOC(\mathrm{t})\right) = \beta_{i,1} e^{-\beta_{i,2} SOC(\mathrm{t})} + \beta_{i,2}, \quad i = 1,2 \tag{5.5}$$

The circuit behaviour is described as follows:

$$\frac{d}{dt} u_i(t) = -\frac{u_i(t)}{c_i r_i} + \frac{i_{\mathrm{bat}}(t)}{c_i}, \quad i = 1,2 \tag{5.6}$$

$$u_t(t) = u_{\mathrm{oc}}(t) - \sum_{i=1}^{2} u_i(t) - r_3 i_{\mathrm{bat}}(t). \tag{5.7}$$

For this research project, measurement inaccuracies have been neglected, therefore, Ah counting is used to estimate SOC, as follows:

$$SOC(t) = SOC\left(t_0\right) + \int_{t_0}^{t} -\frac{i_{\mathrm{bat}}(t)}{Q_{\mathrm{bat}}} dt. \tag{5.8}$$

5.1.6. Auxiliary loads model

In this study we assume the auxiliary loads to be constant, while in reality these might fluctuate. The relationship between auxiliary load power P_{aux} and the auxiliary current i_{aux} for the 3-phase electrical network is described by [11]:

$$P_{aux}(t) = 3 u_g(t) i_{aux}(t) cos(f_p), \tag{5.9}$$

where f_p is a power factor, and u_g the per-phase voltage.

5.1.7. Propeller model

The propeller model is used to give the relationship between the thrust, torque and propeller speed. The 4-quadrant open water diagram is used to model this relationship. This diagram gives the relationship between the hydrodynamic pitch angle B, the propeller torque M_p in Nm, and torque and thrust coefficient respectively C_T and C_Q. The propeller thrust T_p in N, can be computed as follows [52]:

$$\beta(t) = \arctan\left(\frac{v_a(t)}{0.7\pi n_p(t) D_p}\right) \tag{5.10}$$

$$v_a(t) = (1 - f_w)\, v_s(t) \tag{5.11}$$

$$T_p(t) = \frac{C_T(t)\left(1 - t_p\right)}{\frac{1}{2}\rho\left(v_a^2(t) + \left(0.7\pi n_p(t) D_p\right)^2\right)\frac{\pi}{4}D_p^2} \tag{5.12}$$

$$M_p(t) = \frac{C_Q(t)}{\frac{1}{2}\eta_{rr}\rho\left(v_a^2(t) + \left(0.7\pi n_p(t) D_p\right)^2\right)\frac{\pi}{4}D_p^3} \tag{5.13}$$

5.1.8. Gearbox and shaft-line model

[39] proposes to use values at the propeller curve and generator line to predict the gearbox losses across the full gearbox. The gearbox torque loss in Nm, $M_{l_{nom}}$, and resulting gearbox output torque M_{gb} also in Nm, can be represented by:

$$M_l(t) = M_{l_{\text{nom}}}\left(a_{gb} + b_{gb}\frac{n_e(t)}{n_{e_{\text{nom}}}} + c_{gb}\frac{M_e(t)}{M_{e_{nom}}}\right) \tag{5.14}$$

$$M_{l_{\text{nom}}} = \frac{P_{l_{\text{nom}}}}{n_{p_{\text{nom}}}} \tag{5.15}$$

$$M_{gb}(t) = M_e(t) i_{gb} - M_l(t), \tag{5.16}$$

where a_{gb}, b_{gb} and c_{gb} are the gearbox loss function parameters, $P_{l_{\text{nom}}}$ is the nominal gearbox loss power in W and $n_{p_{\text{nom}}}$ is the nominal gearbox output shaft speed and also the nominal propeller speed in rev/s. These function parameters can be extrapolated from manufacturer data or from a thermal network model presented in [53].

The shaft-line losses can be modelled with a linear loss percentage, namely the shaft-line efficiency η_{sl}, on the output torque of the gearbox. This is a constant. The relationship is represented by:

$$M_{sl}(t) = \eta_{sl} M_{gb}(t), \tag{5.17}$$

where M_{sl} are the shaft-line losses in Nm. The equations of motion for the coupled gearbox, shaft-line, and propeller is described by:

$$\frac{dn_p(t)}{dt} = \frac{M_{gb(t)} - M_{sl(t)} - M_p(t)}{2\pi J_t} \tag{5.18}$$

$$J_t = J_e i_{gb}^2 + J_{gb} + J_{sl} + J_p + J_{ew}, \tag{5.19}$$

where J_t is the total moment of inertia of the shaft and all connected rotating equipment in kgm^2. J_{gb}, J_e, J_{sl}, J_p and J_{ew} are the moments of inertia of the gearbox, diesel engine, shaft-line, propeller, and entrained water respectively, all in kgm^2.

5.1.9. Hull dynamics

The chosen hull dynamics model is a single degree of freedom model in the surge direction. The model provides an estimate of the relationship between hull resistance R_v in N and vessel speed v_s in knots. The resistance of the ship is estimated using empirical methods such as towing tank tests. In this project the resistance will be found using a look-up table, that is also used in [39]. The equation of motion in the single DoF of the ship is represented by:

$$\frac{dv_s(t)}{dt} = \frac{\left(k_p T_p(t) - \frac{R_v(v_S(t))}{1-f_t}\right)}{m}, \tag{5.20}$$

where f_t is the thrust deduction factor, k_p is the number of propellers, T_p is the propeller thrust, and m is the ships mass in kg.

5.1.10. Wave model

Waves can cause significant disturbances on the loading of diesel engines when a ship sails in high sea states [39], therefore, it is important to model the waves. The selected model considers the wave speed at the propeller centre, as follows [54]:

$$v_w(t) = \zeta \omega e^{k_w z} \sin\left((-k v_s - \omega)\, t\right), \tag{5.21}$$

$$k_w = \frac{\omega^2}{g}, \tag{5.22}$$

where ω is the wave radial frequency in rad/s, ζ is the significant wave amplitude in m, k_w is the wave number in 1/m, g is the standard gravity in m/s^2 and z is the water depth in m at the propeller centre.

5.2. Conclusion

In this chapter the selected powertrain model and its sub-models have been described. The models capture advanced dynamic behaviour of the engines and batteries. The drawback of the model is that only a single degree of motion of the ship is considered. For the generation of more valuable data a multi-DoF model is better, as it can provide more information on maneuvering behaviour of the ship. The maneuvering behaviour, if captured in data, can provide a valuable asset in shaft power forecasting. Maneuvering operations are often slow, and it would allow the forecasting model to know in advance the power demand. However, due to time constraints of the project, the powertrain model will not be altered to incorporate these changes.

6

Power load forecasting model

In this chapter power load forecasting models will be discussed and research question 3 will be answered. For convenience the research question is stated below. Research question 3a has been addressed in the literature review in chapter 2. Question 3b is answered in sections about data, namely section 6.1 and section 6.5. Question 3c addresses the hyperparameters of the chosen forecasting methods, and is naturally discusses throughout the description of the methodology. Question 3d is the comparison of the performances of the forecasting methods, this question will be answered in section 6.7.

Research question 3: What is an effective data driven model for power load forecasting with a prediction horizon of two minutes while maintaining high levels of accuracy, given the data set of the Holland-class offshore patrol vessel?

(a) What are the state-of-the-art data-driven methods currently employed for power load forecasting, and which is the most effective in terms of accuracy and prediction horizon?

(b) Which data attributes should be included in input space $\mathbb{X}$, and which data cleaning and preparation steps are required for the provided data set?

(c) What are the relevant hyperparameters for the selected data-driven method, and what are their optimal settings, evaluated with model selection criteria of k-fold cross-validation and MSE?

(d) What is the performance of the model evaluated with MAE, MSE, R^2, and sMAPE, and their respective confidence intervals? How does the model performance compare to state-of-the-art data driven methods for power load prediction?

Unfortunately, the shared data set of the Holland-class patrol vessel has very few data features. The scarcity of data features implies that many state-of-the-art forecasting models will not be feasible; Methods such as neural networks, kernel-regularized least squares (KRLS) and support vector machines (SVM). Therefore, first some univariate forecasting methods will be used: Linear regression, moving averaging, and ARIMA. These methods will be discussed in detail in the following sections. Afterwards, using the powertrain model described in the previous chapter, some synthetic data will be generated for a selection of data features, described in section 6.5. With the additional data features it becomes possible to use the state-of-the-art forecasting methods. Therefore, the method recurrent neural network (RNN) with a long-short-term-memory (LSTM) will be used in conjunction with the generated synthetic data. The reasons for choosing the RNN method as well as the RNN model selection and methodology is described in section 6.6. Due to time constraints of the project it is not possible to use multiple state-of-the-art forecasting methods such convolutional neural networks, KRLS, and SVM.

The structure of the chapter is as follows: First the data is described and the data preparation steps are discussed for the univariate prediction methods in section 6.1. Secondly, for the linear regression (section 6.2), moving average (section 6.3) and ARIMA (section 6.4) the methodology is discussed, the implementation and the results. Thirdly, the synthetic data generation is discussed in section 6.5. The RNN its data preparation steps, methodology, implementation and results can be found in section 6.6. And finally, the conclusion and answer to research question 3 can be found in section 6.7.

6.1. Data

6.1.1. Data description

The data features available are discussed in chapter 3, and are repeated below in Table 6.1.

X	Data description
x_1	Available power main engine starboard in [%]
x_2	Available power main engine portside in [%]
x_3	Power of induction machine starboard in [kW]
x_4	Power of induction machine portside in [kW]
x_5	Main engine shaft speed starboard in [rpm]
x_6	Main engine shaft speed portside in [rpm]
x_7	Main engine power starboard in [kW]
x_8	Main engine power portside in [kW]
x_9	Total shaft power starboard in [kW]
x_{10}	Total shaft power portside in [kW]
x_{11}	Vessel speed set point in [%]

Table 6.1: Data features & extrapolated data features of the shared time series.

Onboard the OPV the total shaft power that is required at time t is not available to the controller, unless by prediction. Neither are all the other data features, with the exception of x_{11} the operational speed. It will be assumed that the operational speed is an operator set-point and is therefore available at timestep t. Data features x_9 and x_{10} are additive compositions of x_1, x_2, x_3 and x_4. The individual power of induction machines and main engines are not interesting to the controller since determining the power split between electric and diesel engines is one of the jobs of the controller, one does not want the power split to be dictated by data. Additionally, the four data features do not capture any trends that aren't already captured by x_9 and x_{10}. Therefore, these data features x_1, x_2, x_3 and x_4 do not hold additional predictive power compared to x_9 and x_{10}, and for that reason they are not included in the prediction models in this research.

Additionally, the energy management as well as the powertrain model are only attuned to linear motion of the ship; Maneuvering actions are not captured by the model. Therefore, only either starboard or portside data is required. Once a side is chosen they are assumed to be equal for both sides of the ship. The justifications for choosing a single degree of freedom model is previously discussed in chapter 5.

In conclusion, the only remaining data feature to be used in shaft power forecasting, is past values of the shaft power, as well as the operational speed. However, since the operational speed is directly extrapolated from the main engine shaft speed, which is directly proportional to the shaft power, it also does not hold additional predictive power. Therefore, univariate prediction methods will be employed. Namely, linear regression, moving averaging, and ARIMA are applied on the univariate time series of total shaft power. As described in the introduction, an RNN model will also be described in this chapter. It uses the total shaft power, shaft speed and a few extra synthetic data features, these are described in subsequent chapters.

6.1.2. Data preparation

Only data preparation steps relevant to the linear regression, moving averaging and ARIMA will be discussed here. The full data preparation process for the RNN with be discussed in section 6.6.

Data cleaning Data cleaning is the first step in the data preparation process. Three sources of data cleaning are identified: selection of data attributes, missing data, and outliers. Selection of data attributes was discussed in the previous section. The presence of missing data can be solved by interpolation or removing the affected row of data. Due to the abundance of available data, and the accuracy issues related with data interpolation, data elimination was opted for. This means that rows with missing data were eliminated. Outliers in the dataset were removed where the shaft power values do not fall within the feasible range of $P_{sh} \in [0, 5400] kW$. Similarly, for the the main engine shaft speed outliers

outside the feasible range $n_{sh} \in [330, 1000]$ were removed. The engine shaft speed should be zero, $n_{sh} = 0$, when the main engine not is not in operation, this has also been confirmed by inspection.

Defining prediction variable y The aim of the prediction methods is to predict the total shaft power at each step of a prediction horizon $y = [P_{sh}(k), \cdots, P_{sh}(k+N)]$. Sequences of data in the range $[t-\Delta^-, t-1]$ will be used to predict the shaft power. This input-output relationship is graphically presented in Figure 6.1.

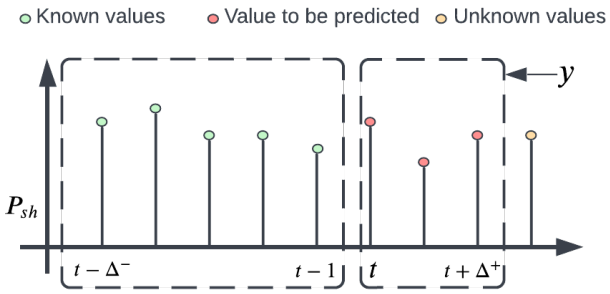

Figure 6.1: Input-output relationships for the univariate prediction models.

Data sequencing As previously explained, the models take sequences of data as input, where each sequence has data points in the range $[t-\Delta^-, t-1]$, with a different t for different sequences. These sequences can be constituted after the other data preparation steps.

6.2. Linear regression

Since we are dealing with a univariate time series and the operational profile shows 'flat' spots. A linear regression model can be used to make short-term predictions on that shaft power; In the order of seconds. Linear regression involves a linear approach for modelling the relationship between a response variable and a dependant variables. A moving time window of data in $[t-\Delta^-, t-1]$ is used to estimate a linear model, and compute Δ^+ seconds ahead, in time window $[t, t+\Delta^+]$. The linear model can be described as [40]:

$$y_t = \beta_0 + \beta_1 t + \varepsilon_t, \tag{6.1}$$

where the coefficients β_0 and β_1 denote the intercept and the slope of the line, respectively. ε_t is an error term that denotes effects on y_t other than time. y_t is the shaft power are time t and is the variable to be predicted. There are a few assumptions when using a linear model that are important to take note off. Namely, (a) the errors of the linear model should have a mean zero, (b) the errors are not related to the predictor variables [40]. the first assumption should hold true, else it would imply that the linear approximation is systematically bias; A better approximation could have been found. The second assumption should hold true, because otherwise there should have been more information included in the systematic part of the model, thus more variables should have been included. The second assumption is unfortunately not adhered to for the shaft power time series in this project. Since using only past values of the shaft power to predict the shaft power at time t, as previously mentioned, is not sufficient to capture all the information of the time-series. Regardless, linear regression will be used here, if only to show the relative effectiveness of other methods in the following chapters.

6.2.1. Model approximation

In order to approximate the values of β_0 and β_1, the linear least squares method (LSM) is used. The LSM is a way of choosing the coefficients by minimising the sum of the squared errors. The mathematical formulation of the errors is as follows:

$$\sum_{t=1}^{T} \varepsilon_t^2 = \sum_{t=1}^{T} (y_t - \beta_0 - \beta_1 t)^2, \tag{6.2}$$

with T the number of data samples. The formulation of the linear problem can be written in matrix form in:

$$\begin{bmatrix} y_1 \\ y_2 \\ \dots \\ y_T \end{bmatrix} = \begin{bmatrix} t_1 & 1 \\ t_2 & 1 \\ \dots & \dots \\ t_T & 1 \end{bmatrix} \begin{bmatrix} \beta_1 \\ \beta_0 \end{bmatrix}, \tag{6.3}$$

or in short notation it can be written as $y = Xc$. Then, to solve for the set of coefficients c, the solution is [55]:

$$c = (X^T X)^{-1} X^T y \tag{6.4}$$

6.2.2. Modelling process

Below the modelling process has been shows graphically in Figure 6.2. First, the data sequence in time window $[t - \Delta^-, t - 1]$ is loaded. Secondly, the least squares problem is formulated, as shown in Equation 6.2. Thirdly the minimization process is executed and coefficients are approximated for β_0 and β_1, using the solution presented in Equation 6.4. Finally, forecasts can be computed given the established linear regression of the data. Once the forecasts have been saved and passed on to the controller, the next timestep is initiated and the process starts over. Note that the models are not regularized. This is a step that could have been implemented to potentially obtain better results, as regularization can prevent over- and underfitting of the model on the data. Regularization has been excluded for linear regression as well as the other methods, due to time constraints of the project. However, in future, regularization of the model can provide a way to obtain models that generalize better.

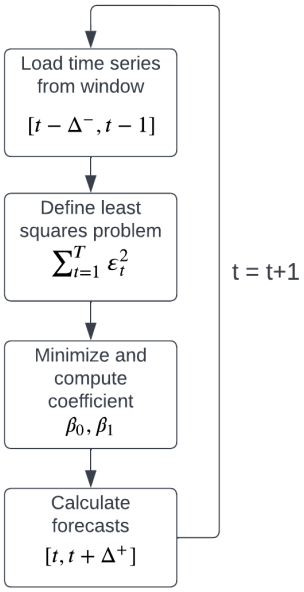

Figure 6.2: Linear regression modelling process.

6.2.3. Linear regression results

The results of the linear regression methods are shown below in various graphs and tables. First, it should be established that the maximum allowable prediction error is 5% mean absolute percentage

error (MAPE) is established for this research. [56] states that 5% MAPE is considered as an indication that the forecast is acceptably accurate. The MAPE is a measure of prediction accuracy of a forecasting method, and is mathematically presented by:

$$\text{MAPE} = \frac{100\%}{n} \sum_{t=1}^{n} \left| \frac{A_t - F_t}{A_t} \right| \tag{6.5}$$

where A_t is the actual value, F_t the predicted value and n the number of data samples. Below in Figure 6.3 the MAPE values are shown for an increasing prediction horizon. Note that the prediction horizon increases with steps of 3 seconds, according to the provided sampling time of the data. From this graph it can be seen 18 seconds is the maximum prediction interval of the horizon. Therefore, the prediction horizon of 18 seconds is used to compute the remaining results in this section for the linear regression method. Note that the values of the MAPE functions were achieved using varying values of Δ^-.

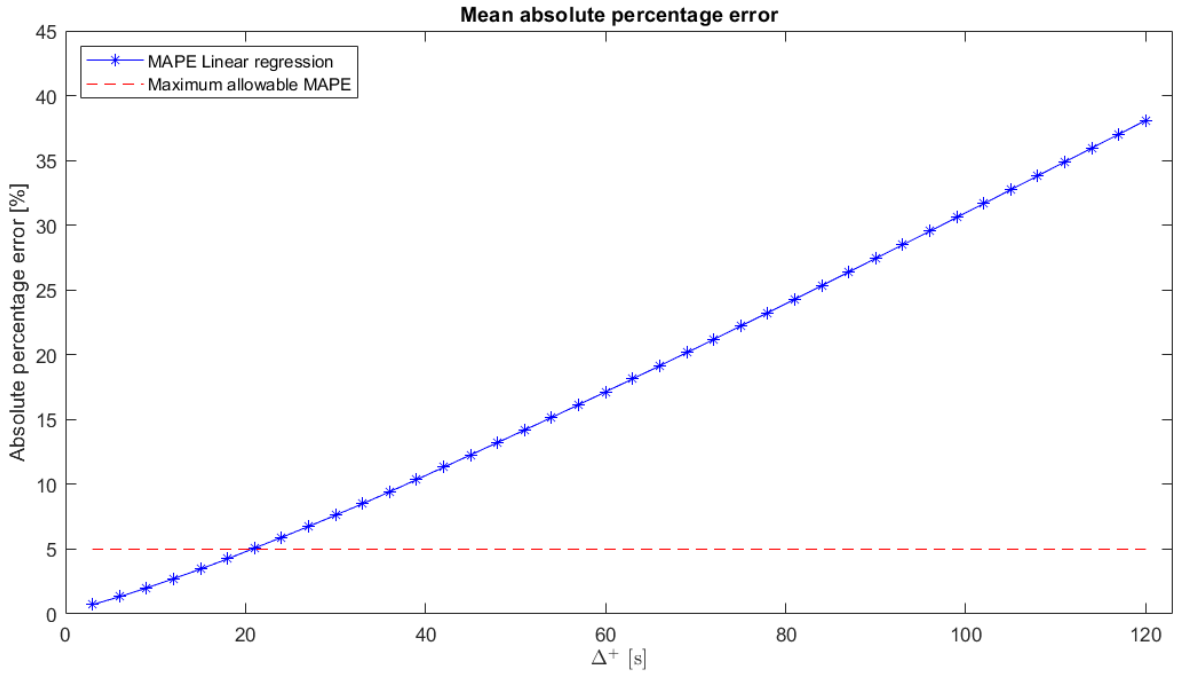

Figure 6.3: Mean absolute percentage error for the linear regression model.

Below in Table 6.2, the relationships between Δ^+ and Δ^- is shown. For an increasing horizon with Δ^+, various data ranges $[t - \Delta^-, t - 1]$ were evaluated; In order to find the optimal combination of prediction horizon and data sequence used to predict the prediction horizon. It can be noted from the table that using more data, thus a larger Δ^-, to make predictions does not lead to improved prediction accuracy for the linear regression method. This is likely because for more datapoints the data is less linear; thus a linear approximation of more datapoints leads to worse results. The optimal Δ^- is 9[s]. Therefore, the remaining results for the linear regression methods are computed with a combination of $\Delta^- = 9$ [s] and $\Delta^+ = 18$ [s].

Δ^- [s] \ Δ^+ [s]	3	6	15	30	60	90	120
9	0.72	2.00	3.46	7.70	17.59	28.38	39.75
15	0.86	2.07	3.52	7.62	17.14	27.44	38.41
30	1.44	2.72	4.16	8.25	17.53	27.45	38.09
90	4.40	5.85	7.38	11.48	20.43	30.03	39.66
180	8.93	10.40	11.92	15.88	24.23	32.82	41.43
360	16.97	18.36	19.77	23.39	30.95	38.79	46.75

Table 6.2: MAPE [%] of the linear regression model for different combinations of Δ^- and Δ^+.

In Figure 6.4, the distribution of actual shaft power, a scatter plot (actual versus predicted), and the relative frequency distribution of absolute errors is shown. As mentioned, the results are for $\Delta^+ = 18[s]$, with $\Delta^- = 9[s]$. The red line in the scatter-plot is the line that shows the correct prediction values for the actual values, which is a 45° angle line. As can be seen from the scatter-plot there is a tight grouping of predicted values around the line, indicating relatively accurate predictions. The relative frequency distribution of the absolute percentage errors also clearly indicates a high frequency of 'close-to-zero' errors rather than larger errors. The outliers, can be explained by the big jumps in the operating profile of the shaft power, as these can not be predicted accurately. For confidentiality the dimensionality of the data has been changed.

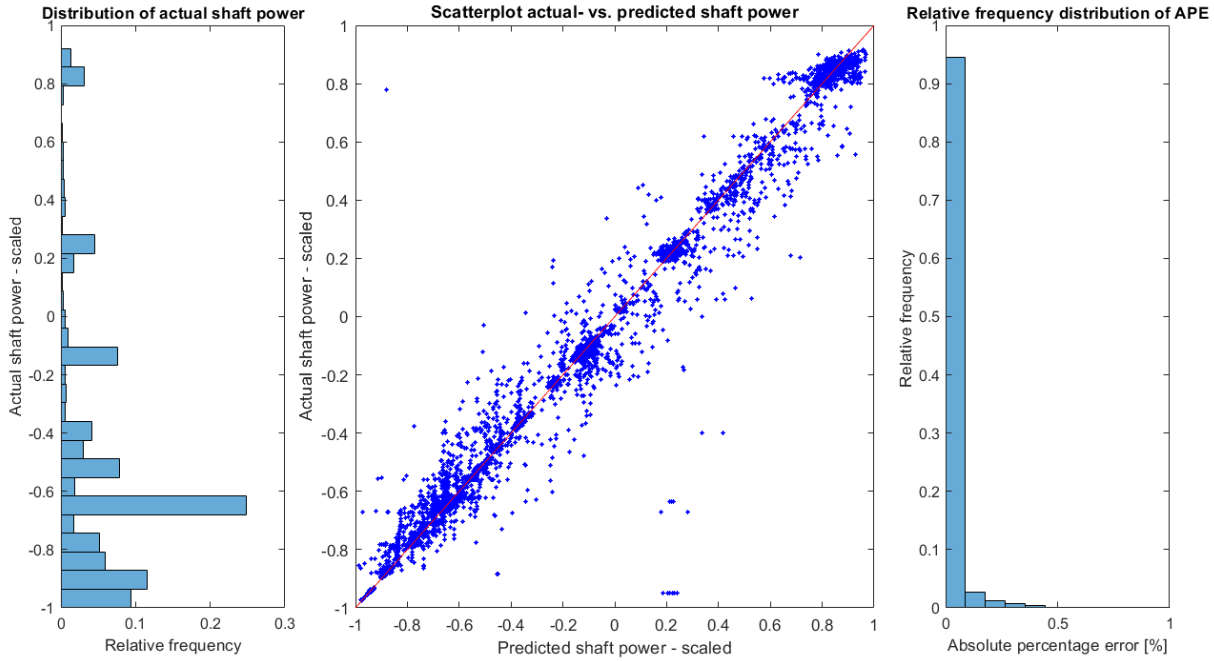

Figure 6.4: Distribution of actual shaft power, scatter plot (actual versus predicted), relative frequency distribution of AE. Results are for $\Delta^+ = 18[s]$, with $\Delta^- = 9[s]$. n = 19110 samples.

To further illustrate the predictive capabilities of the linear regression method a trend in time is shown in Figure 6.5. This graph shows that the trend in time of the actual shaft power can clearly be followed by the predicted shaft power 18 seconds in the future. It should be noted however, that the predicted shaft power shows relatively erratic behaviour compared to the actual shaft power. This can be explained by the fact that the predicted shaft power is merely a linear regression based on 3 data samples ($\Delta^- = 9$ [s]). This leads to an estimation of a slope fitting these 3 data samples, but not fitting to the larger trend in the shaft power. This is also the reason why the linear regression can not be used for medium-term predictions, in the order of minutes.

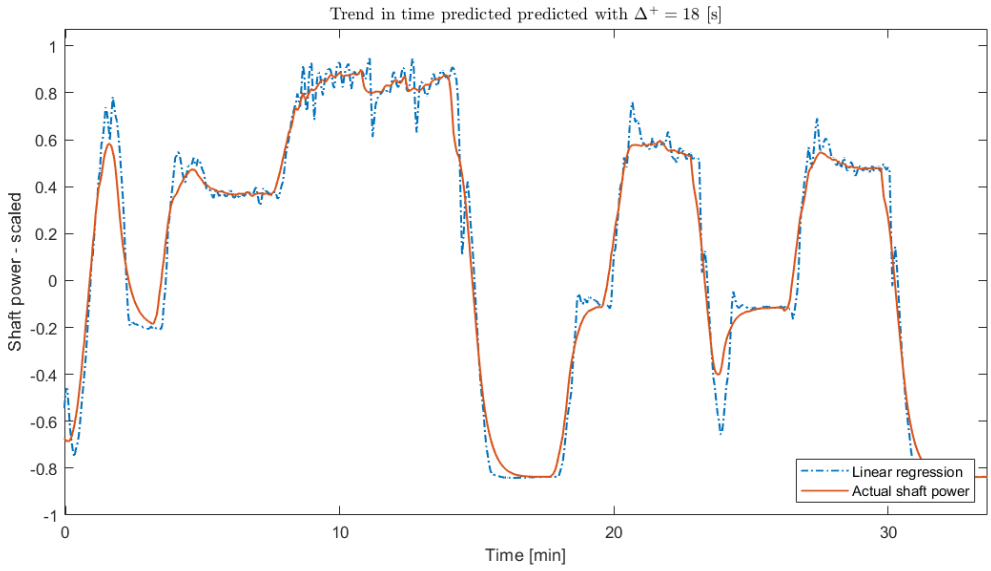

Figure 6.5: A section of the trend in time (actual versus predicted) shaft power. Results are for $\Delta^+ = 18[s]$, with $\Delta^- = 9[s]$.

Finally, the root mean squared error, mean absolute error and Mean absolute percentage error are noted for the combination of $\Delta^- = 9$ [s] and $\Delta^+ = 18$ [s]. The Mean Absolute Error (MAE) is a measure of errors between paired observations, in this case the actual and forecasted shaft power demand. Mathematically the MAE can be written as:

$$\mathrm{MAE} = \frac{\sum_{i=1}^{n} |A_t - F_t|}{n} \tag{6.6}$$

The MAE of 40.466 kW indicates that the average error between predicted and actual shaft power is 40.466 kW. Based on the fact that the maximum shaft power is 5400 kW, this can be considered a relatively small error. The root mean squared error (RMSE) is another measure showing the predictive accuracy of a method. It measures the average difference between values predicted by a model and the actual values. It can be mathematically described by:

$$\mathrm{RMSE} = \sqrt{\frac{\sum_{t=1}^{n} (A_t - F_t)^2}{n}} \tag{6.7}$$

RMSE [kW]	MAE [kW]	MAPE [%]
241.394	40.466 ± 3.370	4.251

Table 6.3: RMSE, MAE, and MAPE, for $\Delta^+ = 18$ [s], and $\Delta^- = 9$ [s].

6.3. Moving average

A rather simple model that can be used is the moving average or order m, mMA. The average value of the moving window time-series in range $[t - \Delta^-, t - 1]$ is computed using the following formula:

$$mMA = \frac{1}{m} \sum_{k=1}^{\Delta^-} y_{t-k}, \tag{6.8}$$

where is the number of samples in data range $[t - \Delta^-, t - 1]$. The mean value is used as the prediction for prediction horizon $[t, t + \Delta^+]$. The method is not very advanced, however, it can be used comparatively to other models to benchmark their performances.

6.3.1. Moving average results

Similarly to the linear regression the MAPE values have been presented graphically, in Figure 6.6. It can be seen that the maximum acceptable prediction horizon is where $\Delta^+ = 27$ [s].

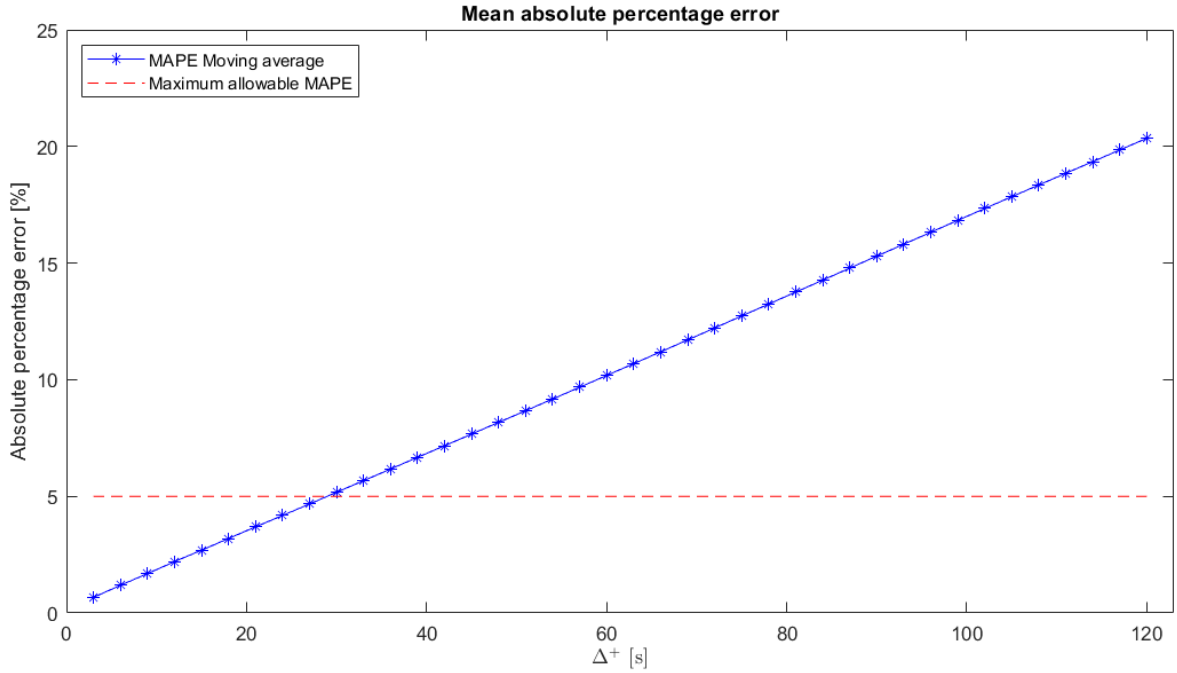

Figure 6.6: Mean absolute percentage error for the moving average.

Below in Table 6.4, the relationships between Δ^+ and Δ^- is shown. For an increasing horizon with Δ^+, various data ranges $[t - \Delta^-, t - 1]$ were evaluated; In order to find the optimal combination of prediction horizon and data sequence used to predict the prediction horizon. It can be noted from the table that using more data, thus a larger Δ^-, to make predictions does not lead to improved prediction accuracy for the moving average method. The optimal Δ^- is 3[s]. Therefore, the remaining results for the linear regression methods are computed with a combination of $\Delta^- = 3$ [s] and $\Delta^+ = 27$ [s].

Δ^- [s] \ Δ^+ [s]	3	6	15	30	60	90	120
3	0.67	1.69	2.69	5.17	10.18	15.30	20.35
9	1.15	2.17	3.17	5.65	10.67	15.79	20.83
15	1.64	2.65	3.65	6.14	11.17	16.29	21.31
30	2.87	3.86	4.86	7.36	12.41	17.52	22.49
90	7.77	8.76	9.76	12.27	17.30	22.25	27.04
180	15.08	16.05	17.02	19.44	24.20	28.74	33.01
360	27.65	28.46	29.28	31.29	35.20	38.94	42.50

Table 6.4: MAPE [%] of the moving average model for different combinations of Δ^- and Δ^+.

Note that $\Delta^- = 3$[s] indicates that a single datapoint is used for the average. Which means that for this optimal solution the value of shaft power at $t - 3$[s] is said to be the prediction value for all steps in prediction horizon $[t, t + 27]$[s]. This is nicely shown in Figure 6.7, which shows a section of the trend in time of the actual shaft power versus the predicted shaft power 27 seconds in the future. It can be seen that the graph is simply shifted 27 seconds. But these 'predictions' are still enough to stay under the 5% MAPE limit.

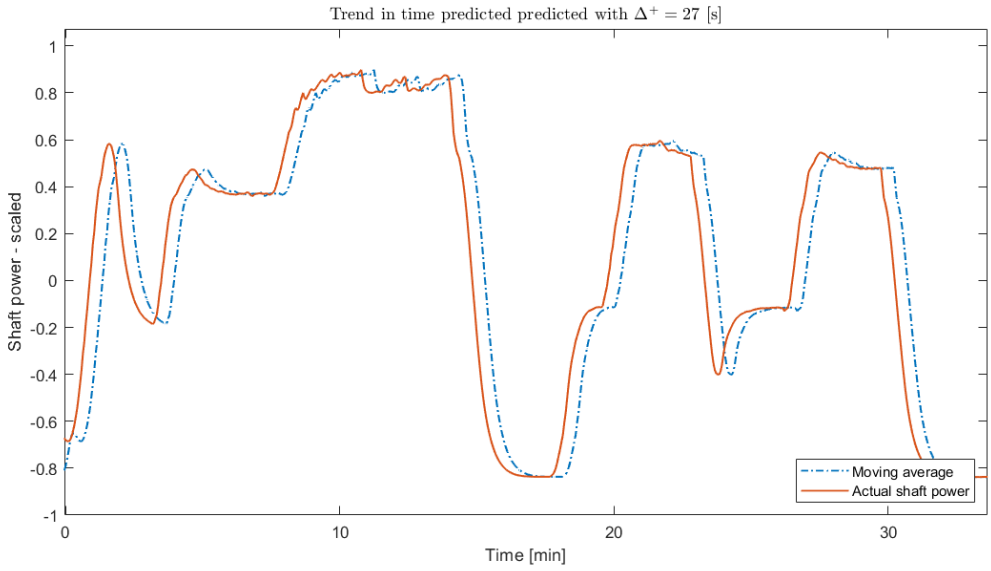

Figure 6.7: A section of the trend in time (actual versus predicted) shaft power. Results are for $\Delta^+ = 27[s]$, with $\Delta^- = 3[s]$.

Below, in Figure 6.8, the distribution of actual shaft power, a scatter plot (actual versus predicted), and the relative frequency distribution of the absolute errors are shown. Results are for $\Delta^+ = 27[s]$, with $\Delta^- = 3[s]$. From the scatter-plot it is clear that predictions show a wider spread than those of the linear regression method. However, more data samples are closely grouped to the diagonal, indicating an overall strong predictive accuracy. Again, the relative frequency distribution of the absolute percentage errors show that most error are close to zero.

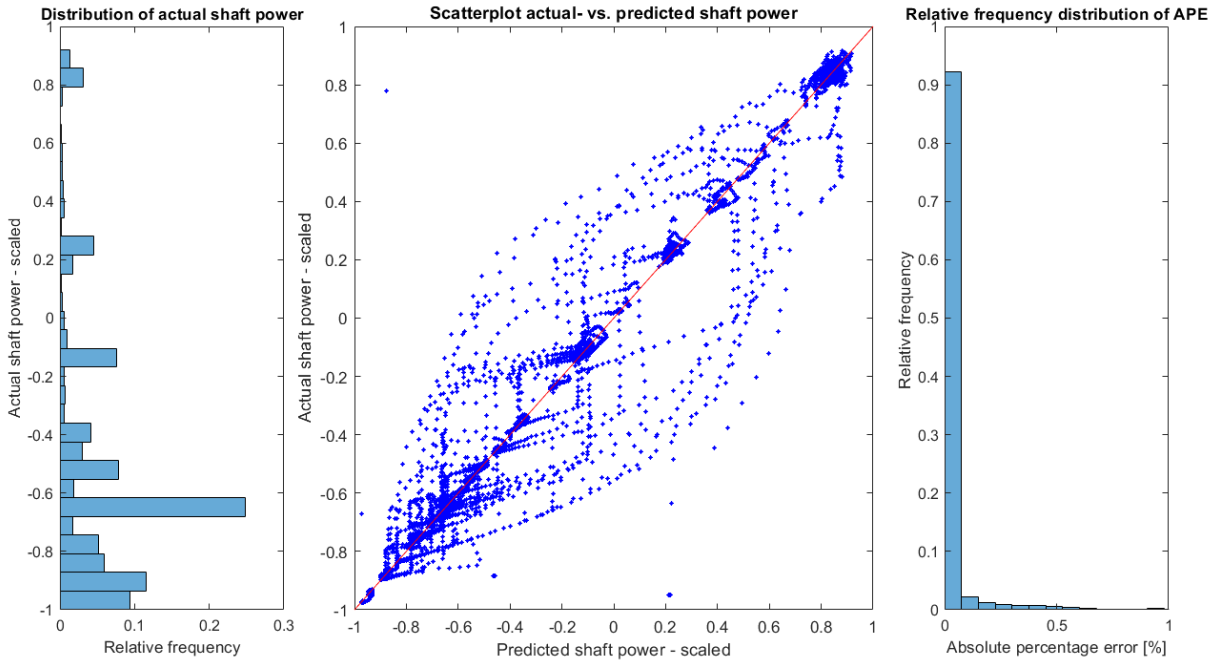

Figure 6.8: Distribution of actual shaft power, scatter plot (actual versus predicted), and relative frequency distribution of AE. Results are for $\Delta^+ = 27[s]$, with $\Delta^- = 3[s]$.n = 19110 samples.

Finally, the RMSE, MAE and MAPE values are shown for the combination of $\Delta^- = 3$ [s] and $\Delta^+ = 27$ [s], for the moving average method. A MAE of 54.608 kW is an acceptable error compared to the

maximum shaft power demand of 5400 kW. And as indicated earlier a MAPE value under 5% is also acceptable.

RMSE	MAE	MAPE
228.842	54.608 ± 2.345	4.673

Table 6.5: RMSE [kW], MAE [kW],and MAPE [%] for $\Delta^+ = 27[s]$, and $\Delta^- = 3[s]$.

6.4. ARIMA

In order to improve on the performance of a simple moving average, and linear regression, a method is employed that can use polynomial regression, namely the Auto-Regressive Integrated Moving Average (ARIMA) model will be used. ARIMA models are one of the most widely used approaches to time series forecasting [40]. ARIMA models aim to describe the auto-correlations in the data. Therefore, it is an appropriate choice for univariate load predictions. ARIMA models combine the use of an auto-regression model with a moving average model. In this section the full procedure to applying the ARIMA model is explained. Throughout the section at each step, a example is shown of the application of the step on one of the operational profiles presented in Figure 3.3. Towards the ends of the section an overview of the full method is graphically shown for reader convenience.

6.4.1. Auto-regression model

In a regression model the variable of interest is forecasted using a linear combination of predictors. In an auto-regression model, the variable of interest is forecasted using a linear combination of past values of the variable. In this case, the shaft power is predicted based on past values of the shaft power. The auto-regressive part of the ARIMA model of order p can be written as

$$y_t = c + \phi_1 y_{t-1} + \phi_2 y_{t-2} + \cdots + \phi_p y_{t-p} + \varepsilon_t, \tag{6.9}$$

where ε_t is the white noise, y_t the shaft power at time t, and $\phi_i, i \in [1, p]$ are parameters at time $t-i$ that are fitted in order to obtain an accurate prediction. Some constraints on the fitting parameters of the auto-regressive model apply. These constraints aim to prevent the polynomial from diverging to infinity or minus infinity. Based on the order p of the auto-regressive model these constraints get increasingly complex, these exact constraints will not be discussed here. Auto-regressive models are normally restricted to stationary data [40], the implications of this will be explained later.

6.4.2. Moving average model

The second ingredient to an ARIMA model is the moving average model. In this case the moving average is applied to the forecasting errors ε_t, where the error is assumed to be white noise. The moving average model of order q is described as:

$$y_t = c + \varepsilon_t + \theta_1 \varepsilon_{t-1} + \theta_2 \varepsilon_{t-2} + \cdots + \theta_q \varepsilon_{t-q}, \tag{6.10}$$

where y_t is a weighted moving average of of the past forecasting errors, and $\theta_i, i \in [1, q]$ are parameters at time $t-i$ that are fitted in order to obtain an accurate relationship between errors and output. Similarly to ϕ_i, θ_i are subject to constraints that get increasingly complex for increasing q. The constraints' purpose is to prevent the model from diverging.

6.4.3. Differencing

As mentioned previously, the ARIMA model requires a stationary time series to make predictions. From the operational profiles in Figure 3.3 it is clear that the shaft power operational profile is not a stationary time series. To transform the operational profile into a stationary time series we can apply the process of differencing. Differencing is the computation of the differences between consecutive observations. Mathematically, this can be written as:

$$y'_t = y_t - y_{t-1} \tag{6.11}$$

As an example the results to differencing operational profile 1 can be viewed in Figure 6.9. Differencing once ($d = 1$) may not be enough for certain time series, in those cases the data may be differenced multiple times until the time series is stationary. Since it not always obvious whether a series is stationary by view, unit root tests can be applied. Unit root tests are statistical hypothesis tests that test the stationarity of the time series, and are designed to ascertain whether differencing is required. Two commonly applied tests are the Kwiatkowski-Phillips-Schmidt-Shin (KPSS) test [57], and the augmented Dickey-Fuller (ADF) test [58]. The KPSS test assesses the null hypothesis that a univariate time series is stationary. The test employs a model with structure

$$y_t = c_t + \delta t + u_{1t}, \tag{6.12}$$

$$c_t = c_{t-1} + u_{2t}, \tag{6.13}$$

where δ is the trend coefficient, u_{1t} is a stationary process and u_{2t} is an independent and identically distributed process with mean 0 and variance σ^2. The null hypothesis is that $H_0 : \sigma^2 = 0$, and the alternative hypothesis is that $H_1 : \sigma^2 > 0$. If the statistical test with significance α shows a p-value sufficiently large (e.g. p>0.05), then the null hypothesis can be rejected and the time series is not stationary. This test can be computed for y_t with respect to samples y_{t-i} in the past, where i is the number data points, or lags, in the past. An accepted or rejected KPSS test for a certain defined number of lags does not ensure the same result for an increased number of lags. Therefore, stationarity of the time series should be proven for n lags (data points) in the past. Stationarity of n lags is relevant to determine what the order of the auto-regressive function p, and order of the moving average q can be. Or alternatively, given a predefined maximum order p, q and d, stationarity should be proven for $n = p + d$ lags [40].

The ADF test for a unit root assesses the null hypothesis of a unit root with a model:

$$y_t = c + \delta t + \phi y_{t-1} + \beta_1 \Delta y_{t-1} + \ldots + \beta_p \Delta y_{t-p} + \varepsilon_t, \tag{6.14}$$

where δ is the deterministic trend coefficient, c is the drift coefficient, p the number of lagged difference terms, Δ is the differencing operator such that $\Delta y_t = y_t - y_{t-1}$, and ε_t white noise. The null hypothesis is $H_0 : \phi = 1$, and the alternative hypothesis $H_1 : \phi < 1$. If the statistical test with significance α shows a p-value sufficiently large (e.g. p>0.05), then the null hypothesis can be rejected and the time series is stationary. Similarly to the KPSS test, the ADF test should be repeated for different lags. The reason to use both the ADF and KPSS test is because they are complementary. The ADF test is common and nicely proves stationarity with the absence of a unit root, the KPSS test is variance based and can be insightful when the variance of the time series is varying.

Combining the auto-regressive model, moving average model and differenced time series ($d = 1$) the ARIMA(p,d,q) model can be described as

$$y'_t = c + \phi_1 y'_{t-1} + \cdots + \phi_p y'_{t-p} + \theta_1 \varepsilon_{t-1} + \cdots + \theta_q \varepsilon_{t-q} + \varepsilon_t, \tag{6.15}$$

where p is the order of the auto-regressive part, q is the order of the moving average part, and d the degree of differencing involved.

The example below provides some insights, shown in Figure 6.9.

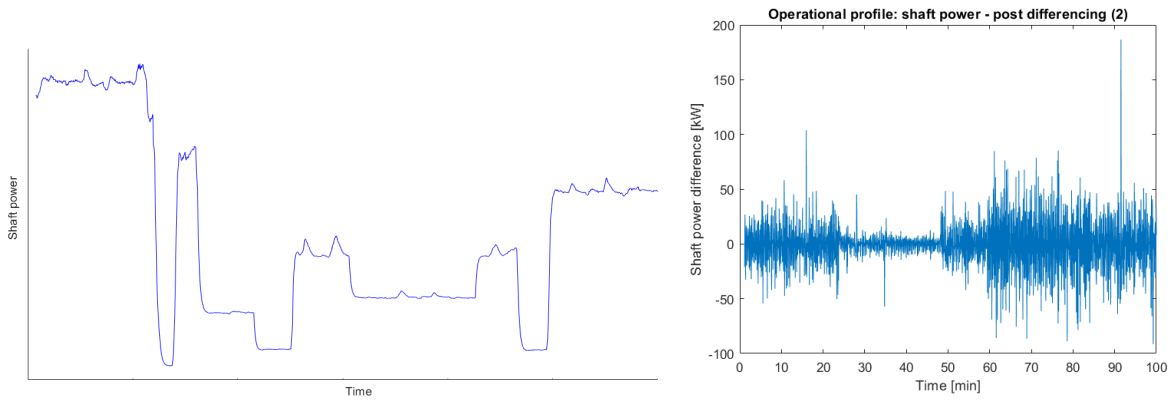

Figure 6.9: Original operational profile of the shaft power (left), and twice differenced operational profile of the shaft power (right).

The differenced time series looks stationary, but the KPSS and ADF tests show this is not the case. It passed the ADF test for lags $k \in [1, 10]$ but fails the KPSS test for lags $k \in [8, 10]$. Differencing the time series again results in successfully passing both stationarity tests for the 10 lags intervals. However, if the maximum order p to be used is smaller than 7, then differing once would be enough. since stationary of $n = p + d = 7 + 1 = 8$ lags was already proven after differencing once.

6.4.4. p, d, q tuning

It is often not immediately evident what the optimal settings of p, and q for the ARIMA(p,d,q) model are. However, this is an important task. The order of p, and q determines the goodness of fit of the ARIMA model with respect to the original data. Sometimes it is possible to determine the parameters by inspecting the auto-correlation function (ACF) and partial auto-correlation function (PACF). The ACF plot shows the auto-correlations which measure the relationship between y_t and y_{t-k} for different values of k. When two concurrent samples are correlated the next sample must also be correlated. For instance, if y_{t-2} and y_{t-3} are correlated, then y_{t-3} and y_{t-4} must also be correlated. This implies that y_{t-2} and y_{t-4} are also correlated, however it is uncertain whether this is because they are simply both correlated to y_{t-3}. It is important to make this distinction, since if y_{t-4} does not have a true correlation to y_{t-2} then it does not hold more information that would help in predicting y_{t-2}. The PACF overcomes this issue by filtering out these effects. Thus the PACF graphically shows the relationship between y_t and y_{t-k} after removing the effects of lags $[1, k-1]$.

Unfortunately, if both p and q are non-zero then the plots do not help in finding suitable values of p and q. If either p or q is zero then the ACF and PACF are useful. The data may follow an ARIMA(p,d,0) model if the ACF and PACF plots of the differenced data show the following patterns [40]: (a) the ACF is exponentially decaying or sinusoidal or (b) there is a significant spike at lag k in the PACF and none beyond lag k. The data may follow an ARIMA(0,d,q) with the following patterns [40]: (a) the PACF is exponentially decaying or sinusoidal or (b) there is a significant spike at lag k in the ACF and none beyond lag k. As an example the ACF and PACF are of the differenced operational profile 1 are shown in Figure 6.10.

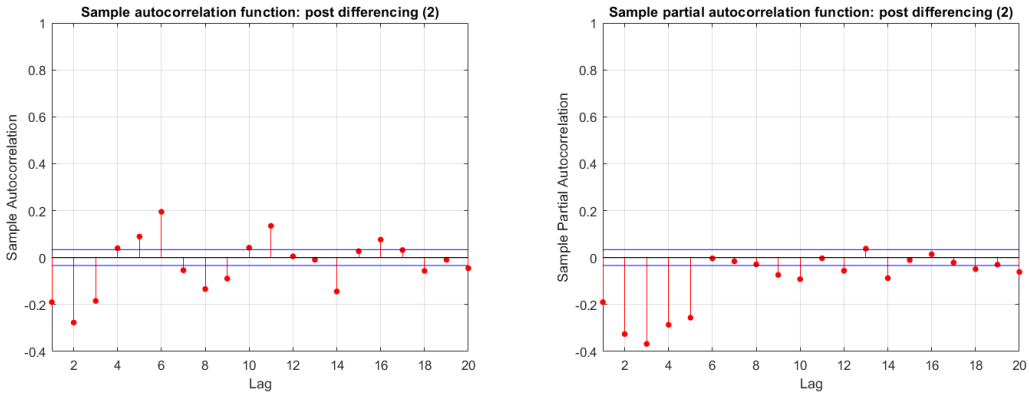

Figure 6.10: Auto-correlation function (left), and partial auto-correlation function (right) of the twice differenced time series.

Note that both the ACF and PACF show sinusoidal trends, and the PACF shows an exponential decay. However, there are no significant spikes followed by statistically insignificant spikes. Therefore, p and q can not be determined by inspecting the ACF and PACF. When that is the case one can test multiple combinations of p and q in order to determine the ARIMA(p,d,q) model that best fits the data. The data is fitted to the ARIMA model by estimating the model parameters c, $\phi_i, with \in [1, p]$ and $\theta_i, withi \in [1, q]$. This estimation happens through a maximum likelihood estimation (MLE). MLE estimates the parameters by maximizing a likelihood function so that, under an assumed statistical model, the observed data is most probable. For the purpose of this project, this process is considered a black box model, and is simply executed by a Matlab function.

For each combination of p, d, and q a model should be fitted to the data, evaluated and compared. The evaluation of the fit of an ARIMA model to the data can be done with Akaike's Information Criterion (AIC) [59]:

$$AIC = -2log(L) + 2(p + q + k + 1), \tag{6.16}$$

where L is likelihood of the data, k is a parameter that is equal to 1 when $c \neq 0$ and 0 and when $c = 0$. Note that the second part of the function evaluated the complexity of the model. Since a lower AIC value is considered better, a complex model is penalized. Alternative evaluation methods such as adjusted R-squared $\bar{R}^2$, BIC, and AICc can be considered as well. [40] states that $\bar{R}^2$ tends to favour overly complex models (high p and q), and BIC tends to work particularly well when there is a true underlying model. Since the shaft power is randomly effected by mariner decisions, a true underlying model does not exist. AICc is an adjusted version of the AIC model; AIC can be considered a first-order model that evaluated information loss, and AICc a second-order model. [40] states that AICc often outperforms the AIC, as it gives a more refined representation of fit. Therefore, the AICc criterion will be selected as evaluative parameter for selecting the optimal ARIMA(p,d,q) model. The AICc model is as follows:

$$AICc = AIC + \frac{2(p + q + k + 1)(p + q + k + 2)}{T - p - q - k - 2} \tag{6.17}$$

To complete the example, an ARIMA(p,d,q) model has been selected using the above procedure. With $p \in [0, 8]$ and $q \in [0, 8]$, and $d = 2$. The ARIMA(6,2,7) model showed the lowest AICc value and therefore shows the best fit to the differenced data.

6.4.5. Model residuals

The final step before making forecasts with the ARIMA model, is to inspect the model residuals. It is important to check that all auto-correlations in the ACF are within the threshold limits. When this is the case, it means that the residuals are behaving like white noise, which was one of the assumptions for using the ARIMA model. If the residuals are not within the threshold limit it proves that there are statistically significant correlated errors, and this implies that not all the relevant relationships between data samples have been captured in the model. Secondly, the residuals should be normally distributed, which was another assumption for using the ARIMA model.

To prove that the residuals behave like white noise a statistical test can be performed: The Ljung-box test. It tests whether any of a group of auto-correlations of a time series are different from zero. The null hypothesis specifies that the data is independently distributed. The alternate hypothesis specifies that the data shows serial correlation.

For the example of operational profile 1, the Ljung-box test shows a p-value of $p = 0.0153$. The p-value is smaller than 0.05 indicating that the residuals behave like white noise. This is further supported by the ACF graph that shows the auto-correlations of most of the residuals are statistically not significant, since they fall within the threshold limits. The residuals are normally distributed also. The ACF, and distribution or the residuals are shown in Figure 6.11. Since the model passed these tests it can be assumed to be ready to make predictions.

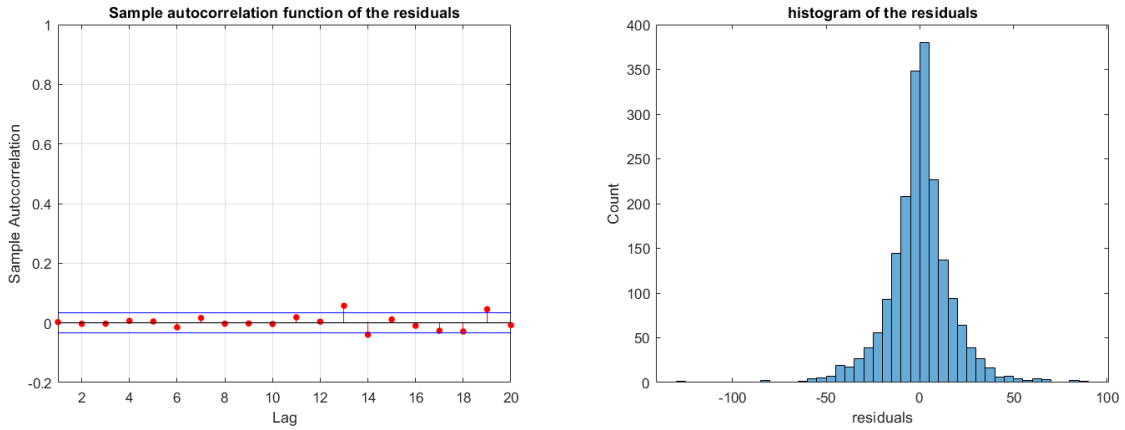

Figure 6.11: Residual plots for the ARIMA(6,2,7) model.

6.4.6. Forecasting

Point forecasts can be obtained by rewriting the ARIMA model equation, Equation 6.15, to [40]:

$$y_t = (1+\hat{\phi}_1)\,y_{t-1} - (\hat{\phi}_1 - \hat{\phi}_2)\,y_{t-2} - \cdots - (\hat{\phi}_{p-1} - \hat{\phi}_p)\,y_{t-p} - \hat{\phi}_p y_{t-p-1} + \hat{\theta}_1 \varepsilon_{t-1} + \cdots + \hat{\theta}_q \varepsilon_{t-q} + \varepsilon_t. \quad (6.18)$$

where $\hat{\phi}_i, i \in [1,p]$, and $\hat{\theta}_i, i \in [1,q]$ are fitted parameters obtained in the model training and selection phase previously. Note that the remaining values on the right-hand side of the equation are also known; $y_{t-i}, i \in [1,p+1]$ are known historical values, and $\varepsilon_{t-i}, i \in [1,q]$ are known residuals of fitting y_{t-i} to the trained ARIMA model. The only value not known is ε_t, since this is the error of fitting y_t to the ARIMA model. Which is the timestep we are forecasting. Therefore, $\varepsilon_t = 0$ is assumed in the model. The right-hand side of the formula can be filled in and y_t can be computed. To predict y_{t+1}, Equation 6.18 can be rewritten where t is replaced with $t+1$. This results in a term of y_t in the right-hand side of the function, this one can be replaced by the previously calculated predicted value of $\hat{y}_t$. Mathematically, this becomes clear:

$$y_{t+1} = (1+\hat{\phi}_1)\,\hat{y}_t - (\hat{\phi}_1 - \hat{\phi}_2)\,y_{t-1} - \cdots - (\hat{\phi}_{p-1} - \hat{\phi}_p)\,y_{t-p+1} - \hat{\phi}_p y_{t-p} + \hat{\theta}_1 \varepsilon_t + \cdots + \hat{\theta}_q \varepsilon_{t-q+1} + \varepsilon_{t+1}. \quad (6.19)$$

Note that values of both ε_{t+1} and ε_t are not known, and have to be replaced by 0. Thus, the moving average part of the ARIMA model has a depreciating influence on the outcome of long term predictions. It should be clear from the equations that any number of point forecasts can be obtained by continually shifting the time parameter t. It should be noted that the above equations are derived based on differencing the data once. With higher order differencing come more complex multipliers on the past samples of y_t, and more complex constraints. These equations will not be discussed here. What one can learn from the equations is that $p+d$ samples of past values are used in evaluating the variable on the left-hand side of the equation. Therefore, it stands to reason that stationarity of up to $p+d$ lags should be proven with the unit root tests, as was already incidated earlier.

6.4.7. Modelling procedure

An overview of the modelling procedure for an ARIMA model is shown in Figure 6.12. The complete procedure is listed on the left side of the figure. It is a summary of the previous sections of this report.

To use the ARIMA model in conjunction with an online optimization-based controller, an ARIMA model should be selected every timestep. Therefore, the luxury of graphically inspecting the time-series for stationarity, and the correlations in the ACF and PACF are not feasible. Instead, an ARIMA model is created every timestep based on a moving window of time-series data of the shaft power. This sequence of data can be defined as time range $[t - \Delta -, t - 1]$. For this sequence of data the unit root tests KPSS and ADF are calculated for lags in range $k \in [1, 4]$. If the tests show the data to be non-stationary, the data is differenced until the tests are passed. Only 4 lags are considered since this is the range applied to the p and q is [0,3]. The reason for this range is that evaluating more elaborate models is time consuming and not feasible for an online process. Secondly, higher order p and q models often have diminishing returns. They are more likely to be a good fit for the data, but that does not guarantee improved forecasting abilities [40].

Once the data is stationary candidate models are defined. The optimal model is selected by evaluating the goodness of fit of the models with the AICc criteria. Unfortunately, due to the automation of the process, stationarity can never be truly ensured. Therefore, a try and catch approach is required. If a model under evaluation diverges and causes an error it can be caught and eliminated. The fact that it diverges also means it was not a good fit. That being the case, the fact that the model is not further evaluated does not mean a feasible model was eliminated. Once an optimal model is selected, a Ljung-box test is performed on the residuals. If the test shows the residuals to be correlated a forecast is still performed. This does mean, however, that the model did not fully capture all the relevant information at all lags, which is to be expected with lower p and q values. It also implies that the assumption of the ARIMA model that the error term is white noise is not adhered to. In practise, when this test is not passed the forecasting method for the timestep could be replaced by one of the previously discussed prediction methods of simple linear regression, polynomial regression or moving average. But for the purpose of this project, where the effectiveness of the prediction tool is estimated, this will not be implemented. The automated procedure of ARIMA modelling is presented below in Figure 6.12. The process is repeated at every timestep.

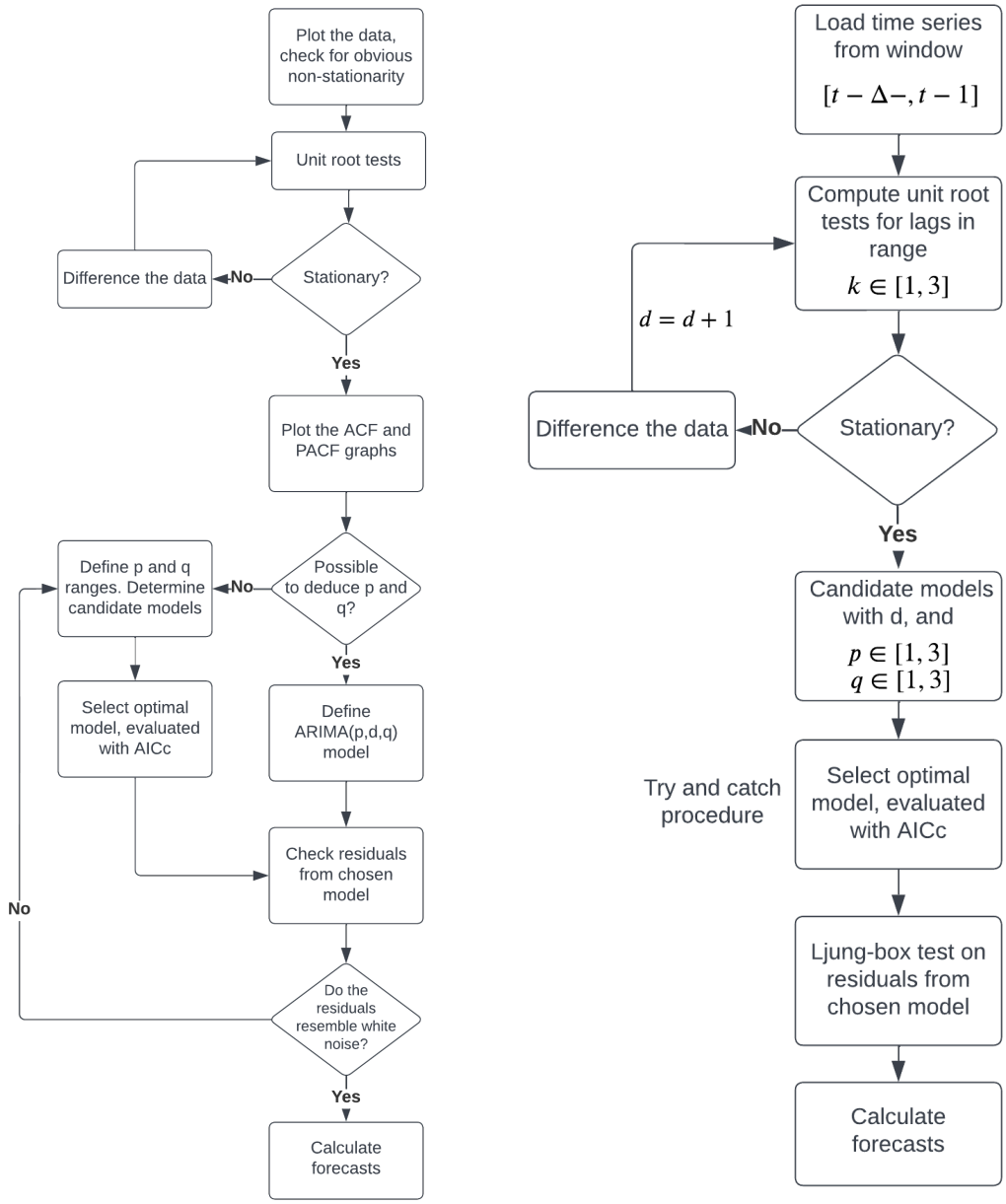

Figure 6.12: Modelling procedure for an ARIMA model (left). Automated modelling procedure for an ARIMA model (right).

6.4.8. ARIMA Results

Similarly to the linear regression and moving average methods the first result to be shown is Figure 6.13, which shows the MAPE values for the ARIMA method for an increasing prediction horizon. Unfortunately, the method does not perform great, and is only able to predict 3 seconds in the future. This is a direct result from divergence of the polynomials that occur sometimes. These divergent prediction show very high or very low prediction values and have a large influence of the mean of the absolute percentage errors.

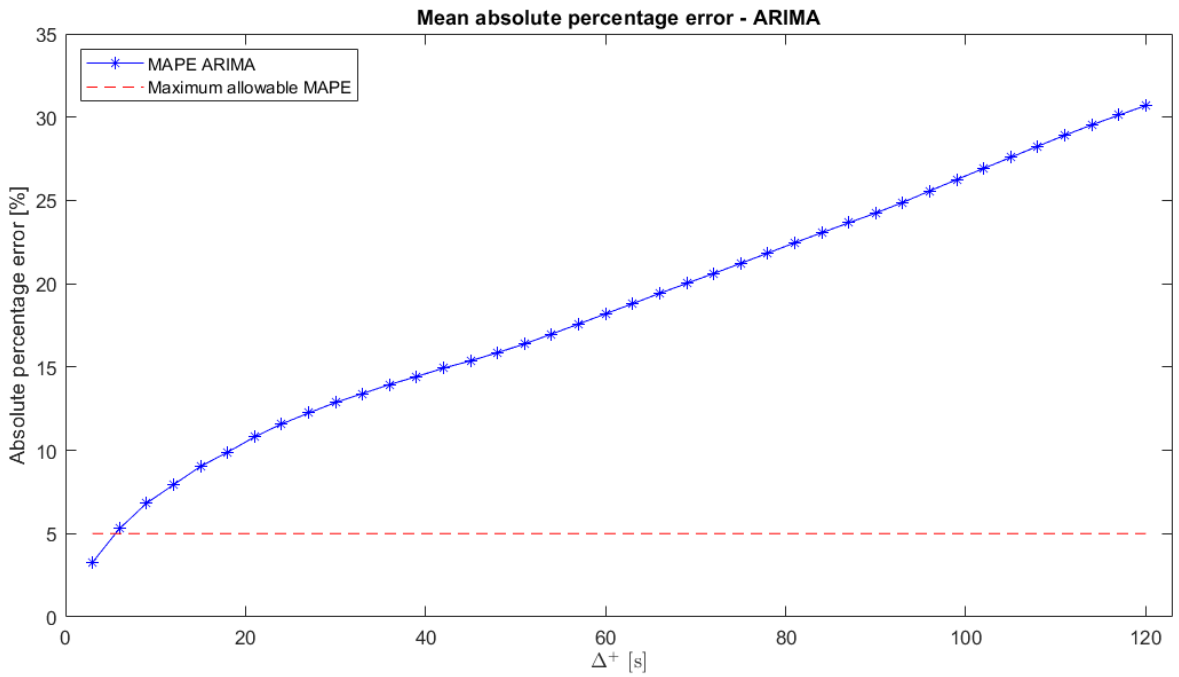

Figure 6.13: Mean absolute percentage error for the ARIMA model.

This effect of diverging predictions is nicely shown in Figure 6.14. Which shows the trend in time for the actual and predicted shaft power for 3 seconds in the future. As can be seen, even for a prediction horizon of 3 seconds there are large outliers.

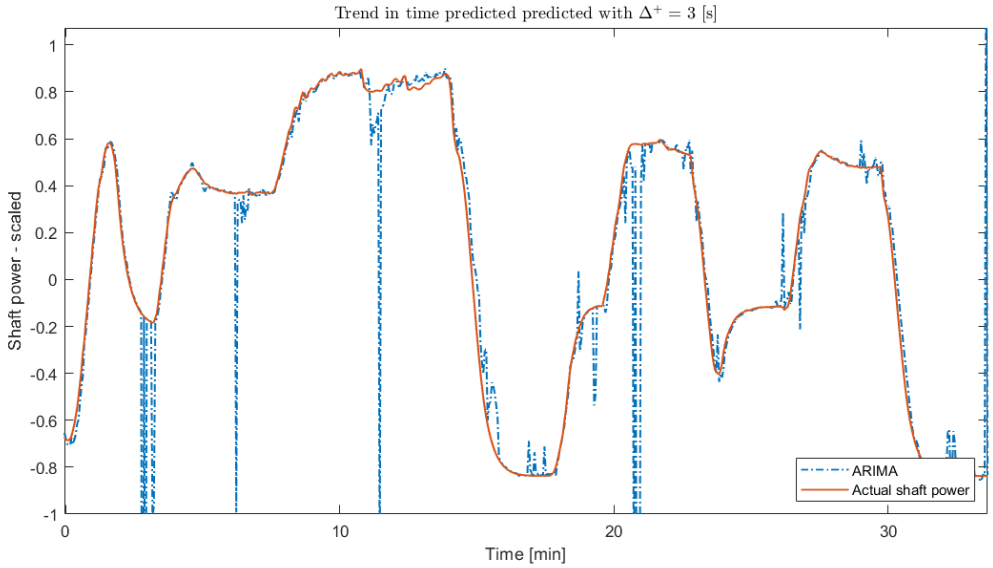

Figure 6.14: A section of the trend in time (actual versus predicted) shaft power. Results are for $\Delta^+ = 3[s]$, with $\Delta^- = 180[s]$.

In Figure 6.15 the distribution of actual shaft power, a scatter-plot (actual versus predicted), and the relative frequency distribution of the absolute errors is shown. The predicted values lie close to the actual values, as can be seen in the scatter-plot. However, larger outliers can be noticed as well. Note that the sample size for this plot is 2401 samples. Whereas, for the linear regression and moving average the sample size was 19110 samples. Due to computational times, fewer samples for the ARIMA method were used. This does have the effect that the outliers have a larger contributing factor

to the mean errors. The relative frequency distribution of the absolute percentage errors shows that predominantly close-to-zero errors occur.

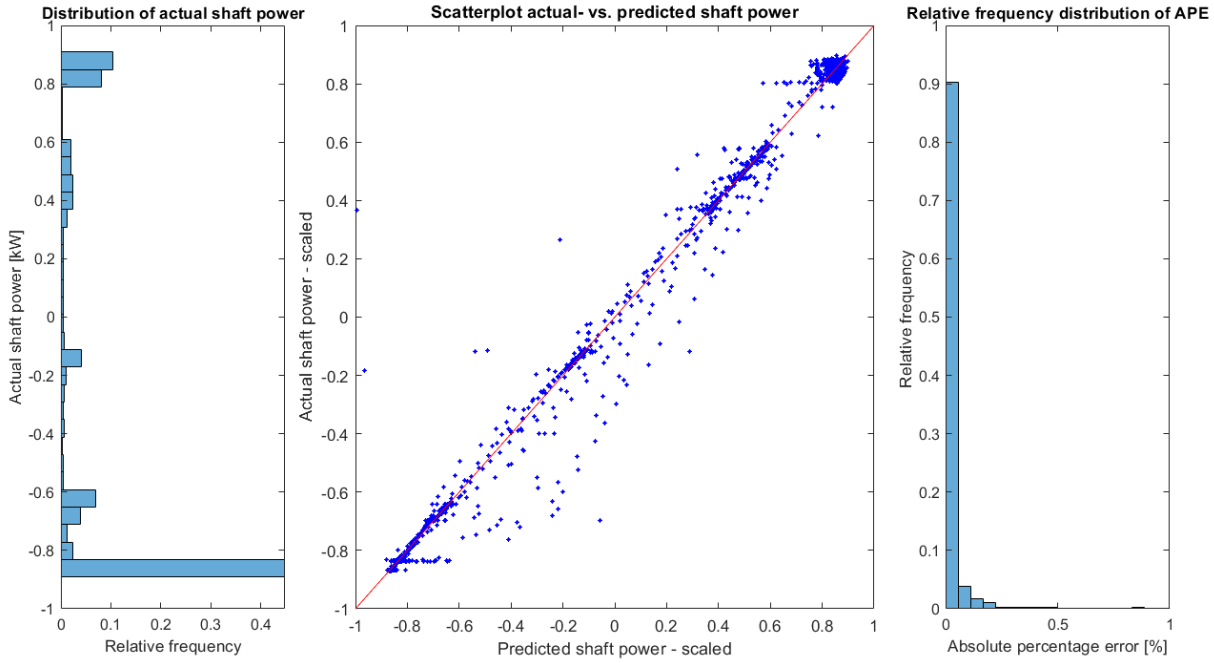

Figure 6.15: Distribution of actual shaft power, scatter plot (actual versus predicted), and relative frequency distribution of AE. Results are for $\Delta^+ = 3[s]$, with $\Delta^- = 180[s]$.n = 2401 samples.

The RMSE, MAE and MAPE of the ARIMA model are shown in Table 6.6. It can be noted that even though the MAPE value is lower than for the linear regression and moving average, the prediction horizon is only 3 seconds. Additionally, the MAE is larger, namely 72 kW, and shows a much larger confidence interval. This indicates the prediction have a larger spread around the mean. Which is not favorable for prediction purposes.

RMSE	MAE	MAPE
268.944	72.073 ± 11.365	3.276

Table 6.6: RMSE [kW], MAE [kW],and MAPE [%] for $\Delta^+ = 3[s]$, and $\Delta^- = 3[s]$.

6.5. Synthetic data

In order to improve on the performance of univariate forecasting methods, some synthetic data is generated. The powertrain model described in chapter 5, in conjunction with controllers for the main engines, induction machines, diesel generators and the operational profiles described in Figure 3.3, are used to generate the data. The control design is directly taken from [11], and graphically shown below in Figure 6.16.

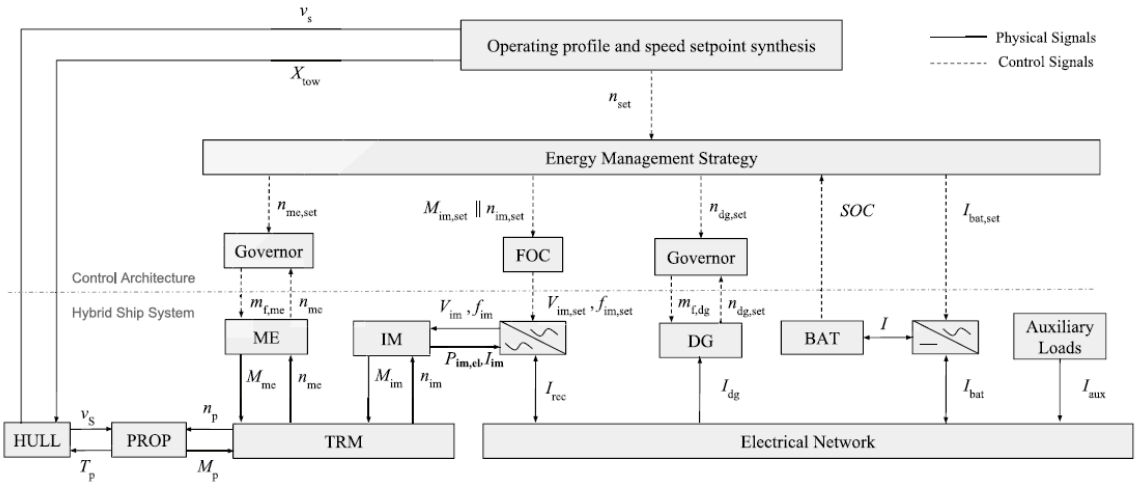

Figure 6.16: Schematic presentation & causality graph of the simulation model (propulsion and control system) showing coupling between models. Image retrieved from [11]

Where TRM is the transmission, FOC is field oriented control, and the governor is a control unit. For a full description and understanding the interested reader is referred to [11]. The model is supplied by Damen, and was appended slightly in order to adjust for the power ratings of the powertrain components of the HCOPV.

The input data to the model is the operational profile of shaft power, as well as the operational profile of vessel speed. The recorded data features are listed below in Table 6.7. These data features are used as input to the RNN, along with historical data on the shaft power.

X	Data description
x_{12}	Main engine shaft speed in [rpm]
x_{13}	Pitch ratio
x_{14}	Propeller torque M_p in [Nm]
x_{15}	Propeller thrust T_p in [N]
x_{16}	Vessel speed v_s in [knots]

Table 6.7: Generated data features.

More information can be extracted from the model on the battery and induction machines. However, their behaviour is directly a result of the energy management system. Therefore, the predictive potency of these features are contingent on if the power load forecasting model would be used in conjunction with this particular EMS again. Since, the EMS used in generating the data is not the same as the one developed in the project, these features are left out.

6.6. Recurrent neural networks

In this section the approach to the RNN design is elaborated. In Figure 6.17 a flow diagram is presented showing the various steps involved in data preparation, employing an RNN, as well as processing results. An explanation of all the steps involved is given in subsequent sections. Recurrent neural networks builds on top of the basic functionality of an artificial neural network (ANN). Therefore, first the theory behind ANNs is elaborated followed by the theory on RNNs. The hyperparameters and their impact on model performance is discussed also. Furthermore, the choices of the set-up of the RNN for this project have been justified and explained.

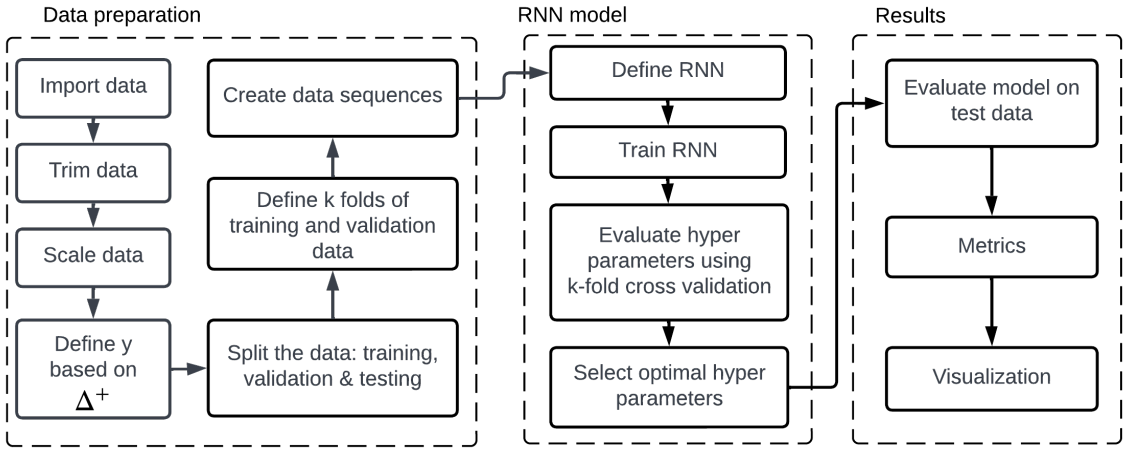

Figure 6.17: Flow diagram of the steps involved in data preparation, employing an RNN, as well as processing results.

6.6.1. Data Preparation

The data cleaning process has already been discussed previously, and will not be restated here. This was the process of removing outliers, selecting data features and handling missing data. The remaining data preparation steps for the RNN are data scaling, defining output y, data splitting, k-fold cross validation and data sequencing.

The reason to split the data and use k-fold cross validation is that, unlike the univariate methods that obtain a new model for each data sequence, the RNN aims to obtain a generalized model that is trained, and then can be used for all future prediction operations. Therefore, for the RNN it is imperative that the right model is obtained with the most optimal settings and correct indicated performance. The validation and testing data in combination with the cross validation method ensure that the trained model, is judged accurately on unseen data. The univariate methods do not have a single set of model setting that are used for all future prediction operations. Rather, these methods obtain new model parameters every timestep. For that reason the methods have different approaches.

The data on which the RNN is tested is the latter 10% of the data. The other methods have been tested on the full dataset. Consistency between results can be assumed because the latter 10% of the data still gives a good overview of the data as it shows a wide range of shaft power values, and variability in the data. The full dataset is used for the other methods, since more data sequences lead to better model performance estimation.

Data scaling The data of the various data attributes have different orders of magnitudes, in order for the neural networks to learn and understand the problem more easily, all attributes are scaled down to a specific range. The range is determined by the activation function used in the neural network. The choice of activation function and its implications is normally a hyperparameter that will be explained later, in subsection 6.6.2. The activation functions considered for neural networks in this project are the sigmoid and hyperbolic tangent activation functions, they have data scaling ranges of [0,1] and [-1,1], respectively.

Defining output y The aim of the neural networks is to predict the shaft power demand P_{sh} in range $[t,\ t + \Delta^+]$. The RNN uses a sequence of data, namely data points in the range $[t - \Delta^-,\ t - 1]$, as input. These input-output relations are graphically presented in Figure 6.18. Where the input space $\mathbb{X}_{\mathbb{1}}$ is presented by the data features shown in Table 6.7.

Splitting the data The next data preparation step is to split the data in training, validation and testing data. The latter 10% of the data is set aside for testing. The remaining 90% is used for training and validation. It is important to grab the latter sections of the data for testing, to ensure the neural network is not trained with data from the future and tested on data in the past.

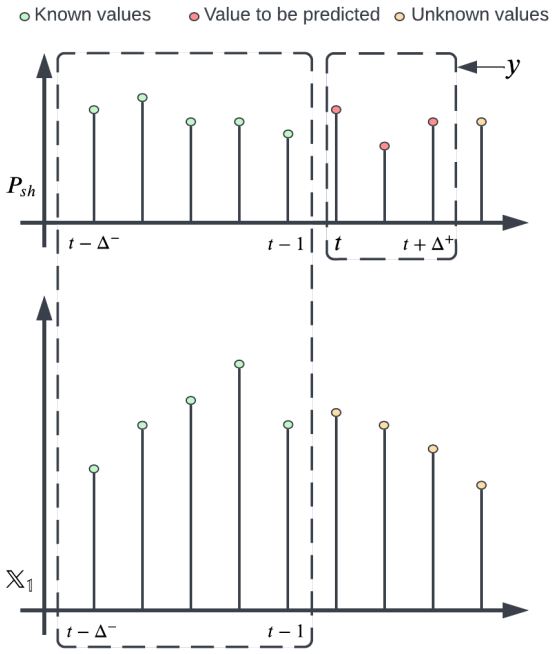

Figure 6.18: Input-output relationship for the RNN.

K-fold cross validation K-fold cross-validation is used for model validation, and allows for more accurate model selection. The aim of cross-validation is to test the model's true ability of predicting y, given input vector X, using unseen data. Multiple folds are used in order to improve the robustness of cross-validation in judging the models' ability. Since the RNN deals with time-series predictions it is important to retain a time continuity, namely the data used for validation cannot be prior to the data used to train the model in time. Therefore, for each fold the amount of training data available decreases. This is graphically presented in Figure 6.19.

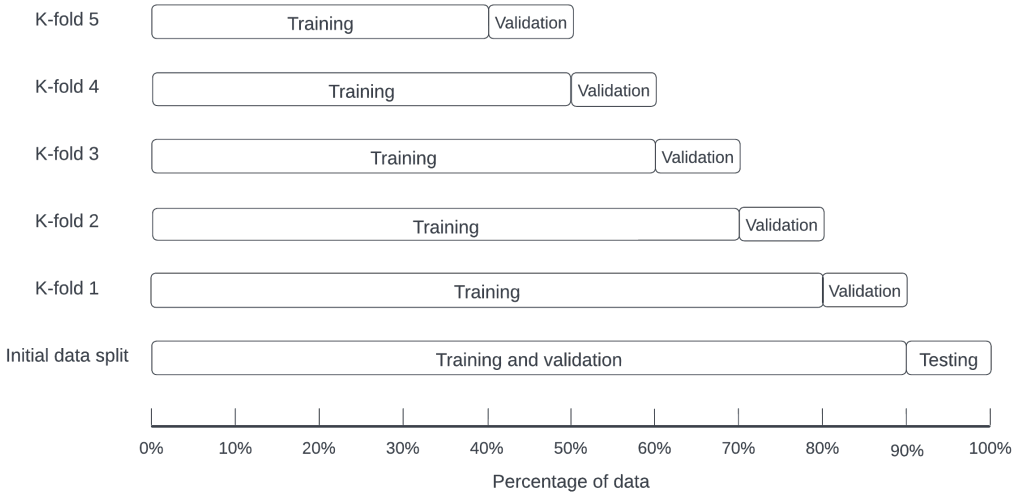

Figure 6.19: Data splitting and k-fold cross validation for the RNN, where $k = 5$.

Data sequencing As previously explained, the RNN takes sequences of data as input, where each sequence has data points in the range $[t - \Delta^{-}, t - 1]$, with a different t for different sequences. These sequences can be constituted after the k-folds have been defined and the time continuity has been ensured. Once the sequences are created they are shuffled.

6.6.2. Artificial neural network

Artificial neural networks (ANN), are supervised learning systems that aim to learn regression or classification tasks. An ANN includes an input layer, hidden layer and output layer. The layers are connected via nodes, the connections between the nodes and the nodes themselves make up the neural network. The nodes in an ANN are also called neurons. The input layer of the ANN, for this particular application, has 6 input neurons with the various data attributes of the input data $\mathbb{X}_{\mathbb{1}}$ and the past values of the shaft power. These 6 neurons are densely connected to *n* neurons in the hidden layer. The value of a hidden layer neuron, h_i, is calculated as follows:

$$h_i = \psi((\sum_{j=1}^{6} w_{i,j} X_j) + b_i), \tag{6.20}$$

where ψ is the activation function on the hidden layer, $w_{i,j}$ is the weight on the connection between input node j, and hidden node i, and b_i is the bias on node i. Predicted output $\hat{y}$ can be computed with:

$$\hat{y}_t = \Psi((\sum_{i=1}^{n} w_{y,i} h_i) + b_y), \tag{6.21}$$

where Ψ is the activation function on the output layer, and $w_{y,i}$ is the weight on the connection between hidden neuron i and output y, and b_y the bias on the output neuron. A graphical representation of the artificial neural network is shown in Figure 6.20. The learning process of the neural network is to find the optimal weights and biases of the neural network so that the network gives accurate shaft power predictions $[\hat{y}_t, \hat{y}_{t+\Delta^+}]$, for an input space $\mathbb{X}$. In the learning process of a neural network with a regression problem, such as the prediction of the shaft power, the predicted values $[\hat{y}_t, \hat{y}_{t+\Delta^+}]$ are confronted with the real shaft power y, and evaluated through a loss function. The loss function used in this research is the mean squared error E, described by:

$$E = \frac{1}{m} \sum_{k=1}^{m} (y_k - \hat{y}_k)^2, \tag{6.22}$$

where, m is the number of data samples used for training the network. By taking the derivative of the loss function with respect to the weights and biases, and then shifting these parameters to minimize the loss function the neural network can learn, this is called backpropagation. Determining which weights and biases should be shifted is achieved through gradient descent.

Many parameters to initialize and define a neural network are required, these parameters are called hyperparameters. The hyperparameters for an artificial neural network are: The number of neurons in the hidden layer, the number of hidden layers, the type of activation functions, the weight initialization matrix of the network, the type of gradient descent optimizer, learning rate and momentum of the optimizer, number of epochs and batch size. Finding the best hyperparameters is an important task as each of these hyperparameter affects the performance of the network, thus they directly effect the model selection. Each parameter also affects the influence of other hyperparameters on the network. Consequently, sets of hyperparameters have to be evaluated rather than individual hyperparameters. To evaluate the set of hyperparameters, the NN is trained with training data and subsequently evaluated by computing the mean squared error of the network when used with the validation data, and k-fold cross validation. Below, the various hyperparameters are discussed and their effects on the network.

Hidden layer: number of neurons and layers Choosing the correct number of neurons in the hidden layer is not an arbitrary task. If too few neurons are present, underfitting and statistical biases will occur. Whereas too many neurons may lead to overfitting, high variance in neuron values, and the training time of the network increases. Since the network is evaluated using new data, the validation data, that

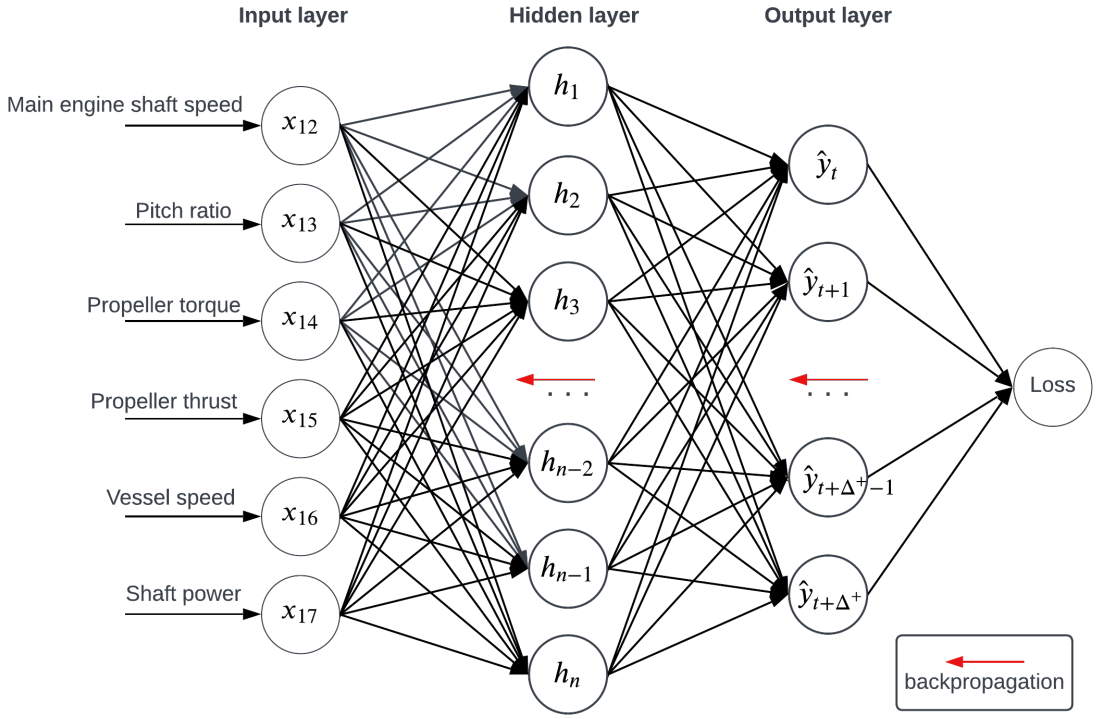

Figure 6.20: Graphical representation of the ANN, with 6 input data attributes, *n* neurons in the hidden layer, and output **y**.

was not used to train the network, whether the system is over- or underfitting will become evident. For the purpose of this project a single hidden layer will be used in the NN. It is common practise to start tuning the number of neurons in the hidden layer, n, with the average of the number of input and output layer neurons, and increase the number of neurons from there. In this case there are 6 input neurons and 40 output neuron, so the minimum value for n will be considered 23. From there, doubling intervals are chosen to tune the number of neurons. The range considered can be viewed in Table 6.8.

Activation functions Activation functions are used to map the output of a neuron to a specific range. In effect, the activation function has to the ability to decide whether a neuron should be activated, as it determines whether the neuron's output is crucial in the process of predicting the shaft power, or not. So it is the job of the activation function to derive an appropriate output value from a certain range, given a set of input values, as shown in Equation 6.20 and Equation 6.21. The main benefit of the activation function is that it allows the introduction of non-linearity to the system, using non-linear activation functions. Without a non-linear activation function, the neurons would simply be performing linear transformations using the weights and biases. In that case, it would be impossible to learn complex tasks as the network would behave as a linear regression model.

The non-linear activation functions considered in the scope of this project are the sigmoid (σ) and hyperbolic tangent (*tanh*) activation functions. The sigmoid activation function, has the benefit of scaling the neuron output to the range of [0,1], the sigmoid function is also differentiable and provides a smooth gradient. The smooth gradient is a beneficial property during backpropagation. The shape of the sigmoid function can be viewed in Figure 6.21, the function definition is:

$$f(x) = \frac{1}{1 + e^{-x}}. \tag{6.23}$$

The *tanh* activation function scales the neuron output to the range [-1,1], which means the output is centered around zero, which is a useful property for some applications. The *tanh* function has the same properties as the sigmoid function of being differentiable with a smooth gradient. The function of the

hyperbolic tangent function is:

$$g(x) = \frac{e^x - e^{-x}}{e^x + e^{-x}}. \tag{6.24}$$

The right choice of activation function is application dependent, and its performance is also contingent on other hyperparameters. These non-linear activation functions are used on the hidden layer. A linear activation function is used on the output layer in order to linearly scale the hidden layer values to a valid output value.

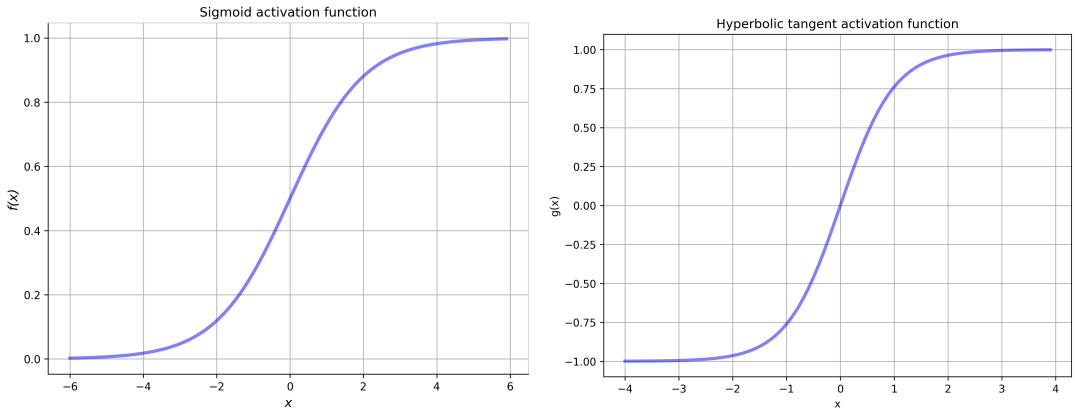

(a) Sigmoid activation function. (b) Hyperbolic tangent activation function.

Figure 6.21: The two non-linear activation functions used on the hidden layer of the neural network.

Weight initialization matrix The weight initialization matrix is the matrix of initial values for weights $w_{i,j}$ and $w_{y,i}$. The aim of weight initialization is to prevent exploding or vanishing effects of weights in artificial neural networks with multiple hidden layers. Since a single hidden layer was selected for the research, weight initialization processes will be omitted. Also, as will become evident later, the application of the long-short-term memory (LSTM) will prevent exploding or diminishing weights.

Optimizers: types, learning rates and momentum The optimization algorithm for gradient descent of the network is called the optimizer. Depending on the application, data and other hyperparameter settings, an appropriate optimizer should be selected. Unfortunately, just as the other hyperparameters this is a trial and error process to find the optimal one. Some of the more common optimizers are stochastic gradient descent (SGD), root mean Square propagation (RMSProp) and adaptive moment optimization (Adam). SGD replaces the actual gradient with a stochastic estimate in order to obtain faster convergences for high-dimensional spaces, like in neural networks, at the cost of convergence accuracy. RMSProp is an optimizer that uses an adaptive learning for each parameter.

The learning rate of the optimizer can be viewed as the step size by which the optimizer aims to find a minimum. With larger learning rates, the optimizer will make quick improvements on the weights and biases of the system, and thus quickly improves the performance of the neural network. The drawback is that, due to the larger step size, the optimizer might overshoot the global minima, and instead roam around the optimal solution. When choosing a smaller learning rate, these global minima will not be missed by the optimizer. However, the smaller learning rates come at the cost of longer computational times, as well as the risk of getting stuck in local minima. The adaptive learning rate employed by RMSProp, aims to capture the benefits of both smaller and larger learning rates.

In the search of global minima of the optimizer, along with the gradient of the current step of the optimizer, the idea of momentum can also be incorporated in determining which direction to go by the optimizer. The momentum is an accumulation of the gradients of the past steps, and can therefore provide valuable additional information on where to go next, and for that reason improves the optimizers route towards a global minimum. Adam combines the idea of momentum with the RMSProp method in order to further improve performance. Initial testing showed Adam to have the best performance on

the training data used in the project, and will therefore be selected as the optimizer. The update rule for the Adam optimizer is as follows:

$$\theta_{t+1} = \theta_t - \frac{\alpha}{\sqrt{\hat{v}_t(\beta_2^t) + \epsilon}} \hat{m}_t(\beta_1^t), \tag{6.25}$$

where θ_t is an update parameter, α the stepsize or learning rate, $\hat{v}_t$ the second moment estimate, $\hat{m}_t$ the first moment estimate, and the moment estimates are a function of β_1^t and β_2^t the exponential decay rates for moment estimates. The first and second moment estimates are computed from the gradients and bias-corrected through an adaptive decay rate. The initial decay rate β_1 and β_2 are hyperparameters that can be tuned. For simplicity only β_1 is tuned. The values considered for α and β_1 are presented in Table 6.8.

Epochs The number of epochs of the neural network indicates how many times the entire training dataset has been passed through the network. Since the network learns through gradient descent, and since the method is iterative, updating the weights and biases using one epoch is not enough. Using one epoch would lead to underfitting, and more complex trends in the data would not be captured by the neural network. However, using a number of epochs that is more than necessary, will lead the neural network to learn patterns that are specific to the training dataset. This makes the network lose generalization capacity by overfitting the training data, and will result in a poor accuracy on new data. Therefore, tuning the number of epochs is a valuable hyperparameter that is able to provide the neural network with enough passes of training data to find better weights and biases.

Batch size The entire training dataset can not be processed by the neural network in one pass, instead the data is divided into batches. The batch size effects the gradient step size, and therefore affects the learning process of the neural network. Namely, when the error gradient is estimated using one of the optimizers, using a larger batch size will likely allow the optimizer to find a more accurate error gradient. Consequently, the weights and biases can be shifted more accurately as well. This improved accuracy comes at the cost of additional computation, as more predictions are made per update-step of the weights and biases. Reducing the batch size will lead to faster computation but less accurate updates. However, more updates could be computed in the time it takes for larger batches to compute. By increasing the number of epochs for instance and lowering the batch size accurate results can still be achieved. However, in practise larger batch sizes often lead to better results. The chosen batch size in this research is 32, which is the default batch size for NN python packages.

6.6.3. Recurrent neural network

A recurrent neural network (RNN) is a type of ANN which uses sequential data as input, time-series data for instance. Within the RNN the internal state of the hidden layer is recurrently updated, and information from one time-step is passed on the next time-step. The computational flow diagram that illustrates this principle can be seen in Figure 6.22. Initially, the first datapoint from the sequence is fed into the network, it is multiplied by a set of weights w_1. The state of the hidden cell h_t, which is the state of the hidden layer for a particular datapoint at time t in the sequence, is calculated with:

$$h_t = tanh(w_2 h_{t-1} + w_1 x_t), \tag{6.26}$$

where w_2 is the set of weights applied on the connections between hidden cells and their neurons, and x_t the input datapoint in the sequence at time t. So the hidden layer is recurrently updating itself using the datapoint at a particular time-step of the input sequence and the internal state of the hidden layer of the previous time-step. The activation function *tanh* is default for basic recurrent neural networks. Once all datapoints of the sequence have been processed the output can be estimated used the formula:

$$\hat{\mathbf{y}}_n = w_3 h_{t-1}, \tag{6.27}$$

where $\hat{\mathbf{y}}_n$ is the set of predicted shaft speed in range $[t, t + \Delta^+]$ at recurrence step n, and w_3 the set of weights applied on the connections between the neurons of the hidden layer and the output layer. At each recurrence step the output $\hat{\mathbf{y}}_n$ is computed and evaluated in the loss function.

Similarly to the ANN, backpropagation is used in RNN models to allow the network to learn, by taking the gradient of the loss function with respect to weights and biases in the system and shifting them to minimize the loss function. The difference, however, is that there is now backpropagation through time. The effects of the weights on the loss function now backtrack through numerous hidden cell update steps. These update steps, as shown in Equation 6.26, all involve a non-linear activation function, and each hidden cell update increases the multiplicity of the set of weights. This introduces some problems of vanishing and exploding gradients. Namely, for larger sequences, where there are a larger amount of hidden cell update steps, the multiplicity of the backpropagation procedure leads the gradient to converge to zero or explode to large numbers. In either case the learning ability of the system is lost, since the gradients no longer capture accurately which weights and biases should be shifted.

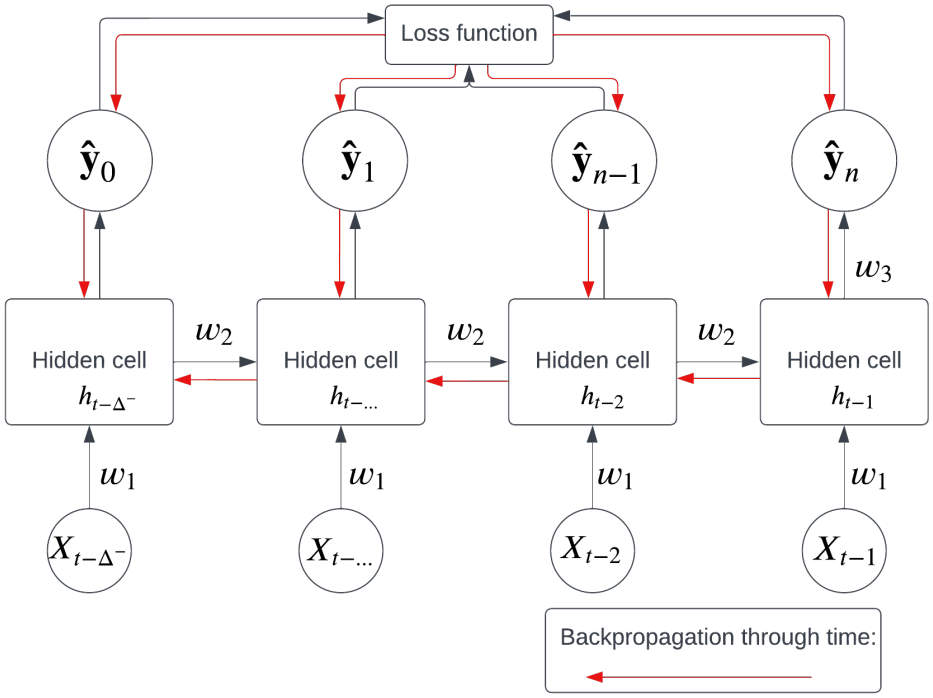

Figure 6.22: Computational flow diagram of a recurrent neural network.

To solve this problem alternate RNN models were developed such as long-short term memory (LSTM) and gated recurrent unit (GRU). For the purpose of this research LSTM was employed as some testing on the network showed that LSTM outperforms the GRU. An LSTM network has four basic operations it performs per recurrent update computation, namely forget, store, update and output. The graphical representation of a LSTM hidden cell is shown in Figure 6.23.

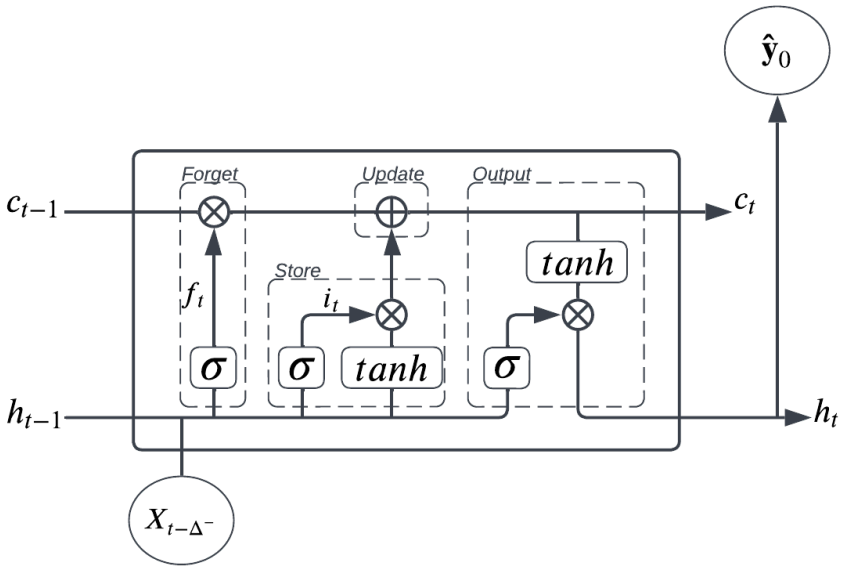

Figure 6.23: A graphical representation of a gates and operations in a LSTM cell.

The first step in the LSTM hidden cell, the forget step, is to decide what information is going to be discarded from the self state. This is represented by function, f_t, and is a function of the previous state h_{t-1} and input X_t. Therefore, it can decide which data is relevant from both the input data as well as the previous hidden state. The second step of the LSTM is to decide which of the new data is relevant, and should be stored to the self state of the hidden cell, denoted by i_t. The third step is to selectively update the cell state, denoted by c_t, using the previous cell state c_{t-1} and the new data that was selected in step two. And finally, step four is to provide an output, h_t. The output gate controls what information that is encoded in the self-state, is used as input to the next time-step, and send to the output layer. Throughout each of these four steps, various non-linear activation functions are used in order to capture the complexities of the data and to capably adapt to it. And through these dynamic actions of forgetting, storing and updating, the gradients can be prevented from exploding or vanishing, allowing the system to learn from larger data sequences as well as during more epochs.

Many of the parameters that are required to initialize and define a recurrent neural network are the same as the ones discussed for an ANN. To restate, these are: the number of neurons in the hidden layer, the number of hidden layers, the type of activation functions, the weight initialization matrix of the network, the type of gradient descent optimizer, learning rate and momentum of the optimizer, number of epochs and batch size. Since the RNN deals with data sequences, and can predict Δ^+ seconds into the future, two additional hyperparameters to be tuned are Δ^+ and Δ^-. The tuning of these parameters will show the optimal data sequence with range $[t - \Delta^-, t - 1]$, to provide the network with optimal accuracy in predicting shaft power P_{sh} at time-steps $[t, t + \Delta^+]$.

6.6.4. RNN Results

Below, in Table 6.8, the hyperparameters ranges for the RNN model selection are presented. The optimal solution found is presented in grey. Obviously, the optimal results are found for a small Δ^+ as it is easier to predict the future shaft power demand a few seconds than a few minutes. The best model performance is achieved with a larger data sequence $[t - \Delta^-, t - 1]$. Only 3 epochs were used in order to cut down on computation times, since run time increases proportionally to the number of epochs. Additionally, the decay rate was also not tuned, as it proved to be an insensitive setting in the model selection process.

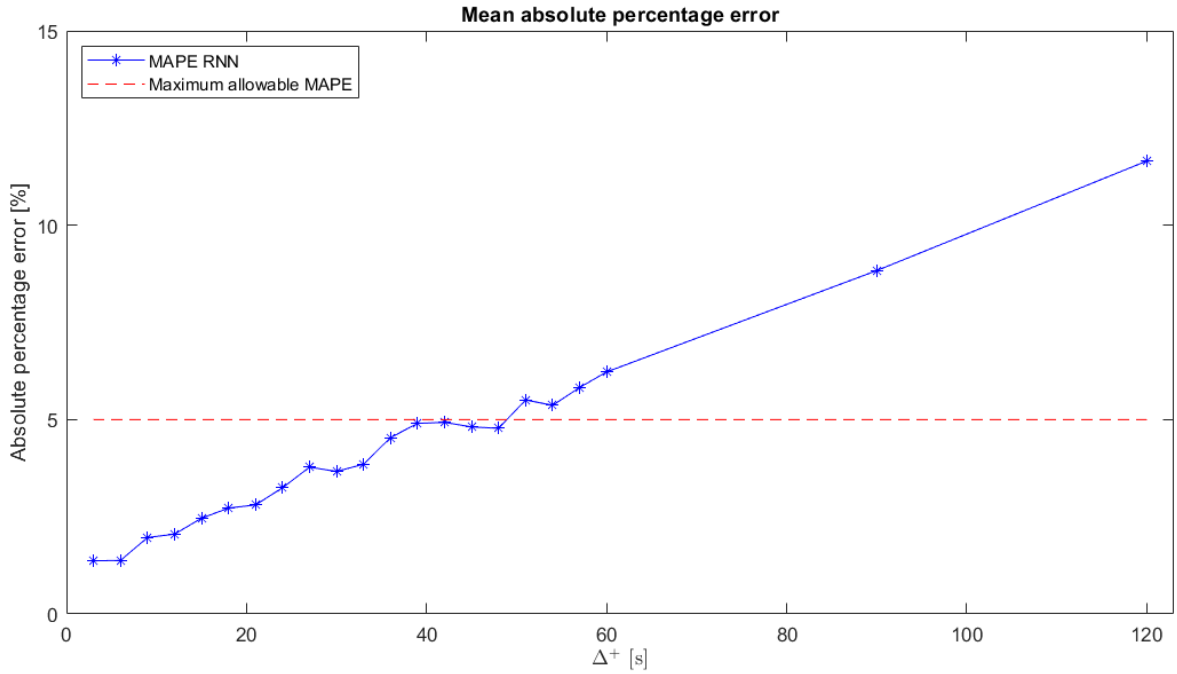

Figure 6.24: Mean absolute percentage error for the recurrent neural network.

Hyperparameter	Evaluated values
Δ^+ [s]	3 9 15 30 60 90 120
Δ^- [s]	3 9 15 30 90 180 360
Neurons n	25 50 100 200
Learning rate α	0.001 0.01 0.1
Decay rate β_1	0.75
Optimizer	Adaptive moment optimization (Adam)
Epochs	3

Table 6.8: Evaluated hyperparameters for the RNN model and optimal solution (in grey), validated through 3-fold cross-validation.

Higher number of epochs can lead to better model performance. To ascertain an approximation of a valid number of epochs that does not overfit the data, the loss of the prediction model with optimal settings from Table 6.8, is plotted for training and validation data. From this it can be deduced that the optimal epochs is 10, for this number the model does not overfit the training data.

In Figure 6.24 the mean absolute percentage error (MAPE) can be seen for various Δ^+. Assuming 5% MAPE is the maximum allowable percentage error, it can be seen that 48 seconds in the future can be forecasted with an acceptable error, with the RNN. Optimal settings for Δ^-, number of neurons n, and learning rate α, were found for each respective Δ^+. Unlike the linear regression, moving average and ARIMA, the MAPE value for the RNN is computed over the set of predictions $[t, t+\Delta^+]$, rather than over singular predictions at timestep $t+\Delta^+$. This is done because the RNN model is specifically trained to optimize for output window $[t, t+\Delta^+]$. Whereas the univariate methods are regression methods, that neglect to take into account how well the fitted model might work on future data samples. Therefore, a MAPE that falls within the bounds of 5% for RNN, does not guarantee that at each timestep in data range $[t, t+\Delta^+]$ the MAPE value is below 5%.

Below, in Table 6.9, the relationship between Δ^+ and Δ^- is shown in tabular form. It shows that the

MAPE values increase for larger prediction horizons, which is to be expected. Additionally, it shows that it is not clear what the optimal data sequence $[t - \Delta^-, t - 1]$ is; For different prediction horizons, different data sequence lengths are optimal. For the selected $\Delta^+ = 48$ [s], the optimal data sequence is one with $\Delta^- = 180$ [s]. For this combination the remainder of the results are presented.

Δ^- [s] \ Δ^+ [s]	3	9	15	30	60	90	120
15	1.46	1.97	2.46	3.67	6.62	9.13	13.58
30	1.41	2.04	2.80	4.44	6.22	8.83	12.65
90	1.78	2.33	2.89	4.36	6.49	9.52	13.94
180	1.37	2.21	2.58	3.99	6.70	8.99	12.80
360	1.41	2.80	2.75	3.97	6.36	9.28	11.65

Table 6.9: MAPE [%] of the proposed model for different combinations of Δ^- and Δ^+.

For $\Delta^+ = 48$[s], the results are shown in Figure 6.25, Figure 6.26, and Table 6.10.. The results are computed on the test data. As is evident, the MAPE value is not below 5% on the test data, this means the model performed worse on the test data than on the validation data. Figure 6.25 shows the distribution of actual shaft power, a scatter plot (actual versus predicted), and the relative frequency distribution of the absolute errors. From the scatter-plot it can be seen that there are a few tight clusters close to the optimal solution line. However, there are outliers far from the optimal solution. These outliers are a product of a larger data sequence used. The larger data sequence (large Δ^-) causes an increased chance of a shaft power shift to be contained in the data sequence. The shaft power shift is when the ship operator sets a different shaft speed setpoint from one moment to the next. When this happens the RNN is not able to predict the shaft power accurately. As can be seen from the relative frequency distribution of the absolute percentage errors, the errors are most frequently close to zero.

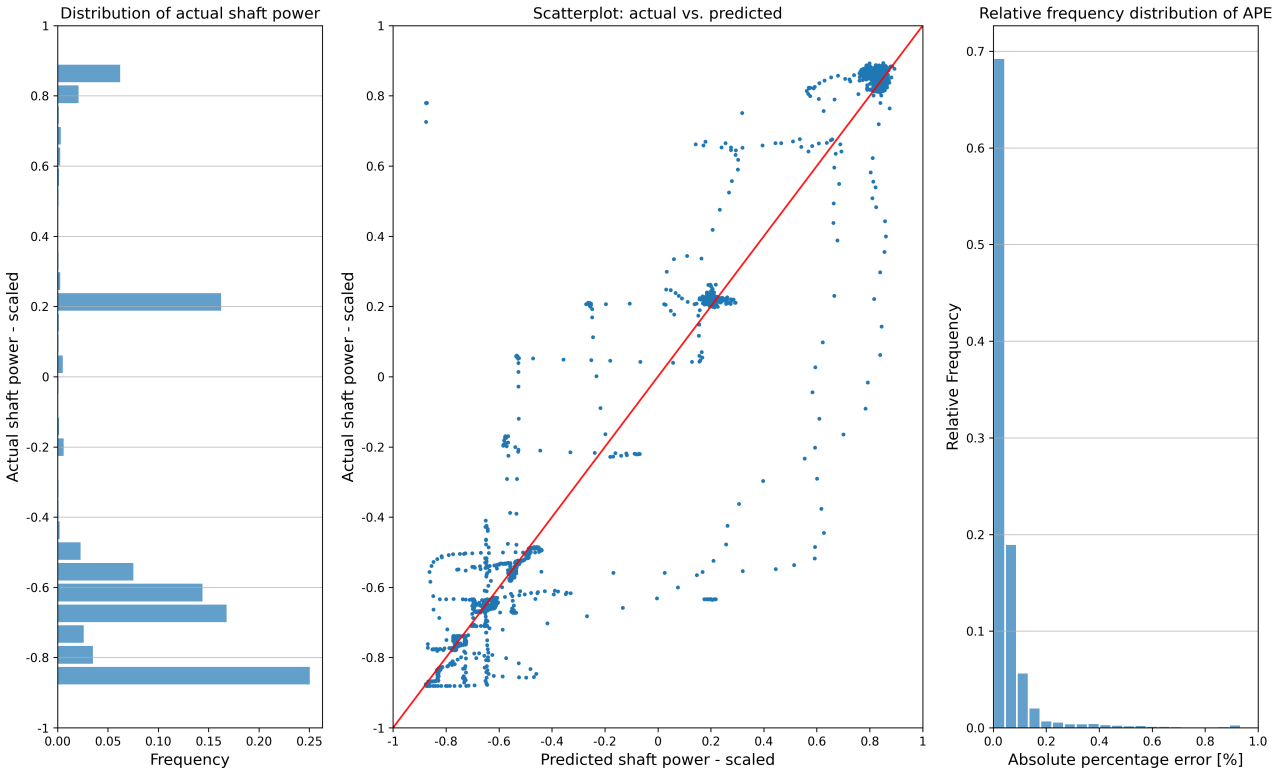

Figure 6.25: Distribution of actual shaft power, scatter plot (actual versus predicted), and relative frequency distribution of AE. Results are for $\Delta^+ = 48$ [s], with $\Delta^- = 180$ [s]. n = 5000 samples.

Figure 6.26 shows a trend in time predicted with the RNN 48 seconds in the future. It can be seen that the trend is clearly followed by the prediction method. The RMSE, MAE, MAPE and R^2 values for the RNN are shown in Table 6.10. The MAE of 90 kW is higher than for the other prediction methods, which is also supported by the fact that the MAPE value is 6.539% which is a bit higher than the allowable MAPE. This is because a good performance of the RNN on the validation, even though k-fold-cross-validation is used, does not guarantee the same performance on the test data. Regardless, a MAE of 90 kW is not bad compared to a maximum shaft power of 5400 kW. The R^2, shows a nice value of 0.960, which indicates a high goodness of fit between the predicted and actual shaft power values.

RMSE	MAE	MAPE	R^2
296.307	90.681 ± 5.484	6.539	0.960

Table 6.10: RMSE [kW], MAE [kW], MAPE [%], and R^2 [-]. Results are for $\Delta^+ = 48$ [s], with $\Delta^- = 180$ [s].

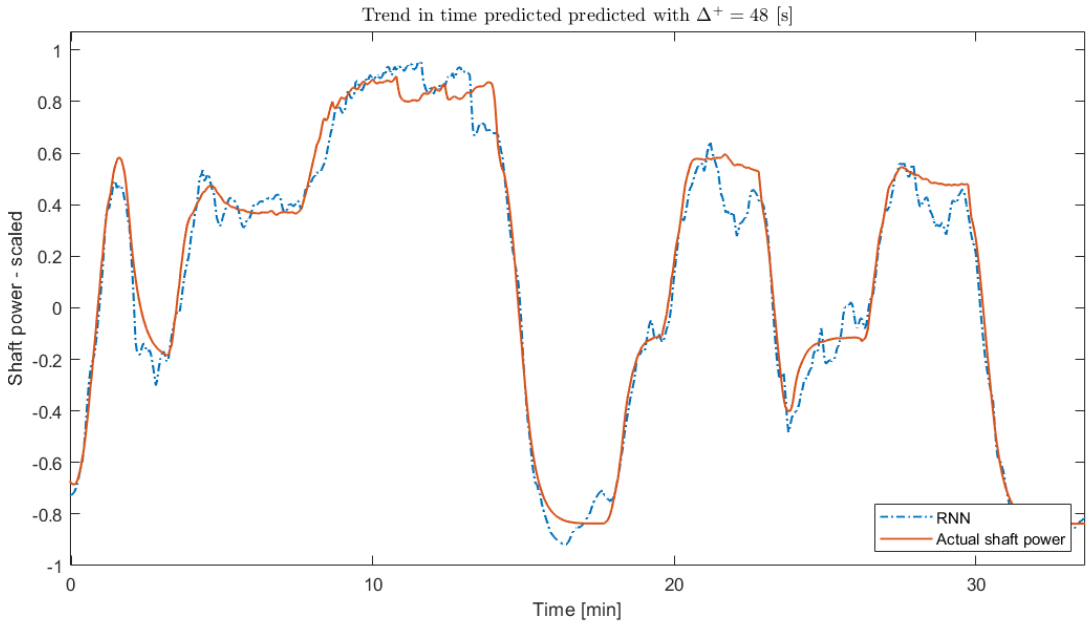

Figure 6.26: A section of the trend in time (actual versus predicted) shaft power. Results are for $\Delta^+ = 48$ [s], with $\Delta^- = 180$ [s].

6.7. Conclusion

As a point of comparison Figure 6.27 summarizes the performance of the four methods: Linear regression, moving average, ARIMA, and RNN. It shows the MAPE over an increasing prediction horizon. It nicely highlights that the RNN outperforms the other methods, and is able to predict further in the future while maintaining a MAPE of under 5%.

Table 6.11 shows the comparison of the four methods in terms of prediction horizon length, RMSE, MAE and MAPE. The variance in MAE can be explained by the test data that they utilized. If the test data contains more datapoints where the shaft power is lower, for instance during electric mode of the vessel, than the MAE is bound to be lower as well. Therefore, the MAPE is a better measure of comparison here, as it looks at the percentage errors.

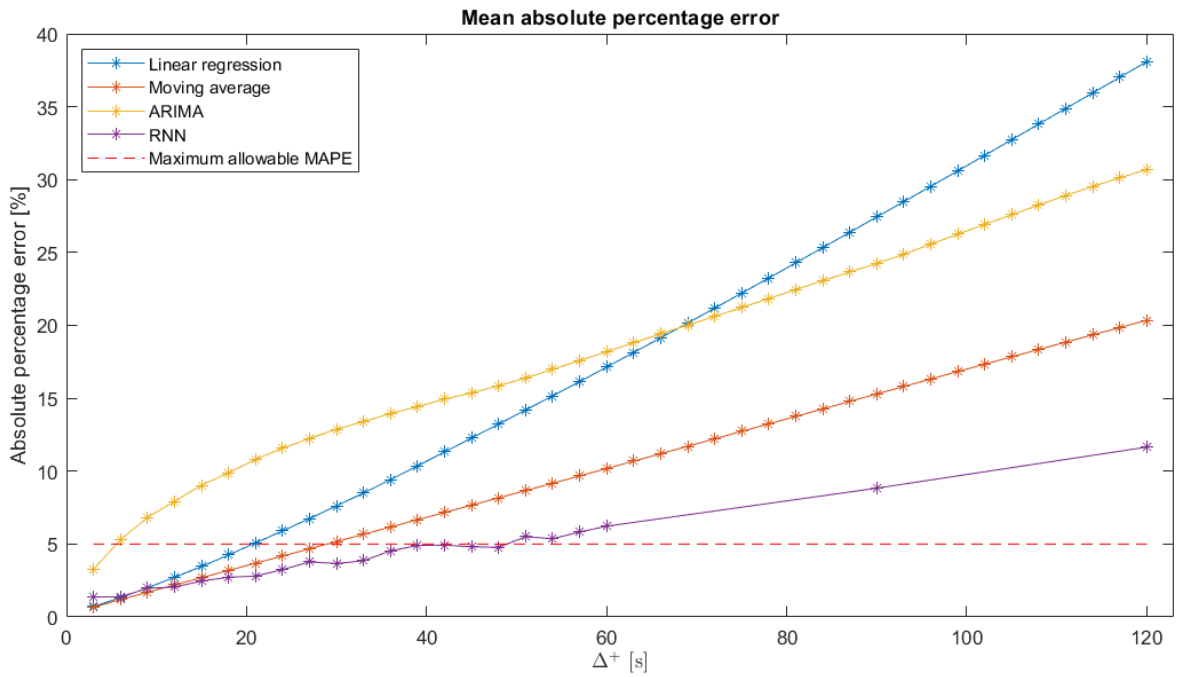

Figure 6.27: Mean absolute percentage error for the linear regression, moving average, ARIMA, and recurrent neural network.

In Figure 6.28 the trends in time for the four prediction methods are shown. It highlights the divergence of the ARIMA methods. It also shows that the RNN comparatively performs worse than the linear regression and moving average in this particular example. This example is chosen since it is a particularly variable load demand, compared to the operational profiles shown in Figure 3.3. This means that RNN is a less reliable prediction method with more varying data. Although overall the RNN outperforms the others methods in accuracy and prediction interval size.

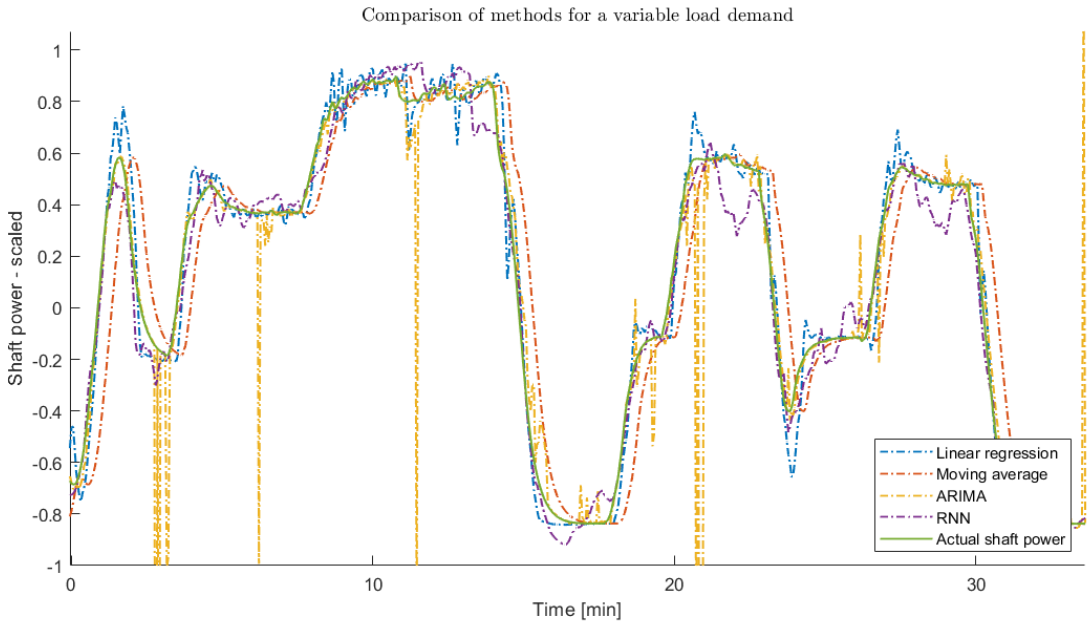

Figure 6.28: A section of the trend in time (actual versus predicted) shaft power. Prediction methods: Linear regression, Moving average, ARIMA and RNN.

Method	Δ^+ [s]	RMSE [kW]	MAE [kW]	MAPE [%]
Linear regression	18	241.394	40.466 ± 3.370	4.251
Moving average	27	228.842	54.608 ± 2.345	4.673
ARIMA	3	268.944	72.073 ± 11.365	3.276
RNN	48	296.307	90.681 ± 5.484	6.539

Table 6.11: Comparison of methods: RMSE, MAE, and MAPE.

Research question 3 is ”What is an effective data driven model for power load forecasting with a prediction horizon of two minutes while maintaining high levels of accuracy, given the data set of the Holland-class offshore patrol vessel?”

The data used to make predictions was real data containing high and irregular variance caused by measurement noise. Additionally, very few data features were made available by Damen of the Holland-class offshore patrol vessel. Given these facts, it was not possible to maintain a high accuracy for a prediction horizon of two minutes. The RNN has the largest prediction horizon of 48 seconds while maintaining a MAPE of under 5%. If higher levels of error would be acceptable, than RNN is still the best option to pursue, as can be seen in Figure 6.27. Therefore, the RNN has been selected as the power load forecasting tool of the energy management system.

7

Energy management strategy

In this chapter the optimization-based controller and the integration of the controller and load prediction tool into a complete energy management tool are presented. This pertains to research question 4. For convenience the research question is stated below. Question 4a, 4b and 4c are answered in section 7.2. Due to time constraints of the project question 4d, dealing with disturbance rejection will be left out. In section 7.5 question 4e is elaborated.

Research question 4: What is an effective controller design given the selected energy management strategy (RQ1), powertrain model (RQ2), and data-driven power load forecasting model (RQ3), that is able to reduce energy consumption & emissions and prescribe power allocation in real-time?

(a) What should be the input vector $\vec{x}$, output vector $\vec{y}$, control vector $\vec{u}$ and disturbance vector $\vec{d}$ of the system?

(b) What is an objective function for the controller that is able to a) find an optimal power split between mechanical and electric drive, b) find an optimal split between diesel generators and battery, and c) reduce energy consumption?

(c) What are appropriate constraints for the states, outputs, control variables, and disturbances of the system, with respect to accomplishing EMS goals and KPI performance?

(d) What is the performance of the model evaluated with selected KPI (RQ1.3)?

First the internal model of the controller will be discussed in section 7.1. The internal model of the controller describes a simplified model of the powertrain components such as the diesel engines, induction machines, diesel-generator sets and the battery. Each of these components is described by their respective fuel consumption, power and torque relationships and power or conversion losses. Second, the optimization problem formulation is given in section 7.2. This includes the objective function and constraints. In **??** the model selection is discussed. This involves a brief description of the nature of the optimization problem and the effects when choosing appropriate optimization algorithms. In the model verification, in section 7.4, some tests are performed in order to verify the correctness of the implemented model. Finally, the results are discussed in section 7.5.

7.1. Internal model controller

Due to confidentiality of the used engine fuel maps in this project, typical representative maps are shown in this chapter rather than the real ones.

7.1.1. Diesel engine

The diesel engine in the internal model of the controller is presented by a fuel efficiency map. An example of such a map is shown in Figure 7.1. Based on an operator set-point for vessel speed, at each timestep, the engine speed is derived. Given the determined engine speed, the relationship between power and specific fuel consumption (sfc) for that engine speed is fed to the controller.

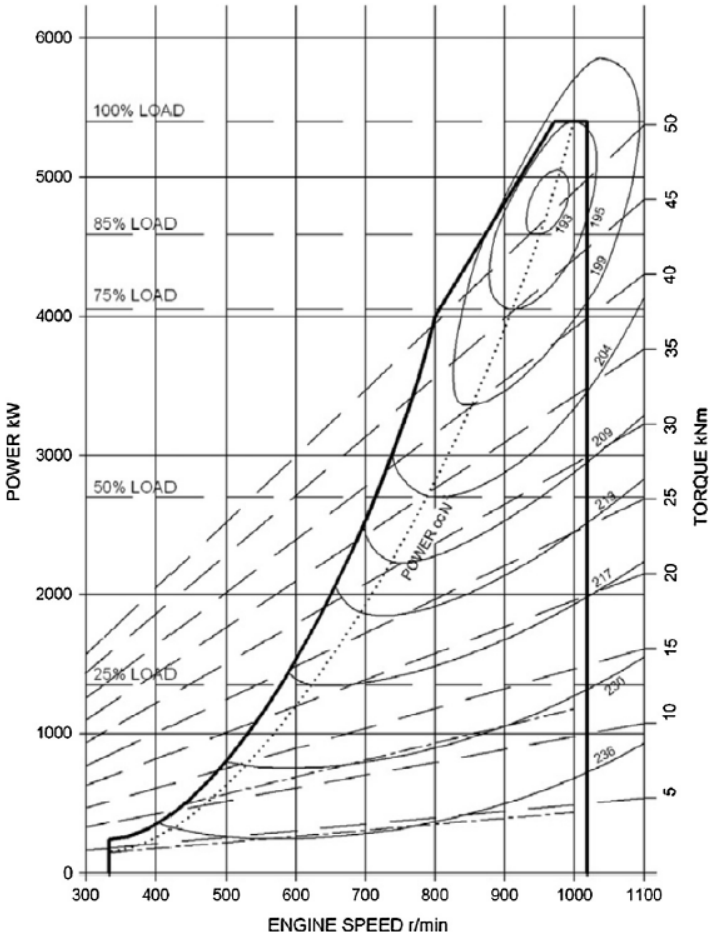

Figure 7.1: Specific fuel consumption of a typical high speed engine. Image retrieved from [39].

The bold bounds in the fuel map show the operating envelope of an engine. The selected power of the controller, given the determined engine speed, must fall within the operating envelope. This is ensured by feeding the power-sfc relationship to the controller only for datapoints within the operating envelope. The fuel consumption rate, $\dot{m}_{f,DE}$ in g/timestep, is calculated using the specific fuel consumption, sfc_{DE} in g/kWh, and engine power, P_{DE} in kW:

$$\dot{m}_{f,DE}(k) = \frac{sfc_{DE} \cdot P_{DE} \cdot \Delta t}{3600}, \tag{7.1}$$

with Δt in seconds, and k the timestep. The diesel engine power P_{DE} is a decision variable of the controller.

7.1.2. Induction machine

Similarly to the diesel engine, the induction machine is represented by a torque-speed efficiency map. The speed setpoint for the induction machine is derived from the operator setpoint of vessel speed. Then, a cross-section of the efficiency map, given the speed setpoint, is fed to the controller, taking into account the operating envelope.

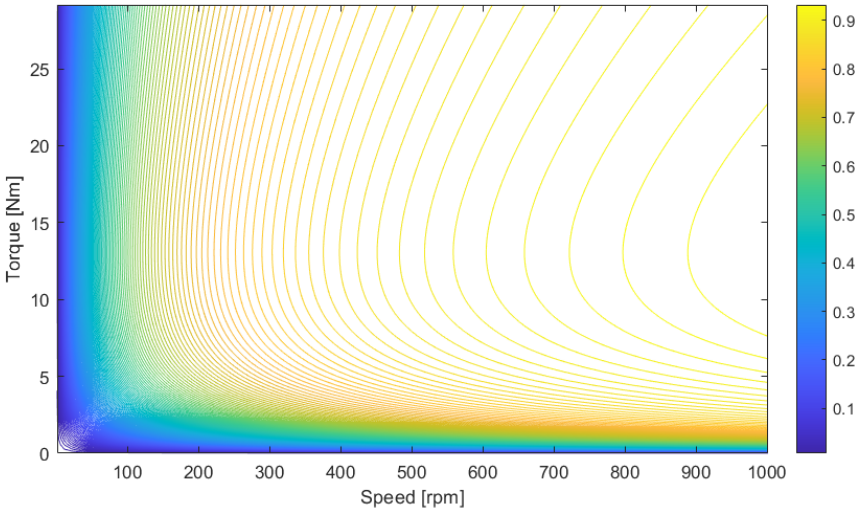

Figure 7.2: The torque-speed efficiency map for the induction machine.

The torque setpoint of the induction machine is a decision variable of the controller. The relationship between induction machine power, P_{IM} and torque $T_{IM,set}$ is given by:

$$P_{IM}(k) = 2\pi T_{IM,set}(k)\frac{n_{sh}(k)}{i_{GB}}, \tag{7.2}$$

where n_{sh} is the shaft speed, and i_{GB} the gearbox ratio. The fuel consumption associated with the induction machine is calculated through the diesel generator or battery, as these two sources provide the energy to the induction machine. The induction machine therefore only has an indirect effect on fuel consumption.

7.1.3. Diesel generator

The power that should be delivered by the diesel generator, $P_{DG,tot,d}$ is the sum of the power demand of the two induction machines P_{IM}, the auxiliary power P_{aux} and the battery power P_{BAT}. Note that the battery power can be both positive and negative depending on whether the battery is charging or discharging. Mathematically this is described as:

$$P_{DG,tot,d}(k) = -P_{BAT,\,\text{set}}(k) + P_{aux}(k) + \frac{2P_{IM}(k)}{\eta_{IM}(k)}, \tag{7.3}$$

where η_{IM} is the corresponding efficiency to the setpoint of the power of the induction machine at a certain speed setpoint. In case of a positive P_{BAT} the battery is discharging, and therefore, the diesel generator has to supply less power to the system. The diesel generator is represented to the controller by a power-sfc relationship similarly to the diesel engine described previously. The difference is, however, that the speed of the diesel generator-set is considered constant, and does not fluctuate with the speed of the ship, graphically this relationship is shown in Figure 7.3. The fuel consumption rate of each of the three generator-sets can be described as:

$$\dot{m}_{f,DG_i}(k) = \frac{sfc_{DG_i} \cdot P_{DG_i} \cdot \Delta t}{3600}\ ,\ i \in [1,3]. \tag{7.4}$$

The three diesel generator-sets should supply the energy demanded by the system. Therefore, the energy supplied by the diesel generator, $P_{DG,tot,s}$ is simply:

$$P_{DG,tot,s}(k) = \sum_{k=1}^{3} P_{DG_i}\ ,\ i \in [1,3]. \tag{7.5}$$

The supply should equal the demand: $P_{DG,tot,s}(k) = P_{DG,tot,d}(k)$, this is a non-linear constraint.

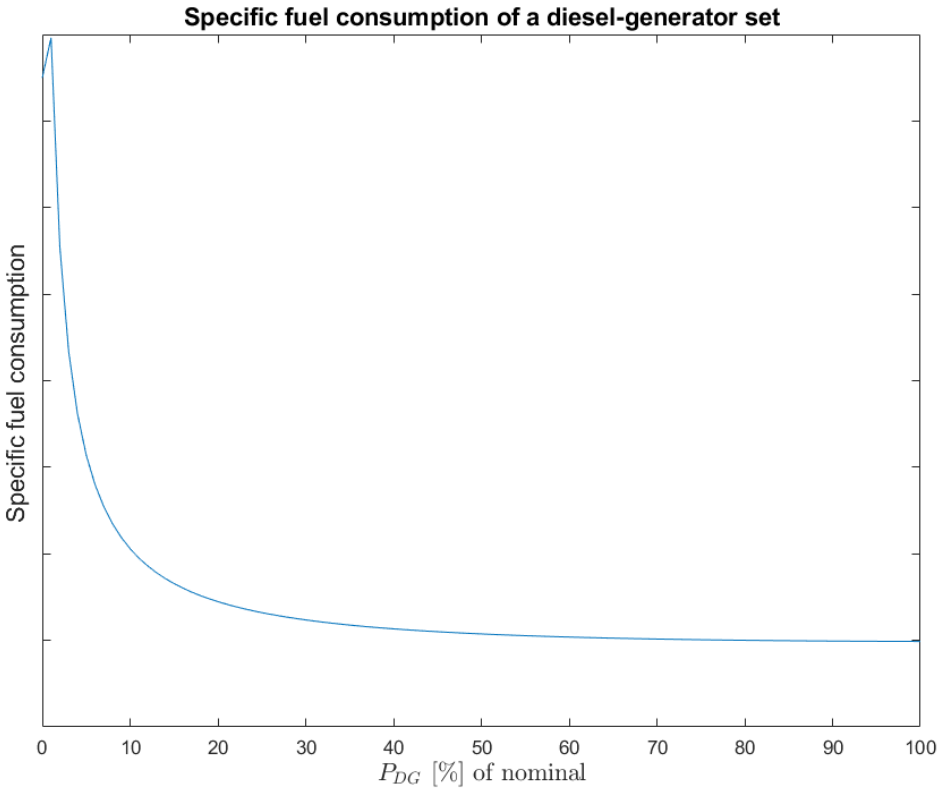

Figure 7.3: Specific fuel consumption curve for the diesel generator-set.

7.1.4. Battery

The current of the battery, I_{BAT}, is a decision variable of the controller. The current is related to the battery power, P_{BAT} in kW, as follows:

$$P_{BAT}(k) = V_{line} \cdot \sqrt{3} \cdot f_p \cdot I_{BAT}(k), \tag{7.6}$$

where V_{line} is a constant line voltage, and f_p a power factor that relates real power to apparent power, for the purposes of this project it is assumed constant at $f_p = 0.8$. To account for the cost of discharging the battery and using the energy, an equivalent specific fuel consumption (ESFC) graph is constructed. This graph represents the associated specific fuel consumption of each power setpoint of the battery. Of course, the battery does not in reality have an associated specific fuel consumption point. The ESFC is merely a tool to incentivize or disincentivize the use of the battery over the diesel generator. When the diesel generator is operating at a sub-optimal setpoint, there are two options, namely: a) Increase the load on the diesel generators to push the generators in a more favorable operating setpoint, while charging the battery. b) Decrease the diesel generator setpoint to a more favorable setpoint, while discharging the battery. In the second case, the setpoint for one of the diesel generators is pushed to 0. Since only partially lowering the load on the diesel generator would create a less optimal setpoint, as indicated in Figure 7.3.

In order to incentivize the battery discharging when the sfc of the generator-set is high, and incentivize charging when the sfc of the generator-set is low, the ESFC of the battery should be the inverse of the sfc graph of the generator set. This is graphically represented in Figure 7.4. Because the operating envelope of the battery is 400 kW, it is only able to cover roughly 40% of the power of one diesel generator-set, which is about 1000 kW. With a more powerful battery with faster discharging capabilities would lead to a more advantageous energy management system; the battery has more versatility in taking over the job of the diesel-generator sets. With this limited battery capacity limited gains can be achieved. As mentioned in the literature review chapter, [19] determined that the fuel consumption savings are partially proportional to the battery capacity.

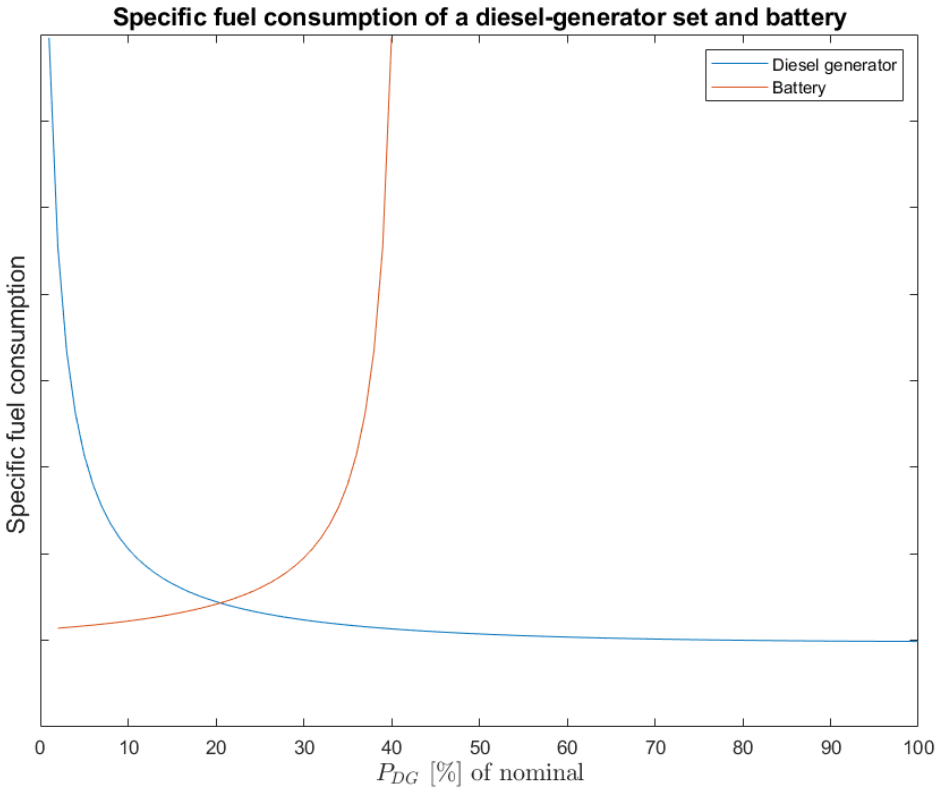

Figure 7.4: Artificial equivalent specific fuel consumption of the battery for discharging mode.

Note that Figure 7.4 only shows the discharging mode, charging mode is an identical but mirrored graph. The complete operating envelope of the battery is shown in Figure 7.5.

To further enhance the performance of the energy management system through this artificial equivalent specific fuel consumption the graph can be fine-tuned to show favorable behaviour. For instance, if shore-charging is the preferred method of charging the battery then the ESFC map can be made to be 'estimated time of arrival (ETA)' dependant; incentivizing discharge of the battery when the ship is known to arrive at shore soon, and disincentivizing charging when close to shore. the ESFC can also be state of charge dependant, where the charging and discharging becomes a function of the SOC of the battery. Additionally, it would be possible to make the ESFC load prediction dependant as well; For instance, if lower shaft loads are expected in the future, it is more likely that battery is to be used in those moments, so in the near future it might then be worthwhile to incentivize charging the battery. These more advanced ESFC for the battery are outside the scope of this project, but provide a valuable and interesting avenue to explore in the future.

In the scope of this project the ESFC will be tuned for a specific operational profile. This is discussed further in section 7.3.

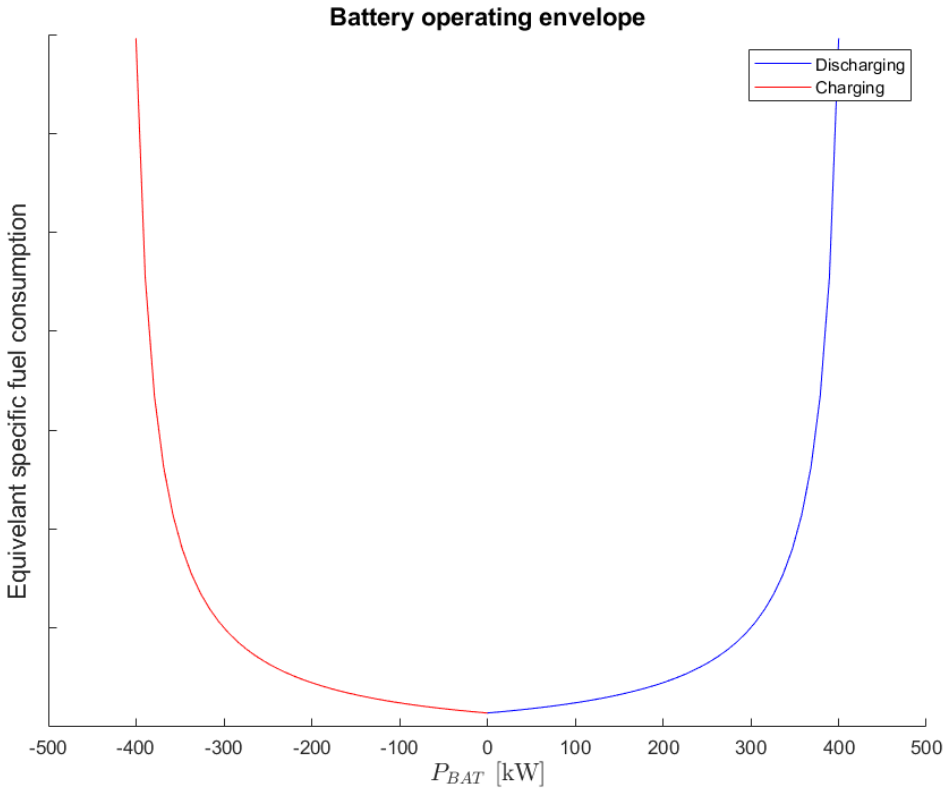

Figure 7.5: Artificial equivalent specific fuel consumption of the battery pack. The complete operating envelope.

The battery fuel consumption can be computed with a string of efficiencies and the ESFC [11]:

$$\dot{m}_{f,BAT}(k) = \frac{sfc_{BAT}(k) \cdot P_{BAT}(k) \cdot \Delta t}{(\eta_{BAT} \cdot \eta_{fc})^{sign(P_{bat})}} \tag{7.7}$$

where, η_{BAT} and η_{fc} are the efficiencies of the battery and the frequency converter respectively. η_{BAT} is battery power dependant, whereas η_{fc} is assumed a constant. The state of charge of the battery is estimated using the coulomb-counting method:

$$SOC(k) = SOC(k-1) - \int_0^{\Delta t} \frac{I_{BAT}(k)}{Q} \tag{7.8}$$

where Q is the capacity of the battery.

7.2. Optimization problem formulation

Since the equivalent fuel consumption for the battery was introduced the optimization problem is an equivalent consumption minimization strategy (ECMS). The objective function of an ECMS is simply the summation of the sources of fuel consumption, as can be seen below. The objective function is subject to system dynamics: Equation 7.10 until Equation 7.20, constraints: Equation 7.21 until Equation 7.30, and boundary conditions: Equation 7.33 until Equation 7.35. The operating envelopes of the engines maps are also constraints, but have been omitted in the description below as they are taken into account as described previously. The state variables, $\vec{x}(k)$, are:

$$\vec{x}(k) = \begin{bmatrix} P_{DE}(k) \\ P_{BAT}(k) \\ SOC(k) \\ n_{sh}(k) \\ \widetilde{P}_{sh,ref}(k) \end{bmatrix}$$

The output variables, $\vec{y}(k)$, are:

$$\vec{y}(k) = \begin{bmatrix} P_{DE}(k) \\ SOC(k) \\ \dot{m}_f(k) \end{bmatrix}$$

The control variables, $\vec{u}(k)$, are:

$$\vec{u}(k) = \begin{bmatrix} T_{IM,set}(k) \\ I_{BAT,set}(k) \\ P_{DG,1}(k) \\ P_{DG,2}(k) \\ P_{DG,3}(k) \\ \dots \\ T_{IM,set}(k+N) \\ I_{BAT,set}(k+N) \\ P_{DG,1}(k+N) \\ P_{DG,2}(k+N) \\ P_{DG,3}(k+N) \end{bmatrix}$$

The objective function of the problem formulation is:

$$\min_{\vec{u}(k)} \; J = \sum_{k=1}^{N} \dot{m}_f(k) \tag{7.9}$$

s.t.:

$$\dot{m}_f(k) = \sum_{i=1}^{2} \dot{m}_{f,DE_i}(k) + \sum_{i=1}^{3} \dot{m}_{f,DG_i}(k) + \dot{m}_{f,BAT}(k) \tag{7.10}$$

$$\dot{m}_{f,BAT}(k) = \frac{sfc_{BAT}(k) \cdot P_{BAT}(k) \cdot \Delta t}{(\eta_{BAT} \cdot \eta_{fc})^{sign(P_{bat})}} \tag{7.11}$$

$$\dot{m}_{f,DG_i}(k) = \frac{sfc_{DG_i} \cdot P_{DG_i,set} \cdot \Delta t}{3600} \;,\; i \in [1,3]. \tag{7.12}$$

$$\dot{m}_{f,DE_i}(k) = \frac{sfc_{DE_i} \cdot P_{DE_i} \cdot \Delta t}{3600} \;,\; i \in [1,2], \tag{7.13}$$

The total reference shaft power $\widetilde{P}_{sh,ref}$ is equal to the sum of the power of the induction machine and power of the diesel engine. It is assumed that both portside and starboard share the same power requirements.

$$\widetilde{P}_{sh,ref}(k) = P_{IM}(k) + P_{DE}(k) \tag{7.14}$$

$$P_{IM}(k) = 2\pi T_{IM,set}(k) \frac{n_{sh}(k)}{i_{GB}} \tag{7.15}$$

$$P_{DG,tot,s}(k) = P_{DG,1}(k) + P_{DG,2}(k) + P_{DG,3}(k) \tag{7.16}$$

$$P_{DG,tot,d}(k) = -P_{BAT}(k) + P_{aux} + \frac{2P_{IM}(k)}{\eta_{IM}(k)} \tag{7.17}$$

$$P_{DG,tot,d}(k) = P_{DG,tot,s}(k) \tag{7.18}$$

$$P_{BAT}(k) = \sqrt{3} I_{BAT,set}(k) V_{line} f_p \tag{7.19}$$

$$SOC(k) = SOC(k-1) - \int_0^{\Delta t} \frac{I_{BAT}}{Q} \tag{7.20}$$

$$T_{IM,min}(k) \leq T_{IM,set}(k) \leq T_{IM,max}(k) \tag{7.21}$$

$$I_{bat,min}(SOC(k)) \leq I_{bat,set}(k) \leq I_{bat,max}(SOC(k)) \tag{7.22}$$

$$P_{DG,min} \leq P_{DG,1}(k) \leq P_{DG,max} \tag{7.23}$$

$$P_{DG,min} \leq P_{DG,2}(k) \leq P_{DG,max} \tag{7.24}$$

$$P_{DG,min} \leq P_{DG,3}(k) \leq P_{DG,max} \tag{7.25}$$

...

$$T_{IM,min}(k+N) \leq T_{IM,set}(k+N) \leq T_{IM,max}(k+N) \tag{7.26}$$

$$I_{bat,min}(SOC(k+N)) \leq I_{bat,set}(k+N) \leq I_{bat,max}(SOC(k+N)) \tag{7.27}$$

$$P_{DG,min} \leq P_{DG,1}(k+N) \leq P_{DG,max} \tag{7.28}$$

$$P_{DG,min} \leq P_{DG,2}(k+N) \leq P_{DG,max} \tag{7.29}$$

$$P_{DG,min} \leq P_{DG,3}(k+N) \leq P_{DG,max} \tag{7.30}$$

Operation of I_{BAT} between 0 and 0.5 indicates charging the battery and between 0.5 and 1 discharging operation.

$$I_{BAT,\min}(\mathrm{SOC}(k)) = \begin{cases} 0.5 & \text{if } \mathrm{SOC}(k) \geq 0.8 \\ 0 & \text{if } \mathrm{SOC}(k) < 0.8 \end{cases} \tag{7.31}$$

$$I_{BAT,\max}(\mathrm{SOC}(k)) = \begin{cases} 0.5 & \text{if } \mathrm{SOC}(k) \leq 0.2 \\ 1 & \text{if } \mathrm{SOC}(k) > 0.2 \end{cases} \tag{7.32}$$

$$\vec{x} \geq 0 \tag{7.33}$$

$$\vec{y} \geq 0 \tag{7.34}$$

$$\vec{u} \geq 0 \tag{7.35}$$

Note that the goal of reducing fuel consumption is enforced through the objective function, the reduction of CO2 emissions is assumed to occur through the reduction of fuel consumption as well. Propulsion availability is ensured through constraint described in Equation 7.18, which equates the demanded power with the supplied power. Finally, a secondary goal of the control formulation is to increase the battery lifetime by keeping state of charge of the battery between 20% and 80%, this is enforced through constraints described in Equation 7.31 and Equation 7.32.

For convenience the variables and their description have been listed below in summary.

- $\widetilde{P}_{sh,ref}(k)$: Total shaft power load reference value
- $\dot{m}_f(k)$: Total fuel rate consumption
- $\dot{m}_{f,DE_i}(t)$: Fuel consumption rate of diesel engine i
- $\dot{m}_{f,DG_i}(t)$: Fuel consumption rate of diesel generator i
- $\dot{m}_{f,BAT}(t)$: Fuel consumption rate of the battery.
- $P_{DG,tot}(k)$: Total power of the diesel generator-sets
- $P_{IM}(k)$: Induction machine power
- $P_{DG_i}(k)$: Diesel generator-set i, setpoint
- $P_{DE_i}(k)$: Power of diesel engine i
- $T_{IM,set}(k)$: Torque set-point for the induction machines.
- $n_{IM}(k)$: Rotational frequency of the induction machines
- $P_{BAT}(k)$: Battery power
- P_{aux} : Total auxiliary power, a constant
- $P_{IM}(k)$: Current power of the induction machines
- $I_{BAT,set}(k)$: Current set-point for the battery
- V_{line} : line voltage of the system, a constant
- f_p : power factor, a constant
- $SOC(k)$: State of charge of the battery
- $I_{BAT,min}$: Minimum current of the battery
- $I_{BAT,max}$: Maximum current of the battery
- sfc_{BAT} : Equivalent specific fuel consumption battery
- sfc_{DE_i} : Specific fuel consumption diesel engine i
- sfc_{DG_i} : Specific fuel consumption diesel generator i

7.2.1. Nature of the optimization problem

The optimisation problem can be classified as a non-linear programming problem (NLP). NLP have the characteristic that their solution time increases exponentially with the number of dimensions of the problem [60]. This indicates that for increasing prediction horizon the solution time increases exponentially, as the decision variables increase linearly with the size of the prediction horizon. For a prediction horizon of 48 seconds, which is the maximum feasible prediction horizon with the RNN, there are 16 prediction steps with 5 decision variables at each step, thus 80 decision variables. It is clear that this is a slow optimization problem.

There are three options to deal with this problem practically. (1) Rather than optimize for each timestep in the prediction horizon only a few timesteps should be considered. For instance at time [t, t+12, t+24, t+36, t+48]. (2) Alternatively, rather than re-optimize every timestep (3 seconds), one could optimize once every 30 seconds or once every minute. (3) Finally, rather than work with a moving horizon, the solutions found for each timestep in the 48 second window can be used to operate the ship for 48 seconds. Then, the next optimization solution has an allowable computation time of 48 seconds. In this case, however, one is operating the ship with relatively outdated information. Once the optimization starts it takes 48 seconds to be implemented, and then 48 seconds to execute, therefore much more relevant data might be available in the meantime. Therefore, the preferred solution is either of the first two options. The selection of the preferred solution is made based on computation times of the optimizer. This is done in the subsequent sections.

The optimization problem is tackled using a multi-start procedure. The multi-start procedure strategically samples the solution space. Each sample is used as a starting point for the solvers to find a local, or preferred, global minimum. Then, the most optimal solution of the multiple starts is selected. The starting points selected in this project were chosen between the upper and lower bounds on the decision variables. These bounds are presented in Equation 7.21 until Equation 7.30. First, given the upper and lower bounds, combinations of the lower and upper bound limits for the decision variables were used as starting positions. Secondly, starting positions between the upper and lower bounds are used; The starting positions are in the middle of the solution space. Thirdly, given the limited amount of probable optimal scenarios, analytically the setpoints for the scenarios were computed and used as starting points also. Two examples of the scenarios include: (1) Diesel engine takes care of the propulsive power demand, induction machine is turned off, diesel generator supplies the electrical power required by the hotel loads, and the battery is off. (2) Induction machines take care of the propulsive power demand, Diesel engines are turned off, diesel generator supplies the electrical power required by the hotel loads and the induction machines, and the battery supplies power as well, pushing the diesel generator setpoint of one of the diesel-generators to zero. Multiple of the scenarios can be thought out, and the corresponding setpoints to these scenarios can be analytically calculated. These scenarios do not necessarily start in feasible solution space. If the starting point did not converge to a feasible solution, the solution is discarded. Fourthly, the optimal solution to the previous timestep is also used as a starting point.

Initially over a 100 starting positions were utilized, however, this led to very large solving times. Upon further review, the number of starting points were reduced to 15. These 15 starting points still converged to the global minimum in the test cases performed. The starting points used are the same for all the evaluated solvers below.

7.2.2. Solver selection

The solvers considered in this project are sequential quadratic programming (SQP), SQP-legacy, active-set method, and interior-point. SQP is an iterative method for constraint non-linear optimization. SQP methods first transform the constraints into linearized versions and the optimization problem into sub-problems each of which becomes a quadratic model [61]. This is mathematically shown below, where an optimization problem such as:

$$\begin{aligned} &\text{minimize} && f(x) \\ &\text{over} \quad x \in \mathbb{R}^n && \\ &\text{subject to} && h(x) = 0 \\ & && g(x) \leq 0, \end{aligned}$$

is transformed into:

$$\begin{aligned} &\text{minimize} && \nabla f\left(x^k\right)^T d(x) + \tfrac{1}{2} d(x)^T B_k d(x) \\ &\text{over} \quad d(x) \in \mathbb{R}^n && \\ &\text{subject to} && h\left(x^k\right) + \nabla h\left(x^k\right)^T d(x) = 0 \\ & && g\left(x^k\right) + \nabla g\left(x^k\right)^T d(x) \leq 0 \end{aligned} ,$$

where B_k is a function of the hessian of $f(x)$. The benefit of SQP methods are the fact that they can deal with non-linear constraints and optimization problems easily. The SQP-legacy method is a MATLAB interpretation of the SQP method where a more refined stepsize is used. This may lead to more accurate, but slower solution. Active-set methods transform inequality constraints into simpler equality constraint sub-problems. The SQP method also uses an active-set implicitly to try and solve the quadratic problem (QP) using the active set of the previous QP sub-problem. The interested reader is referred to [61].

The interior-point (IP) method is a method that can solve linear and non-linear convex problems. The IP method moves from one point to the next in feasible solution space. The interior-point method employs barrier functions that augments the objective function to ensure violations of inequality constraints are not possible. This barrier function thus ensures that the optimal solution falls in feasible solution space.

Below in Table 7.1 the results are presented to implementation of the four algorithms that have been applied to operational profile 7 shown in Figure 3.3. The results are shown for a prediction horizon of one timestep. For comparison, the algorithms have also been tested on more complex solution spaces with a prediction horizon of 5 timestep (thus 25 setpoints). These results are shown in Table 7.2.

Algorithm	Total fuel consumption [kg]	Average fc per timestep [kg]	Average solving time per timestep [s]
Sequential Quadratic Programming (SQP)	1285.117	0.535	1.292
SQP-legacy (SQPL)	1285.117	0.535	1.435
Active-set (AS)	1260.291	0.525	1.844
Interior-point (IP)	1293.861	0.539	2.629

Table 7.1: Comparison of algorithms for non-linear optimization, for 1 timestep, and 5 decision variables.

Algorithm	Total fuel consumption [kg]	Average fc per timestep [kg]	Average solving time per timestep [s]
Sequential Quadratic Programming (SQP)	1253.549	538.929	51.701
SQP-legacy (SQPL)	1324.343	569.365	56.259
Active-set (AS)	1297.750	557.932	53.127
Interior-point (IP)	1463.113	629.025	66.834

Table 7.2: Comparison of algorithms for non-linear optimization, for 5 timestep, and 25 decision variables.

From the results we can see that SQP is the fastest method. For a single timestep horizon the AS method produces the best results in terms of minimizing fuel consumption. However, when the prediction horizon is increased the SQP shows the best results. What can also be noted is that the computational time of a single timestep is already 1.3 seconds. If at every timestep, so every 3 seconds, the controller is to complete an optimization procedure than just 1 timestep can be predicted. Therefore, in order to predict over a time horizon of 48 seconds and still use real-time optimization. Solution (1) and (2) described in the previous section will be used; (1) For the prediction horizon of 48 seconds the steps [t, t+24, t+48] will be predicted using the RNN, and these timesteps will be optimized for with the controller. (2) Since the prediction of 3 timesteps takes on average 20 seconds, every 30 seconds the controller will initiate a new optimization procedure as a moving horizon. These solving times are estimated based on the computational power of the researchers personal laptop. With parallel computing and more powerful processors the optimization procedures can be sped up, and more complex problems can be considered.

7.3. Battery equivalent specific fuel consumption

The operational profiles in Figure 3.3 are all around two hours. The ESFC map of the battery will be fine-tuned to be optimized for a 2 hour operating profile, namely, operating profile 7. This operational profile is chosen as is has a nice balance between electric mode and hybrid mode and will therefore be most illustrative. Note that the fine-tuning of the ESFC is a complex task, and as previously mentioned, the ESFC can be made to be ETA dependant, SOC dependant, and predicted shaft power demand dependant. Here, only the optimal energy consumption over a 2 hour profile is taken into account; the ESFC is tuned specifically to reduce energy cost over the operating profile.

In order to fine-tune the ESFC map two operations are performed on the map shown in Figure 7.5: (1) the map will be shifted higher or lower to have a minimum in range [0,227], and (2) the map will have a maximum value in range [235, 735]. The first operation determined how much the discharging of the battery is incentivized. The diesel generator-set has a sfc minimum value of 197. Therefore, the range was chosen around this value. The second operation is to fine-tune the incentive to charge the battery. For very high peaks, the optimizer will always elect to charge the battery, if the constraints allow it. Visually the two operations and their ranges are shown in Figure 7.6. The maximum range is denoted by C_1, and the shifting range is denoted by C_2. These two variables are control parameters that have mapped the ranges mentioned above in range [0,1]. For instance, $C_1 = 0$ corresponds to a cap of 235, $C_1 = 0.33$ to 400, $C_1 = 0.66$ to 565 and $C_1 = 1$ to 735. Similarly, $C_2 = 0$ corresponds to a minimum of 0, $C_2 = 0.33$ to 75, $C_2 = 0.66$ to 150, and $C_2 = 1$ to a minimum of 227. These values are in grams per kilowatt hour.

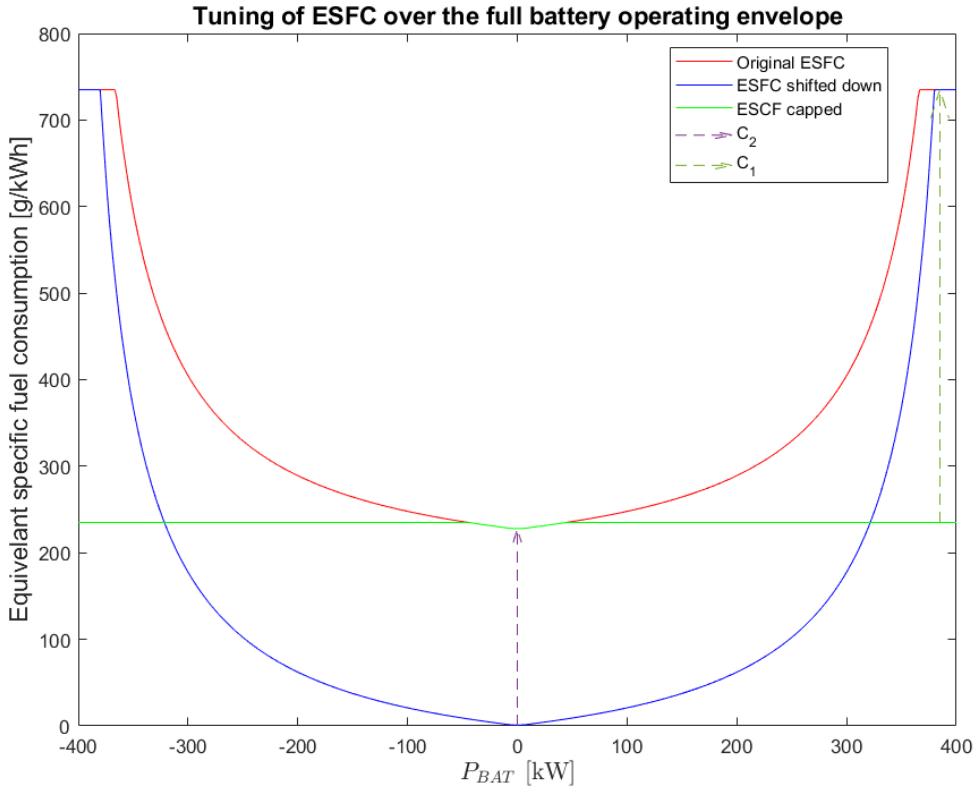

Figure 7.6: Fine-tuning of the ESFC for the battery, showing the two applied shifts.

The results to the tuning procedure are shown in tabular form in Table 7.3. The table shows for each set of evaluated control parameters the total fuel consumption of the main engines and diesel-generator sets over a period of 2 hours. At the start of the simulation the state of charge of the battery is 1, indicating it is completely charged. The table shows the final state of charge of the battery at the end of the 2 hour period. This drop in state of charge is assigned an equivalent fuel consumption cost.

The calculation is done by considering how much it would have cost to charge to battery initially with a diesel generator at its most optimal setpoint. Then, the difference between a fully charged battery and $SOC_{t_{end}}$ is multiplied by this cost to indicate the equivalent cost. Finally, the equivalent cost of the battery and total fuel consumption by the engines are summed and converted to the total energy cost of the 2 hour operation. It is assumed that each calorific value of the diesel fuel is 43 MJ/kg of fuel [62].

It can be noted from Table 7.3 that the total energy spent is almost the same for whichever setting of the battery, the difference between minimum and maximum total energy is 0.3 GJ which is a 0.34% difference in energy usage. This is because the battery capacity is tiny compared to total power required by the system. It is interesting to note that the setting $C_1 = 0$ and $C_2 = 0$ is the setting that used the battery the most, and is also the most optimal setting. These settings incentivized discharging the battery (low minimum cost), while disincentivizing charging (low cap). This result resulted in a significantly lower total fuel consumption by the engines. However, when compensating for the battery cost, the energy cost savings are minimal. Since this is the optimal settings, these settings of the ESFC are used for the simulations in the remainder of the research.

Control parameter settings		Fuel consumption [kg]			Energy battery		Total energy cost [GJ]
C_1	C_2	Main engines	Diesel generator sets	Total	$SOC_{t_{end}}$	Equivalent cost [kg]	
0	1	1461.114	561.863	2022.977	0.976	1.925	87.071
0.33	1	1462.681	560.246	2022.926	0.976	1.934	87.069
0.66	1	1464.969	557.900	2022.869	0.975	1.946	87.067
1	1	1464.969	557.900	2022.869	0.976	1.930	87.066
0	0.66	1464.432	543.397	2007.829	0.800	15.820	87.017
0.33	0.66	1465.183	543.099	2008.283	0.800	15.812	87.036
0.66	0.66	1465.655	542.699	2008.354	0.800	15.820	87.039
1	0.66	1465.018	543.275	2008.294	0.799	15.849	87.038
0	0.33	1463.245	510.566	1973.811	0.362	50.403	87.041
0.33	0.33	1462.311	549.020	2011.331	0.799	15.860	87.169
0.66	0.33	1470.710	541.483	2012.193	0.800	15.839	87.205
1	0.33	1470.436	544.316	2014.752	0.800	15.839	87.315
0	0	1462.906	497.502	1960.408	0.200	63.198	87.015
0.33	0	1465.004	547.893	2012.897	0.799	15.853	87.236
0.66	0	1464.688	547.783	2012.471	0.799	15.881	87.219
1	0	1465.393	546.973	2012.367	0.800	15.807	87.211

Table 7.3: Effect of ESFC tuning on total energy cost.

For settings $C_1 = 1$ and $C_2 = 0.66$, the total energy cost is essentially identical for settings $C_1 = 0$ and $C_2 = 0$, even though for the former settings the battery is only used up for 20%. In this case the battery is used until the constraint on SOC is satisfied: SOC between 20% and 80%. Afterwards the battery is charged and discharged to maintain an 80% state of charge. This is highlighted in the SOC trajectories shown in Figure 7.7.

The state of charge trajectory of the simulation with settings $C_1 = 1$ and $C_2 = 0.33$ nicely show that having a high cap, works as an incentive to charge the battery. However, the optimizer is only able to charge the battery up to 80%, as implemented through a constraint. Comparing SOC trajectories of the of $C_1 = 0$ and $C_2 = 0.33$ and $C_1 = 0$ and $C_2 = 0$ it shows that the C_2 influence the rate of discharge of the battery. It can therefore influence the slope of the SOC trajectory. It also highlights that a more advanced ESFC tuning procedure would be valuable. For instance when ESFC is SOC based the incentives change with the SOC, and the SOC trajectory would not be so linear. Therefore, for implementation in real-life scenarios it is recommended to make more complex ESFC maps that take into account the SOC, estimated time of arrival, or the long-term predicted shaft power demand.

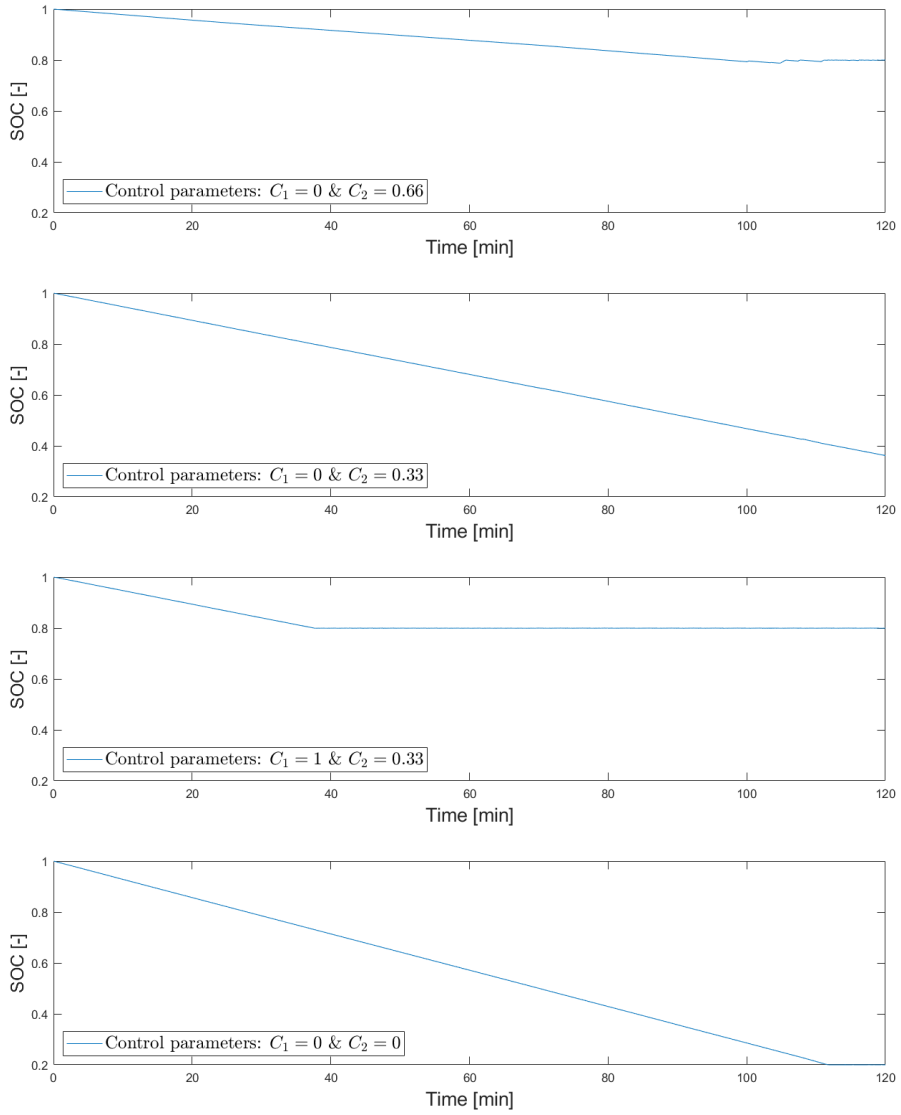

Figure 7.7: Simulation Results of ESFC tuning: SOC trajectories

7.4. Model verification

Some simple tests were performed to show model verification; it shows that the model has been implemented correctly. The checks are presented in Table 7.4.

Nr.	Test	Expected outcome	Result
1.	$P_{sh} = P_{IM} + P_{DE}$	Equality	✓
2.	$\dot{m}_f(k) = \sum_{i=1}^{2} \dot{m}_{f,DE_i}(k) + \sum_{i=1}^{3} \dot{m}_{f,DG_i}(k) + \dot{m}_{f,BAT}(k)$	Equality	✓
3.	$P_{DG,tot,d}(k) = P_{DG,tot,s}(k)$	Equality	✓
4.	$0 \leq SOC(k) \leq 1$	Bounded	✓
5.	Correct non-linear constraint $I_{BAT_{min}}(k)$ & $I_{BAT_{max}}(k)$	Bounded	✓
6.	Operating envelopes engines	Bounded	✓
7.	Correct minimums found for prediction horizon of 1 timestep	Conversion	✓

Table 7.4: verification tests performed on the controller.

These particular checks have been chosen to check the correctness of implementation of the system

dynamics (tests 1-3), constraints (tests 4-6), and correct conversion to the optimal solution (test 7). The results to tests 1-6 were verified graphically and numerically by tracking data during optimization procedures and ensuring these system dynamics and constraints were adhered to. Test number 7 was done by hand for various data points of various setpoints of shaft speed. Optimization could only be verified for a prediction horizon of 1 timestep as the complexity of the verification increases rapidly with increasing size of the prediction horizon. In Figure 8.2 it can be seen that the propulsive power demand is always met by the sum of the induction machine and diesel engine power. Also the diesel generator power and battery power always equate the requested electric power.

7.5. Conclusion

The controller is optimization based using an ECMS (determined in RQ1) and utilizes a power load forecasting tool with RNN methodology (determined in RQ3). The controller designed in this chapter is able to incorporate the use of the battery as an equivalent fuel consumption in the optimization problem. The controller correctly provides the system with an optimal power split between induction machine and diesel engines (Hybrid propulsion). It is also able to find an optimal split for the hybrid power supply; between the battery and the diesel generator-sets. Due to implementation of constraints of the diesel generator-sets individual setpoints for the generators are possible. Additionally, through constraints on the SOC between 20% and 80% the battery is operating at a favourable setpoint, which could prolong battery life. The energy management strategy is evaluated for fuel efficiency in the next chapter.

8

Results & Discussion

In this chapter the performance of the energy management strategy is evaluated and discussed. Afterwards an analysis is given on the influence of the battery size on the total fuel savings.

8.1. Results

The results can be split into four comparative parts, namely:

- Optimization at every timestep for a prediction horizon of 3 seconds.
- Optimization using a trigger
- Optimization with 'perfect knowledge', prediction horizon of 48 seconds with 3 timesteps.
- Optimization with shaft power predictions using RNN, prediction horizon of 48 seconds with 3 timesteps.

The first set of results are when optimizing at every timestep, and using those results for only 1 timestep. The second set of results use a trigger. The trigger tells the controller when a new optimization cycle should begin, until it does, the last setpoints for the engines are maintained. The trigger used in this project is a change in shaft power demand of more than 5% compared to the last optimization cycle or a change in state of charge of more than 5% compared to the last optimization cycle. When an optimization trigger is used it greatly diminishes the effect of the short-term prediction tool. This is because the trigger works on a larger time-scale than the short-term predictions. So where the predictions work in the order of seconds, the trigger works in the order of minutes.

The third set of results show the performance of the controller with a prediction horizon of 48 seconds with acausal knowledge. The controller will have future knowledge on the shaft power in the present, making this an acausal optimization. This result is included as a comparison to the causal set of results. And finally, the fourth set of results show the performance of the controller with a prediction horizon of 48 seconds using power load forecasting with the RNN described in the previous chapter. For the methods using 48 seconds prediction horizon, 3 timesteps are optimized for, namely for t in range [t, t+24, t+48]. For these simulations every 30 seconds a new optimization cycle is initiated. 30 seconds is chosen in accordance with the computation times of the controller on the researcher's laptop. This way, the simulations can be considered as a real-time EMS.

The results in Table 8.1 show that the total energy cost for the four sets of results are almost the same. This is not surprising as in all cases the exact same energy was demanded. So naturally, a very similar amount of energy is going to be expended in order to deliver the required power. Two factors are contributing to the fact that there are no energy cost reductions for the controller when using a prediction horizon. (1) The prediction horizon is short-term, in the order of seconds. It is easy to see that predictions of long-term trends in power demand, would allow the use of the battery to be far more efficient. In those cases the battery can be charged when it is expected that the battery is going to be needed in the future. Instead, battery charging and discharging for short-term load predictions is purely decided on short-term trends. Given the variance in the data of the shaft power, the charging and

discharging in the short-term becomes quite random. Also, since the control horizon of the controller is not executed completely, but instead works with a receding horizon, sometimes sub-optimal setpoints are used as decision variable setpoints. (2) The capacity of the battery, which is 400 kW, is very small compared to the overall power demand. A larger battery capacity would allow more versatility in the use of the battery; it could take over the function of the diesel generator-sets, rather than take over 40% of one diesel generator-set. The effect of the battery on fuel savings is discussed in detail in the next section.

Simulation	Fuel consumption [kg]			Energy battery		Total energy cost [GJ]
	Main engines	Diesel generator sets	Total	$SOC_{t_{end}}$	Equivalent cost [kg]	
1	1462.906	497.502	1960.408	0.200	63.198	87.015
2	1487.794	473.122	1960.916	0.186	64.346	87.086
3	1521.679	470.425	1992.104	0.344	51.856	87.890
4	1516.185	478.354	1994.540	0.382	48.790	87.863

Table 8.1: Simulation results: fuel and energy consumption.

The triggered optimization (simulation 2), and the optimization for simulations with prediction horizon (simulation 3 and 4), do not optimize at every timestep. This means that the shaft power demand at each timestep is also not met exactly. This is nicely highlighted in Figure 8.3, Figure 8.4 and Figure 8.5. Therefore, it is possible that the EMS is delivering slightly more or less power than demanded on the timesteps where an optimization routine did not occur. The MAPE and Mean Percentage Error (MPE) for the four simulations are shown in Table 8.2. It shows the percentage errors for these simulations. A negative MPE indicates that an excess amount of energy was delivered on average. When the total energy cost presented in Table 8.1 is adjusted for the excess delivered energy, the adjusted total energy cost is calculated. This number merely indicates that had all the energy been delivered correctly at the right times, a lower amount of energy would have been needed. Of course this number does not say much, as the excess delivered energy was delivered at the wrong times. In the case of simulation 4, which uses the RNN for shaft power demand forecasting, the prediction accuracy also play a role in incorrectly delivered amount of energy, as the predicted shaft power demand is not exactly equal to the actual desired shaft power.

Simulation	MAPE [%]	MPE [%]	Adjusted total energy cost [GJ]
1	0.00	0.00	87.015
2	1.08	-0.16	86.946
3	3.04	-0.62	87.345
4	5.65	-2.23	85.842

Table 8.2: Error values of the delivered versus requested total shaft power. Adjusted total energy cost based on the MPE.

The SOC trajectories of the four sets of results are shown in Figure 8.1. The trajectories indicate a similar battery use in all simulation; The battery use is relatively cheap compared to the diesel generators, and is therefore used consistently. For simulation 3 and 4 occasionally the battery is charged. For these cases given a control horizon of 48 seconds, charging the battery led to a lower objective function value and was deemed the optimal solution. However, due to the short-term predictions, and short-term control horizon of the controller, longer-term trends were not identified and taken into account, and an overall lower fuel consumption of the EMS could not be achieved in these simulations. It should be noted that simulation 1 has better performance in part due to the ESFC tuning of the battery, which was performed on this particular operational profile. Given more time in the project, it would have been valuable to perform these simulations on a wide array of operational profiles, thus capturing more accurately the true behaviour and power demand of the ship. Regardless, looking at the results of the ESFC tuning, in Table 7.3, the total energy cost is lower for whichever setting of the ESFC, compared to the simulations with the control horizon of 48 seconds. This means that the error in power delivery when not optimizing every timestep is more dominant, compared to fuel savings by ESFC tuning. Given

a larger battery capacity, the dominance of errors will shift to the ESFC tuning.

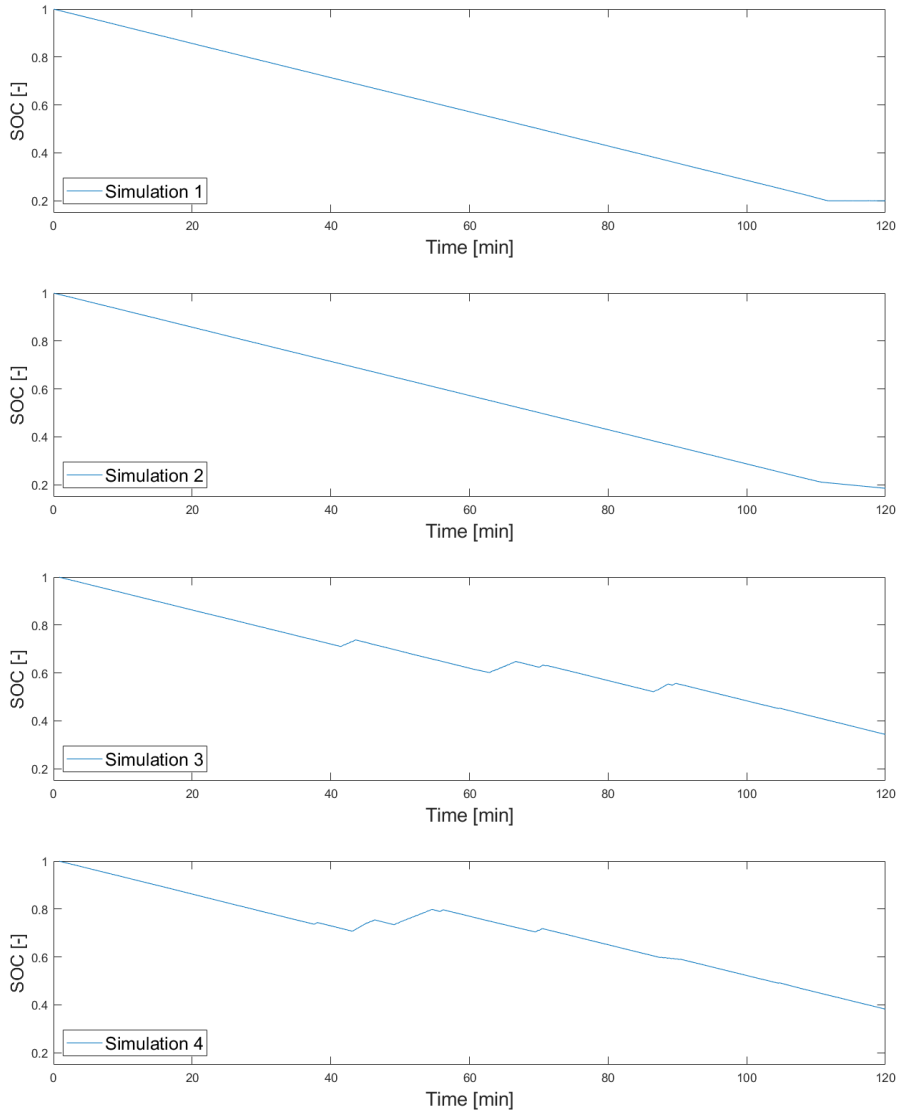

Figure 8.1: SOC trajectories of the four simulations

In Figure 8.2, Figure 8.3, Figure 8.4 and Figure 8.5 the trajectories for the input (shaft power demand) is shown, confronted with the indirect decision variables of induction machine power and diesel engine power for the four simulations. The power of the machines are shown rather than the torque setpoint for the induction machine, since induction machine power is easier to confront with the input shaft power demand, since they are in the same units. Similarly, the electric power demand is confronted with the battery- and diesel generator- power setpoints. The power setpoints are shown rather than the current setpoint of the battery, to be able to show the same units between comparative variables. Thus in these graphs are shown the 5 decision variables for the diesel generators, battery, induction machine and diesel engine, as well as the reference values for the shaft power demand.

For simulation 1 where every timestep the controller re-optimizes, the variable trajectories are shown in Figure 8.2. It shows that at each timestep the shaft power and electric power is met by the engines, motors, generators and battery. The first graph shows the hybrid propulsion: It shows that for lower power requirements the controller prefers the induction machine over the diesel engine. When induction machine cannot deliver all the power at a low-power setpoint the remaining energy is supplemented by the diesel engine. The second graph shows the electric power demand of the ship, and highlights the hybrid power supply behaviour of the vessel. Battery setpoints lower than 0 indicate charging of

the battery, and it can be seen that in those cases, the diesel generator delivers more energy than is demanded by the induction machines and the auxiliary power. It can be seen that in cases where the shaft power is slightly more than what is deliverable by the induction machine, the controller has trouble finding the optimal solution. This is the case because using the induction machine fully, supplementing it with a slight amount delivered by the diesel engines, is very close to the same objective function value as when using the diesel engine alone for that amount of energy.

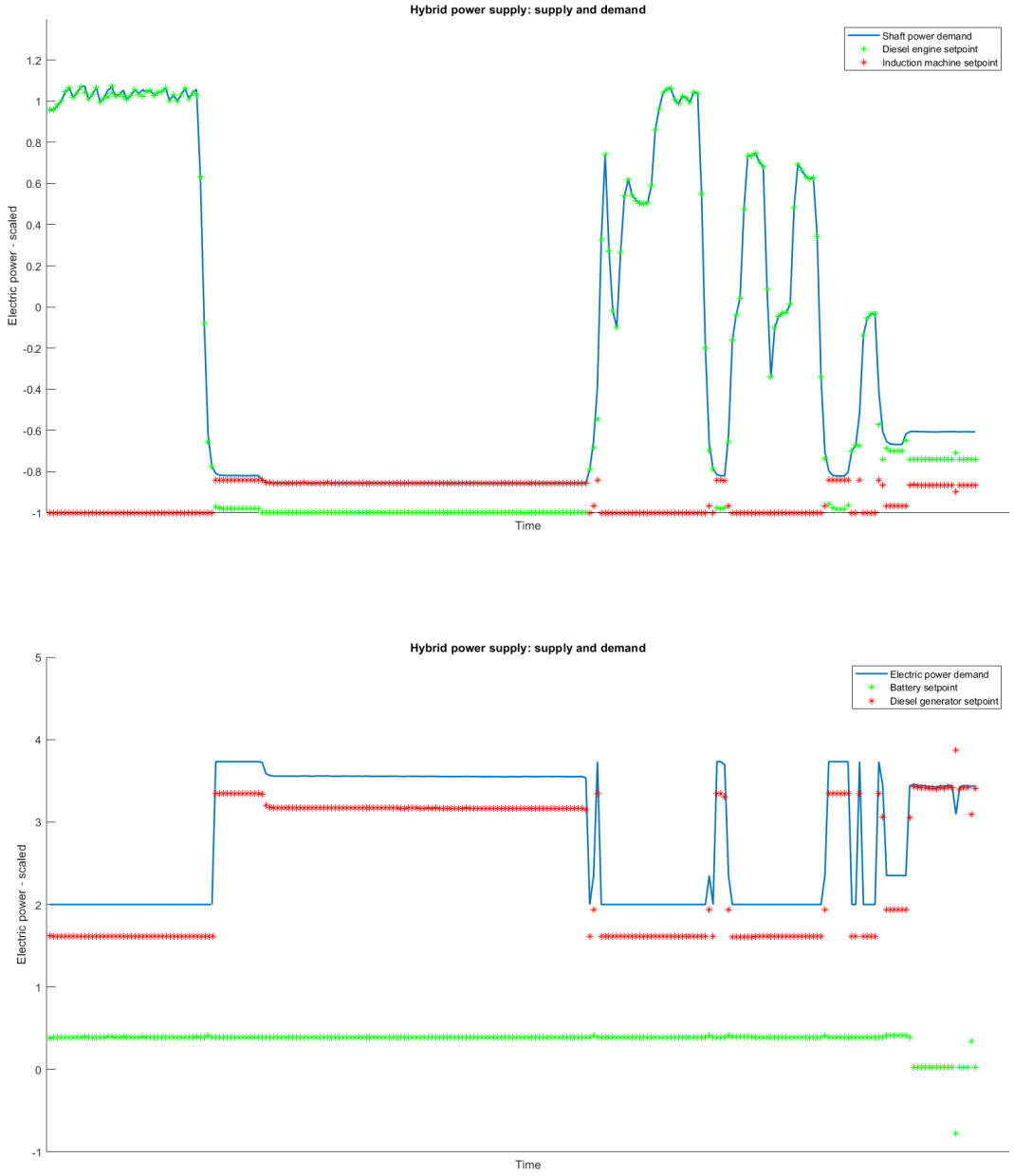

Figure 8.2: Propulsive- and electric power demand and supply. Results are for simulation 1.

Simulations 2, 3 and 4 show that not exactly the correct amount of shaft power is delivered at every timestep. But it does show that these amounts are very close to the correct values. For simulation 2, which uses the triggered optimization procedure, it can be seen that the setpoints for the engines are very similar to simulation 1. From this, it can be deduced that triggered optimization works well.

Simulation results 3 and 4 use a prediction horizon with three timesteps and have therefore 15 decision variables rather than just 5. Because of this, the exact optimal solution is not always found. Rather, an optimum close to the global optimum is reached. This leads to some variance in the battery setpoints and the diesel generator setpoints. Additionally, two first two sets of 5 decision variables (for the first two timesteps) are executed before another optimization cycle begins. The small variance in setpoints of the battery and diesel generators are not a problem. However, sometimes a different solution is found, which is still close to the global optimum, but which indicates a different strategy. This is the case where the battery is charged rather than discharged. In this case charging the battery over a control horizon leads to an objective function value very close to the discharging the battery over the same control horizon. For the reason, sometimes, a switch between these two strategies is noticed. The way to solve this problem is to fine-tune the solver settings more precisely to a control horizon of 48 seconds and three timesteps. Additionally, the tuning of the ESFC curve for the battery should also be done for a control horizon rather than for a single timestep. In this way more optimized results can be found. Unfortunately, for this research, due to time constraints these suggestions can not be incorporated.

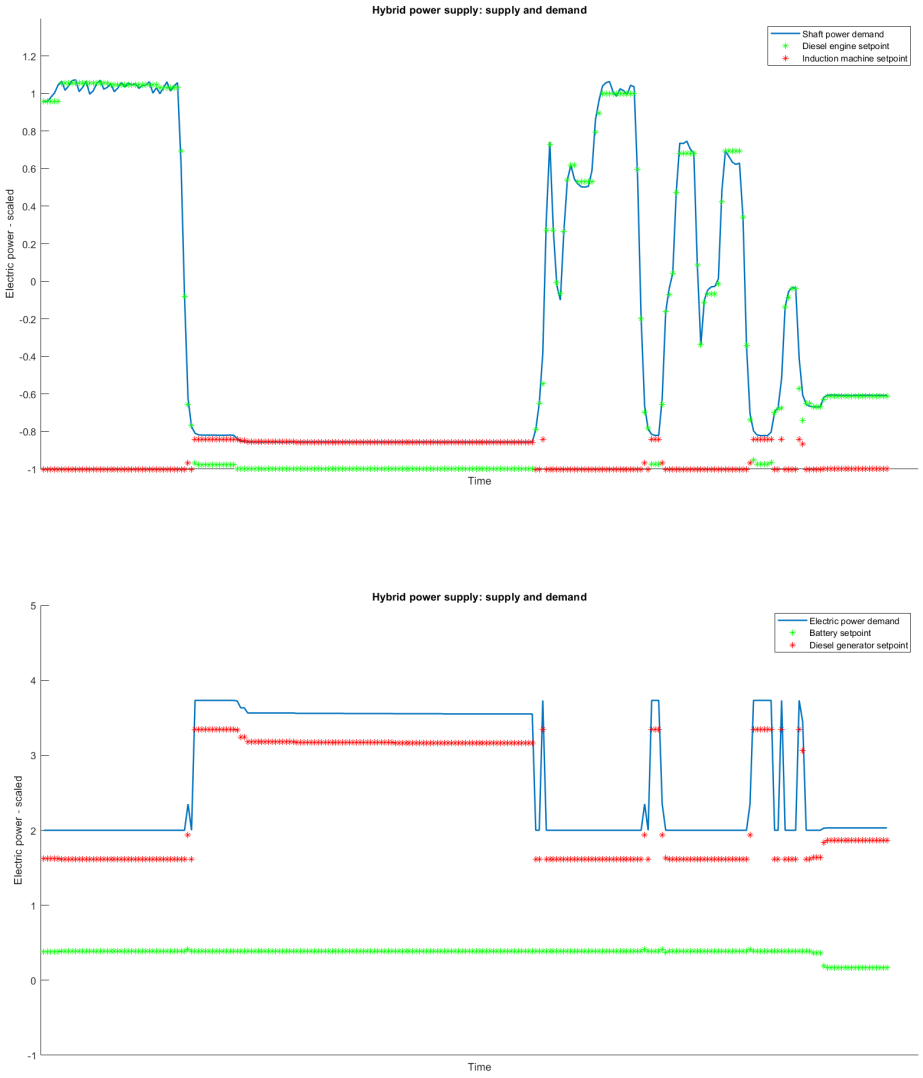

Figure 8.3: Propulsive- and electric power demand and supply. Results are for simulation 2.

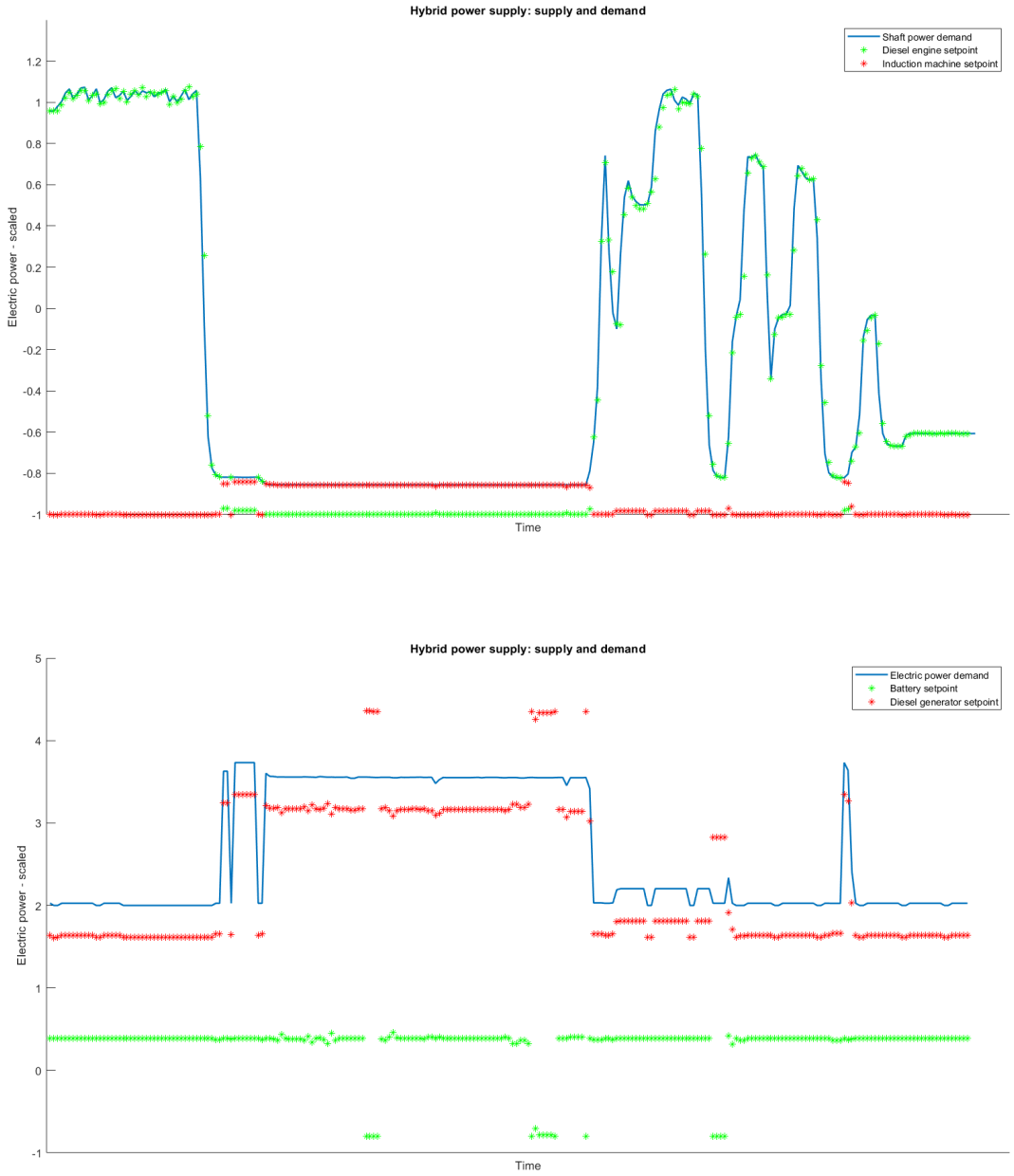

Figure 8.4: Propulsive- and electric power demand and supply. Results are for simulation 3.

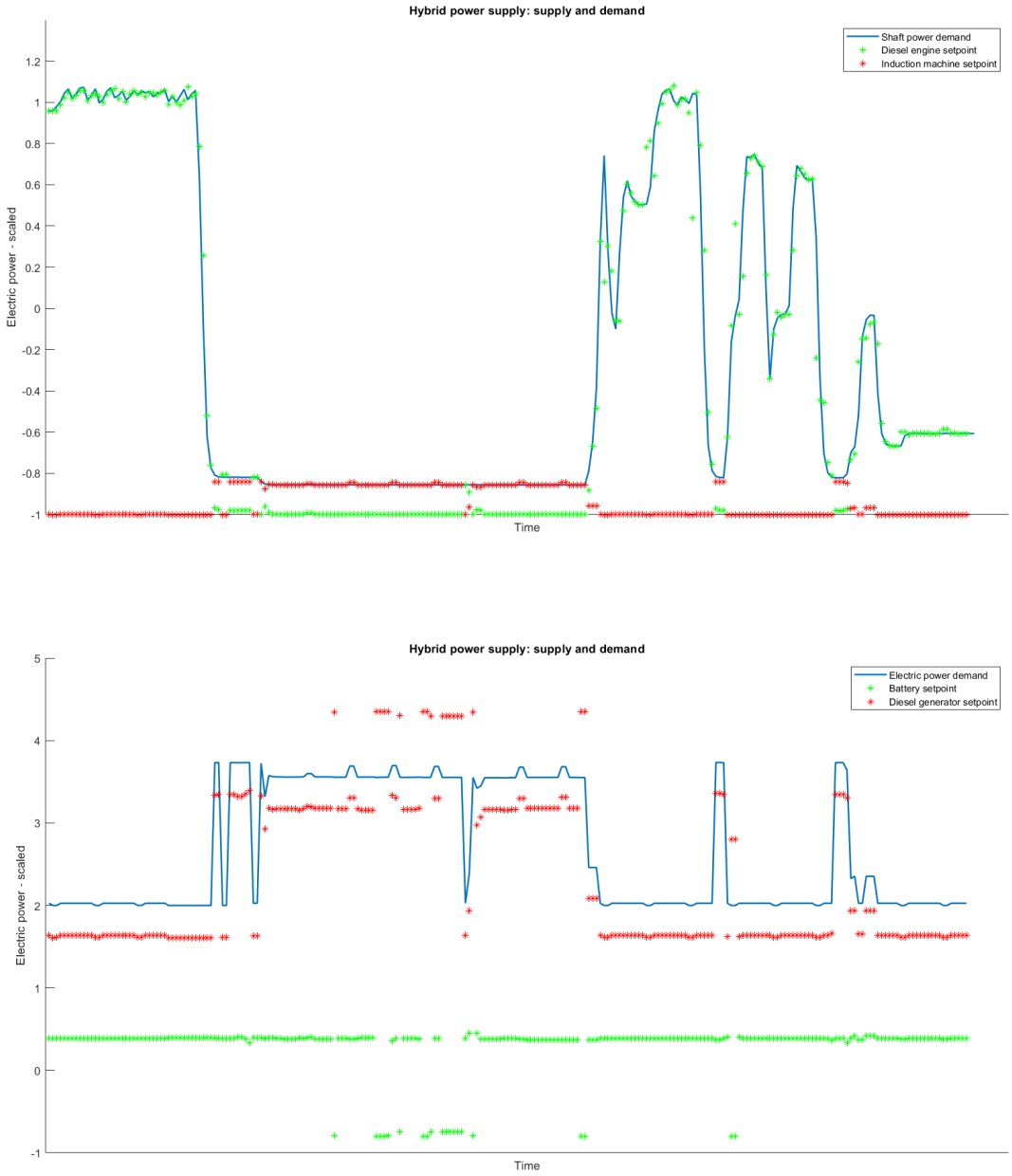

Figure 8.5: Propulsive- and electric power demand and supply. Results are for simulation 4.

8.2. Battery effectiveness

As a point of discussion the effectiveness of the battery is discussed here. It is one the main contributing factors of for the lack of fuel savings, and is therefore worthwhile to explore further. The influence of the battery on the total fuel consumption can be estimated using four simple ratios. The first ratio, R_1, indicates the share of electric power, P_{el}, of the total power demand, P_{tot}, at a given time for the ship. In the case of the Holland-class offshore patrol vessel the maximum energy demand is summing the maximum power of the two diesel engines (5400 kW), the three diesel generators (968kW), and the battery (400 kW). The induction machine is accounted for through the power supply to the machine.

The electric power is the summation of the diesel generators and the battery.

$$R_1 = \frac{P_{el}}{P_{tot}} = \frac{3304}{14104} = 0.23 \tag{8.1}$$

The second ratio, R_2, indicates the share of the electric power delivered by the battery, P_{bat} .

$$R_2 = \frac{P_{bat}}{P_{el}} = \frac{400}{3304} = 0.12 \tag{8.2}$$

The third ratio, R_3, shows the relative fuel savings of using the battery compared to the average specific fuel consumption of the diesel generators, $sfc_{DG,avg}$. The average setpoint for the diesel generators determined through simulations - without using the battery - is around $sfc_{DG,avg} = 210$ [g/kWh]. With the assumption that the cost of charging the battery is 195 [g/kWh], which is considered a favourable setpoint of the diesel generator, the associated specific fuel consumption cost of the battery, sfc_{bat}, becomes 195 [g/kWh].

$$R_3 = \frac{\mathrm{sfc}_{DG,avg} - \mathrm{sfc}_{bat}}{\mathrm{sfc}_{DG,avg}} = \frac{210 - 195}{210} = 0.07 \tag{8.3}$$

Also, by using the battery, the average setpoints of the diesel generator are pushed to a more favourable setpoint, fuel savings achieved this way have not been accounted for yet. This can be captured in an additional ratio, R_4.

$$R_4 = \frac{\mathrm{sfc}_{DG,avg} - \mathrm{sfc}_{DG,avg,new}}{\mathrm{sfc}_{DG,avg}} = \frac{210 - 202}{210} = 0.04 \tag{8.4}$$

The ratios can be combined to show the overall battery effectiveness. It shows the battery's effectiveness at reducing the total fuel consumption of the ship. In this example with the particular operating profile the estimated battery influence on total fuel consumption is 0.3%. Thus if the battery is used optimally, it should be able to reduce the fuel consumption with 0.3%. To refine the estimations more simulation with varying operating profiles should be run to get an estimation for the R_1, R_3 and R_4 values. Due to time constraints of the project, these values could not be estimated more precisely.

$$R_{eff} = R_1 \cdot R_2 \cdot (R_3 + R_4) = 0.23 \cdot 0.12 \cdot (0.07 + 0.04) = 0.003 \tag{8.5}$$

The four ratios are easily influenced by various factors, and the example above is merely an indication for one particular example. The influencing factors on the ratios are shown in Table 8.3. R_1 is heavily influenced by the operating profile and the power demand scenarios that occur. The ratio as calculated above shows the total electric share of power of the total possible power demand. In reality a varying partial total load is delivered and a varying electric load. If the vessel is in electric mode, thus using the induction machines with the diesel engines off, then the ratio R_1 is much higher, namely $R_1 = 1$. Alternatively, in diesel mode with a lower hotel load, leads to a lower R_1 value. If a midway setpoint for the diesel engines is assumed then the ratio is $R_1 = 0.38$. If the size of the induction machines were to be increased, the likelihood of a larger share of electric power increases as well. Of course changing induction machine size is a design consideration, and should not simply be considered to increase the effectiveness of the battery.

R_2 is effected by the battery size compared to the total power deliverable by the diesel generators. If a large battery is chosen that is able to take over the job of all three generators then the ratio is $R_2 = 1$. Alternatively, if a battery is chosen that can at least take over the job of one diesel generator, the ratio is $R_2 = 0.33$. This nicely, highlights that the choice of battery size has a large influence of the total effectiveness of the battery at reducing fuel consumption.

R_3 and R_4 are effected by the operating profile of the vessel and the various power demand scenarios that occur. It could be the case for instance that the combination of the hotel load and induction machines pushes the setpoints for the diesel generators to very unfavourable setpoints. If this is the case, the use of the battery is felt more in the fuel savings. However, if the operating profile indirectly already facilitates relatively favourable setpoints for the diesel generators, then the effect of the battery diminishes. Secondly, the cost of the battery can be effected by the charging procedure. If the battery is charged more efficiently on shore, an idea to influence R_3 is to implement shore charging, and optimizing the equivalent fuel map to deplete the battery by the time the vessel operation ends. Alternatively,

if the battery is charged on-board the battery cost is most likely done at the most favourable setpoint of the diesel generators.

Ratio	Influencing factor
R_1	(1) Operating profile (2) Size of induction machines
R_2	(1) Size of the battery (2) Size of the diesel generators
R_3	(1) Operating profile (2) Charging cost of battery
R_4	Operating profile

Table 8.3: Influencing factors on battery-effectiveness ratios.

It should be noted that the ratios do not take into account the state of charge of the battery. Therefore, these ratios assume the battery power is available. With no battery power available the battery's effectiveness naturally goes to zero.

To show the effect of the 400 kW battery compared to a no-battery scenario two simulation have been run. The simulation with the battery uses the optimal battery fuel map determined in the previous chapter. The results are shown in Table 8.4. From this example it can be shown that fuel savings of 0.77% are achieved. The reason for more fuel savings are achieved as estimated by the ratios, is because R_1 and R_2 are undervalued; A larger share of the total energy is electric, and a larger share is provided by the battery, since not all diesel generators are in operation all the time.

Simulation	Fuel consumption [kg]			Energy battery		Total energy cost [GJ]
	Main engines	Diesel generator sets	Total	$SOC_{t_{end}}$	Equivalent cost [kg]	
Battery (optimal)	1462.906	497.502	1960.408	0.200	63.198	87.015
No battery	1406.035	633.238	2039.273	1.000	0.000	87.689

Table 8.4: Effect of implementing a 400 kW on total fuel consumption.

9

Conclusion

Hybrid propulsion is a promising technology to reduce the environmental footprint of the vessel. It combines the use of mechanical and electrical propulsion, as such, it is able to operate efficiently at a multitude of operational setpoints. Hybrid power supply uses two or more types of power sources to provide electrical power to the propulsive system. For instance, power supply combinations such a battery and diesel generator-sets are quite common. The combination of the hybrid power supply allows for the efficient use of the diesel generator-sets. An energy management system is required to effectively operate the complex systems of hybrid propulsion and hybrid power supply systems. For that reason, in this research an energy management system is developed for a hybrid propulsion and hybrid power supply vessel. The EMS is developed through a case study of the Holland-class offshore patrol vessel. The EMS consists of three main pillars, namely, the powertrain model, shaft power forecasting model, and the controller. The powertrain model was provided through Damen and TU Delft, and was not appended in this project.

Four shaft power forecasting models were developed in the course of this research. The methodologies of linear regression, moving average, ARIMA and RNN were applied. The former three of these methods are univariate methods. Due to the limited data features available, these methods were employed. The linear regression model is able to predict accurately for up to 18 seconds, showing a MAPE of 4.25%. The moving average improved on the performance of the linear regression model and is able to accurately predict 27 seconds in the future, with a MAPE of 4.67%. In order to capture the variance of the shaft power an ARIMA model was applied also. However, due to occasional divergence of the ARIMA model it proved an unreliable prediction tool for the purpose of shaft power prediction. It was only able to accurately predict the shaft power for 3 seconds in the future with a MAPE of 3.28%. In order to improve on the performance of the univariate methods, synthetic data was generated and the additional data features were used to train an RNN. The RNN is able to predict the shaft power 48 seconds in the future while maintaining a MAPE of 4.78%. It should be noted that these predictions were made using real shaft power data, which shows high and irregular variance, and is therefore more difficult to predict. Unfortunately, a prediction horizon of 48 seconds is not enough for the purpose of an energy management system. To effectively make use of the hybrid power supply, medium to long-term predictions are required; in the order of minutes to hours.

The controller is optimization-based using an equivalent consumption minimization strategy. The designed controller is able to incorporate the use of the battery as an equivalent fuel consumption (ESFC) in the optimization problem. The ESFC is tuned for a two hour operating profile. The controller correctly provides the system with an optimal power split between induction machine and diesel engines (Hybrid propulsion). It is also able to find an optimal split for the hybrid power supply; between the battery and the diesel generator-sets. Due to implementation of constraints on the diesel generator-sets, individual setpoints for the generators are possible. Additionally, through constraints on the SOC between 20% and 80% the battery is operating at a favourable setpoint, which could prolong battery life. Four simulation studies were performed in the research to test and compare the effectiveness of the EMS. (1) Optimization at every timestep. (2) Triggered optimization, when a significant change (5%) occurs in SOC or shaft power demand. (3) Non-causal optimization for a prediction horizon of 48 seconds with 3 timesteps in the prediction horizon. (4) Optimization for a prediction horizon of

48 seconds with 3 timesteps in the prediction horizon, using RNN predicted shaft power reference values. The total fuel consumption and SOC trajectories of the 4 simulations are almost identical. The SOC trajectories indicate the battery use, and the fuel consumption indicates the efficiency of the EMS. Energy fuel reduction could not be proven. Given the parameters of the case study this is not surprising: (a) There is limited data availability leading to short-term predictions, and (b) a small battery capacity, leading to limited usefulness of the hybrid power supply system. Short-term predictions and control horizons are not sufficient to effectively utilize the hybrid power supply of the system. A small battery leads to limited effectiveness of the EMS even if long-term predictions were possible; The battery can only take over a fraction of the function of one diesel generator-set.

The effect of battery size on the effectiveness of the battery to reduce fuel consumption is analytically captured by four ratios. The ratios indicate (1) the share of electric power with respect to the total power, (2) the share of electric power that can be delivered by the battery, (3) the fuel savings the battery can provide by taking over the function of the diesel generator, and (4) fuel savings achieved by the battery by pushing the diesel generator setpoint to a more favourable set point. Ratio 2 shows that the battery size influences directly the effectiveness of the battery to reduce fuel savings. With a simulation, reduction of 0.77% of total energy consumption was shown with the implementation of a 400kW battery.

9.1. Future works

Future research has a multitude of directions to focus on. First, incorporation of medium to long-term shaft power demand prediction tools can be developed, this can improve the performance of the energy management strategy presented in this research. This would require more data features and possibly other prediction methodology. Secondly, design and control could be viewed as an inter-correlated problem; for instance, in this research the small battery capacity was a limiting factor in the usefulness of the hybrid power supply system. Therefore, with this EMS as a guideline it could be developed alongside the design phase of a hybrid power supply and hybrid propulsion system. Thirdly, the equivalent specific fuel consumption map of the battery can be greatly improved upon. It can be made to be SOC, ETA and forecasted power demand dependant. If this were to be paired with long-term predictions it would form a powerful energy management system capable of saving significant fuel cost. Fourthly, the objective function in the EMS can be further elaborated to incorporate soft constraints on emissions, variability of battery current, and variability of the diesel power. Fifthly, rather than solely focusing on replacing the short-term predictions with medium or long-term predictions, a second layer of control could be designed for medium or long-term control. This long-term prediction layer would be less accurate, but would focus on capturing major trends. This requires a lot of data, and a somewhat regular operating profile of the vessel. Finally, the effect of the battery size on the fuel consumption savings can be studied.

9.2. Practical applicability

The energy management system (EMS) provided in this research is able to incorporate the use of the battery as an equivalent fuel consumption in the optimization problem. The EMS correctly provides the system with an optimal power split between induction machine and diesel engines (Hybrid propulsion). It is also able to find an optimal split for the hybrid power supply; between the battery and the diesel generator-sets. Due to implementation of constraints on the diesel generator-sets, individual setpoints for the generators are possible. Which allows for use of particular diesel generator-sets to dedicated subsystems of the ship. Additionally, through constraints on the SOC between 20% and 80%, the battery is operating at a favourable setpoint, which could prolong battery life. Reduction of energy fuel consumption could not be proven given the parameters of the case study: (a) limited data availability leading to short-term predictions, and (b) a small battery capacity, leading to limited usefulness of the hybrid power supply system. 0.77% fuel savings were proven in a limited simulation where a hybrid power supply system with a 400kW is compared to a diesel generator power supply system. With a larger battery size, more fuel savings can be expected. However, this is to be proven with more research and more simulations that represent the power profile of the ship better. Furthermore, to increase the usefulness of the hybrid power supply, and electric mode of the vessel, it is recommended to find an optimal pairing of control and powertrain design. For instance, increasing the battery and induction machine sizes, while at the same time taking into account their effects on fuel savings via

an EMS. With the development of medium to long-term load prediction tools the energy management system can prove to save on energy consumption also. However, long term load prediction is infeasible for variable, unpredictable load demand.

Bibliography

[1] Yijie Zhang et al. “Two-level model predictive control energy management strategy for hybrid power ships with hybrid energy storage system”. In: *Journal of Energy Storage* 52 (2022), p. 104763. ISSN: 2352-152X. DOI: https://doi.org/10.1016/j.est.2022.104763. URL: https://www.sciencedirect.com/science/article/pii/S2352152X22007733.

[2] Qiang Wang and Xue Yang. “Imbalance of carbon embodied in South-South trade: Evidence from China-India trade”. In: *Science of The Total Environment* 707 (2020), p. 134473. ISSN: 0048-9697. DOI: https://doi.org/10.1016/j.scitotenv.2019.134473. URL: https://www.sciencedirect.com/science/article/pii/S004896971934464X.

[3] Hulda Winnes, Linda Styhre, and Erik Fridell. “Reducing GHG emissions from ships in port areas”. In: *Research in Transportation Business & Management* 17 (2015). Energy Efficiency in Maritime Logistics Chains, pp. 73–82. ISSN: 2210-5395. DOI: https://doi.org/10.1016/j.rtbm.2015.10.008. URL: https://www.sciencedirect.com/science/article/pii/S2210539515000590.

[4] R.D. Geertsma et al. “Design and control of hybrid power and propulsion systems for smart ships: A review of developments”. In: *Applied Energy* 194 (2017), pp. 30–54. ISSN: 0306-2619. DOI: https://doi.org/10.1016/j.apenergy.2017.02.060. URL: https://www.sciencedirect.com/science/article/pii/S0306261917301940.

[5] Jinyoung Ko et al. “Comparative investigation of NOx emission characteristics from a Euro 6-compliant diesel passenger car over the NEDC and WLTC at various ambient temperatures”. In: *Applied Energy* 187 (2017), pp. 652–662. ISSN: 0306-2619. DOI: https://doi.org/10.1016/j.apenergy.2016.11.105. URL: https://www.sciencedirect.com/science/article/pii/S0306261916317366.

[6] Nikolaos Planakis, George Papalambrou, and Nikolaos Kyrtatos. “Predictive power-split system of hybrid ship propulsion for energy management and emissions reduction”. In: *Control Engineering Practice* 111 (2021), p. 104795. ISSN: 0967-0661. DOI: https://doi.org/10.1016/j.conengprac.2021.104795. URL: https://www.sciencedirect.com/science/article/pii/S0967066121000721.

[7] Bijan Zahedi, Lars E. Norum, and Kristine B. Ludvigsen. “Optimized efficiency of all-electric ships by dc hybrid power systems”. In: *Journal of Power Sources* 255 (2014), pp. 341–354. ISSN: 0378-7753. DOI: https://doi.org/10.1016/j.jpowsour.2014.01.031. URL: https://www.sciencedirect.com/science/article/pii/S0378775314000469.

[8] Omer Berkehan Inal, Jean-Frédéric Charpentier, and Cengiz Deniz. “Hybrid power and propulsion systems for ships: Current status and future challenges”. In: *Renewable and Sustainable Energy Reviews* 156 (2022), p. 111965. ISSN: 1364-0321. DOI: https://doi.org/10.1016/j.rser.2021.111965. URL: https://www.sciencedirect.com/science/article/pii/S1364032121012302.

[9] A. Sciarretta et al. “A control benchmark on the energy management of a plug-in hybrid electric vehicle”. In: *Control Engineering Practice* 29 (2014), pp. 287–298. ISSN: 0967-0661. DOI: https://doi.org/10.1016/j.conengprac.2013.11.020. URL: https://www.sciencedirect.com/science/article/pii/S0967066113002323.

[10] Amam EE Breijs A. “Energy management – adapt your engine to every mission.” In: *Proceedings of the 13th international naval engineering conference* 2 (2016), pp. 1–8.

[11] M. Kalikatzarakis et al. “Ship energy management for hybrid propulsion and power supply with shore charging”. In: *Control Engineering Practice* 76 (2018), pp. 133–154. ISSN: 0967-0661. DOI: https://doi.org/10.1016/j.conengprac.2018.04.009. URL: https://www.sciencedirect.com/science/article/pii/S096706611830090X.

[12] Lino Guzzella and Antonio Sciarretta. *Vehicle Propulsion Systems*. Springer Berlin Heidelberg, 2013. DOI: 10.1007/978-3-642-35913-2. URL: http://dx.doi.org/10.1007/978-3-642-35913-2.

[13] K.E. Bailey, S.R. Cikanek, and N. Sureshbabu. "Parallel hybrid electric vehicle torque distribution method". In: *Proceedings of the 2002 American Control Conference (IEEE Cat. No.CH37301)*. Vol. 5. 2002, 3708–3712 vol.5. DOI: 10.1109/ACC.2002.1024504.

[14] P. Bowles, H. Peng, and X. Zhang. "Energy management in a parallel hybrid electric vehicle with a continuously variable transmission". In: *Proceedings of the 2000 American Control Conference. ACC (IEEE Cat. No.00CH36334)*. Vol. 1. 6. 2000, 55–59 vol.1. DOI: 10.1109/ACC.2000.878771.

[15] K.L. Butler, M. Ehsani, and P. Kamath. "A Matlab-based modeling and simulation package for electric and hybrid electric vehicle design". In: *IEEE Transactions on Vehicular Technology* 48.6 (1999), pp. 1770–1778. DOI: 10.1109/25.806769.

[16] Fabio Massimo Frattale Mascioli et al. "Optimization of Hybrid Electric Cars by Neuro-Fuzzy Networks". In: *Applications of Fuzzy Sets Theory*. Ed. by Francesco Masulli, Sushmita Mitra, and Gabriella Pasi. Berlin, Heidelberg: Springer Berlin Heidelberg, 2007, pp. 253–260. ISBN: 978-3-540-73400-0.

[17] Hyeoun-Dong Lee et al. "Torque control strategy for a parallel-hybrid vehicle using fuzzy logic". In: *IEEE Industry Applications Magazine* 6.6 (2000), pp. 33–38. DOI: 10.1109/2943.877838.

[18] Niels J Schouten, Mutasim A Salman, and Naim A Kheir. "Energy management strategies for parallel hybrid vehicles using fuzzy logic". In: *Control Engineering Practice* 11.2 (2003). Automotive Systems, pp. 171–177. ISSN: 0967-0661. DOI: https://doi.org/10.1016/S0967-0661(02)00072-2. URL: https://www.sciencedirect.com/science/article/pii/S0967066102000722.

[19] E.A. Sciberras and R.A. Norman. "Multi-objective design of a hybrid propulsion system for marine vessels". In: *IET Electr Syst Transp* 2 (July 2012), pp. 148–157. DOI: 10.1049/iet-est.2011.0011.

[20] Atriya Biswas et al. "Comparison of Three Real-Time Implementable Energy Management Strategies for Multi-mode Electrified Powertrain". In: *2020 IEEE Transportation Electrification Conference & Expo (ITEC)*. 2020, pp. 514–519. DOI: 10.1109/ITEC48692.2020.9161549.

[21] G-Q Ao et al. "Fuel economy and NO_x emission potential investigation and trade-off of a hybrid electric vehicle based on dynamic programming". In: *Proceedings of the Institution of Mechanical Engineers, Part D: Journal of Automobile Engineering* 222.10 (Oct. 2008), pp. 1851–1864. DOI: 10.1243/09544070jauto644. URL: https://doi.org/10.1243/09544070jauto644.

[22] Olivier Grondin et al. "Energy management strategy for Diesel hybrid electric vehicle". In: Oct. 2011, pp. 1–8. DOI: 10.1109/VPPC.2011.6043132.

[23] Thanh Long Vu et al. "Power Management for Electric Tugboats Through Operating Load Estimation". In: *IEEE Transactions on Control Systems Technology* 23.6 (2015), pp. 2375–2382. DOI: 10.1109/TCST.2015.2399440.

[24] Yijie Zhang et al. "Two-level model predictive control energy management strategy for hybrid power ships with hybrid energy storage system". In: *Journal of Energy Storage* 52 (2022), p. 104763. ISSN: 2352-152X. DOI: https://doi.org/10.1016/j.est.2022.104763. URL: https://www.sciencedirect.com/science/article/pii/S2352152X22007733.

[25] Ali Haseltalab, Rudy R. Negenborn, and Gabriel Lodewijks. "Multi-Level Predictive Control for Energy Management of Hybrid Ships in the Presence of Uncertainty and Environmental Disturbances**This research is supported by the project ShipDrive: A Novel Methodology for Integrated Modelling, Control, and Optimization of Hybrid Ship Systems (project 13276) of the Dutch Technology Foundation STW." In: *IFAC-PapersOnLine* 49.3 (2016). 14th IFAC Symposium on Control in Transportation SystemsCTS 2016, pp. 90–95. ISSN: 2405-8963. DOI: https://doi.org/10.1016/j.ifacol.2016.07.016. URL: https://www.sciencedirect.com/science/article/pii/S2405896316302129.

[26] Nikolaos Planakis, George Papalambrou, and Nikolaos Kyrtatos. “Predictive power-split system of hybrid ship propulsion for energy management and emissions reduction”. In: *Control Engineering Practice* 111 (2021), p. 104795. ISSN: 0967-0661. DOI: https://doi.org/10.1016/j.conengprac.2021.104795. URL: https://www.sciencedirect.com/science/article/pii/S0967066121000721.

[27] Y. Si et al. “Configuration optimization and energy management of hybrid energy system for marine using quantum computing”. English. In: *Energy* 253 (2022). Cited By :1. URL: www.scopus.com.

[28] Divyajot, Rajesh Kumar, and Manoj Fozdar. “Optimal sizing of hybrid ship power system using variants of particle swarm optimization”. In: *2017 Recent Developments in Control, Automation & Power Engineering (RDCAPE)*. 2017, pp. 527–532. DOI: 10.1109/RDCAPE.2017.8358327.

[29] Bin Wang et al. “Adaptive mode switch strategy based on simulated annealing optimization of a multi-mode hybrid energy storage system for electric vehicles”. In: *Applied Energy* 194 (2017), pp. 596–608. ISSN: 0306-2619. DOI: https://doi.org/10.1016/j.apenergy.2016.05.030. URL: https://www.sciencedirect.com/science/article/pii/S0306261916306249.

[30] M.A. Ancona et al. “Efficiency improvement on a cruise ship: Load allocation optimization”. In: *Energy Conversion and Management* 164 (2018), pp. 42–58. ISSN: 0196-8904. DOI: https://doi.org/10.1016/j.enconman.2018.02.080. URL: https://www.sciencedirect.com/science/article/pii/S0196890418301973.

[31] Lianghong Wu et al. “Multiobjective Optimization of HEV Fuel Economy and Emissions Using the Self-Adaptive Differential Evolution Algorithm”. In: *IEEE Transactions on Vehicular Technology* 60.6 (2011), pp. 2458–2470. DOI: 10.1109/TVT.2011.2157186.

[32] Yongbing Xiang and Xiaomin Yang. “An ECMS for Multi-Objective Energy Management Strategy of Parallel Diesel Electric Hybrid Ship Based on Ant Colony Optimization Algorithm”. In: *Energies* 14.4 (2021). ISSN: 1996-1073. DOI: 10.3390/en14040810. URL: https://www.mdpi.com/1996-1073/14/4/810.

[33] S. Kim and J. Kim. “Optimal energy control of battery hybrid system for marine vessels by applying neural network based on equivalent consumption minimization strategy”. English. In: *Journal of Marine Science and Engineering* 9.11 (2021). Cited By :1. URL: www.scopus.com.

[34] Yi Lu Murphey et al. “Intelligent Hybrid Vehicle Power Control—Part II: Online Intelligent Energy Management”. In: *IEEE Transactions on Vehicular Technology* 62.1 (2013), pp. 69–79. DOI: 10.1109/TVT.2012.2217362.

[35] Ryuta Moriyasu et al. “Diesel engine air path control based on neural approximation of nonlinear MPC”. In: *Control Engineering Practice* 91 (2019), p. 104114. ISSN: 0967-0661. DOI: https://doi.org/10.1016/j.conengprac.2019.104114. URL: https://www.sciencedirect.com/science/article/pii/S0967066119301303.

[36] seaforces. *Holland class Offshore Patrol Vessel / OPV*. URL: https://www.seaforces.org/marint/Netherlands-Navy/Offshore-Patrol-Vessel/Holland-class.htm.

[37] Ministerie van Defensie. *Zr.ms. Groningen*. Mar. 2020. URL: https://www.defensie.nl/organisatie/marine/eenheden/schepen/zr.-ms.-groningen.

[38] *Damen*. URL: https://products.damen.com/en/ranges/opv-holland-class/holland-class-ocean-going-patrol-vessel-3750/deliveries/opv-3750-friesland.

[39] R.D. Geertsma et al. “Pitch control for ships with diesel mechanical and hybrid propulsion: Modelling, validation and performance quantification”. In: *Applied Energy* 206 (2017), pp. 1609–1631. ISSN: 0306-2619. DOI: https://doi.org/10.1016/j.apenergy.2017.09.103. URL: https://www.sciencedirect.com/science/article/pii/S0306261917313855.

[40] Robin John Hyndman and George Athanasopoulos. *Forecasting: Principles and Practice*. English. 2nd. Australia: OTexts, 2018.

[41] D.G. Lainiotis and Konstantinos Plataniotis. “Neural network estimators: application to ship position estimation”. In: Jan. 1994, 4710–4717 vol.7. ISBN: 0-7803-1901-X. DOI: 10.1109/ICNN.1994.375037.

[42] D.G. Lainiotis et al. “Neural network application to ship position estimation”. In: Nov. 1993, I384–I389 vol.1. ISBN: 0-7803-1385-2. DOI: 10.1109/OCEANS.1993.325979.

[43] Lizhu Hao et al. “Recurrent neural networks for nonparametric modeling of ship maneuvering motion”. In: *International Journal of Naval Architecture and Ocean Engineering* 14 (2022), p. 100436. ISSN: 2092-6782. DOI: https://doi.org/10.1016/j.ijnaoe.2022.100436. URL: https://www.sciencedirect.com/science/article/pii/S2092678222000024.

[44] José del Águila Ferrandis et al. *Learning functionals via LSTM neural networks for predicting vessel dynamics in extreme sea states*. Dec. 2019.

[45] Yuchao Wang et al. “Multi-dimensional prediction method based on Bi-LSTMC for ship roll”. In: *Ocean Engineering* 242 (2021), p. 110106. ISSN: 0029-8018. DOI: https://doi.org/10.1016/j.oceaneng.2021.110106. URL: https://www.sciencedirect.com/science/article/pii/S002980182101430X.

[46] Gabriel Khoury et al. “Including core losses in induction motors dynamic model”. In: *2016 3rd International Conference on Renewable Energies for Developing Countries (REDEC)*. 2016, pp. 1–6. DOI: 10.1109/REDEC.2016.7577556.

[47] Mukund R Patel. *Shipboard propulsion, power electronics, and ocean energy*. Boca Raton, FL: CRC Press, Feb. 2012.

[48] R. Stapersma and J. Bosklopper. “Fuel efficiency of diesel, electric and superconductive propulsion systems.” In: *In Proc. 10th INEC* (2010).

[49] Yong Tian et al. “Comparison Study on Two Model-Based Adaptive Algorithms for SOC Estimation of Lithium-Ion Batteries in Electric Vehicles”. In: *Energies* 7.12 (2014), pp. 8446–8464. ISSN: 1996-1073. DOI: 10.3390/en7128446. URL: https://www.mdpi.com/1996-1073/7/12/8446.

[50] O. Erdinc, B. Vural, and M. Uzunoglu. “A dynamic lithium-ion battery model considering the effects of temperature and capacity fading”. In: *2009 International Conference on Clean Electrical Power*. 2009, pp. 383–386. DOI: 10.1109/ICCEP.2009.5212025.

[51] Lijun Gao, Shengyi Liu, and R.A. Dougal. “Dynamic lithium-ion battery model for system simulation”. In: *IEEE Transactions on Components and Packaging Technologies* 25.3 (2002), pp. 495–505. DOI: 10.1109/TCAPT.2002.803653.

[52] J Klein Woud and D Stapersma. *Design of propulsion and electric power generation systems*. Undefined/Unknown. IMarEST, 2002. ISBN: 1-902536-47-9.

[53] M. Godjevac et al. “Evaluation of losses in maritime gearboxes”. In: *Proc IMechE, Part M: J Eng Marit Environ* (2015). Cited By :3, pp. 1–16. URL: www.scopus.com.

[54] Beukelman W. Gerritsma J. “Analysis of the resistance increase in waves of a fast cargo ship.” In: *International Shipbuilding Progress* 19.217 (1972), pp. 285–293. DOI: 10.3233/ISP-1972-1921701.

[55] Dan Margalit and Joseph Rabinoff. *Interactive Linear Algebra*. 2019. URL: https://textbooks.math.gatech.edu/ila/.

[56] David Swanson. *UC Riverside UC Riverside Previously Published Works Title On the Relationship among Values of the same Summary Measure of Error when used across Multiple Characteristics at the same point in time: An Examination of MALPE and MAPE Journal Author Publication Date*. 2015. URL: https://escholarship.org/content/qt1f71t3x9/qt1f71t3x9.pdf?t=o5wul1.

[57] Denis Kwiatkowski et al. “Testing the null hypothesis of stationarity against the alternative of a unit root: How sure are we that economic time series have a unit root?” In: *Journal of Econometrics* 54.1 (1992), pp. 159–178. ISSN: 0304-4076. DOI: https://doi.org/10.1016/0304-4076(92)90104-Y. URL: https://www.sciencedirect.com/science/article/pii/030440769290104Y.

[58] D. Dickey and Wayne Fuller. “Distribution of the Estimators for Autoregressive Time Series With a Unit Root”. In: *JASA. Journal of the American Statistical Association* 74 (June 1979). DOI: 10.2307/2286348.

[59] “Book Reviews”. In: *Journal of the American Statistical Association* 83.403 (1988), pp. 902–926. DOI: 10.1080/01621459.1988.10478680. eprint: https://doi.org/10.1080/01621459.1988.10478680. URL: https://doi.org/10.1080/01621459.1988.10478680.

[60] Frederick S. Hillier. *Introduction to operations research*. McGraw-Hill Education, 2021.

[61] Jorge Nocedal and Stephen J. Wright. *Numerical optimization*. Springer, 2006.

[62] Kok S Ong, Liben Jiang, and Koon C Lai. “4.20 Thermoelectric Energy Conversion”. In: *Comprehensive Energy Systems*. Elsevier, 2018, pp. 794–815.

Appendix A

Optimal Control Energy Management Strategy for Hybrid Propulsion and Power Supply Vessels using Data-Driven Load Forecasting

Simeon Slagter [a,*]

[a] Department of Maritime & Transport Technology, Delft University of Technology, The Netherlands

Abstract—Hybrid technology could significantly reduce fuel consumption and emission for vessels that have high power demand peaks followed by long periods of low loading. Hybrid technology refers to powertrain layouts that consist of hybrid propulsion and/or hybrid power supply. Advanced energy management strategies (EMS) are required to make optimal use of these available power resources. In this paper it is investigated how much fuel consumption reduction can be achieved by applying a causal, real-time equivalent consumption minimization strategy (ECMS) to a hybrid propulsion and hybrid power supply plant with a power load forecasting scheme, for a case study vessel: The Holland-class offshore patrol vessel. The forecasting tools evaluated are Linear regression, moving average, ARIMA and recurrent neural networks (RNN). The RNN outperformed the other methods and is able to predict the power demand for up to 48 seconds, while maintaining a mean absolute percentage error of under 5%. An optimization-based controller is combined with an ECMS approach which assigns an equivalent consumption cost to the battery. The controller is able to identify the power split for the hybrid propulsive system, and the power split for the hybrid power supply. A simulation proved that 0.77% fuel savings are achieved with a 400 kW battery, compared to a no-battery scenario. Fuel savings could not be proven for the EMS with a control horizon of 48 seconds, leveraging power predictions supplied by the RNN, due to limiting factors. The limiting factors are the combination of the small control horizon, the limited battery capacity compared to the overall power demand and the limited tuning of the ESFC curve.

Index Terms — Energy management system · Propulsion control · Hybrid vehicles · Marine systems · Hybrid energy supply

1 Introduction

At present, ocean shipping facilitates 80% of the transportation of global trade [1]. The shipping industry is only expected to grow, and this development is naturally paired by a multitude of environmental problems. The increased carbon and nitrogen oxides (NO_x) emissions resulting from the increased shipping demand is one of these problems [2]. In fact, the shipping industry is one of the fastest growing industries with regard to greenhouse gas emissions [3]. To combat the ever-increasing emissions, regulations have been put in place and are expected to become more stringent over time. Currently, there are restrictions on the weighted cycle NO_x emissions for diesel engines with an output of more than 130 kW [4]. In future, it is expected that there will not only be restrictions on engine specific NO_x emissions but on NO_x emissions per mile also [5]. Additionally, new ships are expected to adhere to a specific Energy Efficiency Design Index (EEDI) [4]. This index is a measure of CO2 emissions of a cargo vessel per mile or per tonne of goods. Given these restrictions as well as the increasing price of energy, it is imperative that the propulsion and power generation plants of ships have ways of reducing fuel consumption and emissions.

For vessels that have high power demand peaks as well as long periods of low loading, hybrid technology could significantly reduce fuel consumption and emissions [6]. Hybrid technology refers to powertrain layouts that consist of hybrid propulsion: a combination of mechanical and electrical propulsion, and/or hybrid power supply: a combination of combustion power supply and energy storage, found mostly in combination with electric propulsion [4]. The hybrid propulsion and power supply powertrains are able to reduce fuel consumption and emissions by 10% to 35% [4]. Advanced energy management strategies (EMS) are required to make optimal use of the available power resources onboard the vessel. The EMS determines setpoints for the engines, motors and energy storage devices, and in this way prescribes the power split between mechanical and electric propulsion as well as the split between combustion power supply and energy storage.

. * Damen Naval provided funding for this research.

1.1 Literature review

In [4] the various powertrain topologies of ships are classified, as well as the control strategies employed for these respective topologies. These different topologies are all the combinations between mechanical and electric drive, coupled with various types of power supply. The control strategies of relevance to this research are the EMSs that have been developed for topologies with hybrid power supplies. These developed control strategies can be classified as heuristic control strategies or optimization-based control strategies [7].

Two common implementation approaches for heuristic control are the map-based and rule-based approaches. In the map-based approach [8, 9, 10], the output setpoints of the EMS are determined by mapped control set points for different speeds and torque request points by the operator. Different maps can be established for a high and low state of charge as well. In some other methods [11, 12, 13], these map

regions are not rigid and can instead be defined using other methodologies such as fuzzy logic. Various articles have presented implementation of rule-based controllers. For instance, [14] presents a control strategy that uses the batteries at low speeds for propulsion rather than the engine, and at higher speeds the battery can electrically assist the engine. The article shows that the strategy is able to reduce fuel consumption, and that these savings are proportional to the battery capacity.

Optimization-based control uses performance indexes, that is either minimized or maximised. The most common and simplest performance index is the fuel mass consumed over a period of time [15]. Rather than just taking into account the fuel mass consumption in the performance index, pollutants can also be incorporated [16, 17]. In the Equivalent Consumption Minimisation Strategy (ECMS), an optimal control problem is formulated that minimises the fuel consumption of the engine and the equivalent fuel consumption of a battery. [18] shows that ECMS can approximate the fuel economy of acausual controllers, with a computationally cheap process and limited calibration of control parameters. [19] proves the effectiveness of ECMS as an EMS in automotive industry, as it outperformed heuristic control. This control method performs particularly well compared to other strategies when the operating profile is not known beforehand. Fuel savings of up to 10% were shown in [20] while using the ECMS strategy compared to rule-based logic. In [6], 6% fuel savings were achieved in a simulation study of a tugboat, with unknown load demand.

To further improve the performance of an optimization-based controller load predictions schemes can be incorporated. The load predictions methods anticipate future load demand based on historical load demand data. Short-term trends (order of seconds) can often be identified and predicted reasonable accurate, where-as long-term trends (order of minutes to hours) are difficult. For this reason [21] designed the two-level MPC; To have accurate short-term predictions and control, combined with capturing a less accurate but broader trend of power consumption in the long-term. [22] also uses MPC to account for future power demand, while also taking into account environmental disturbances and uncertainties. [23] shows that a 9% improvement on the cost function performance compared to the rule-based control of [14] can be achieved by predicting the load.

Of the methods mentioned in this literature review very few have been specifically applied for hybrid propulsion & hybrid energy supply (HPHPS) systems [6, 1, 14]. [1] presents an EMS for a hybrid energy supply leveraging power load forecasting, however, hybrid propulsion was not considered. [14] does consider a HPHPS system but only for optimal powertrain design purposes, and not for an energy management system. [6] considers an optimization-based controller for a HPHPS system using ECMS. However, the method leveraged a limited power load forecasting scheme to further enhance the performance of the EMS. Therefore, what is currently missing is the implementation and evaluation of an energy management systems for HPHPS systems leveraging state-of-the-art power load forecasting methods.

1.2 Aim and contribution

In this paper it is investigated how much fuel consumption reduction can be achieved by applying a causal, real-time ECMS to a hybrid propulsion and hybrid power supply plant with a power load forecasting scheme. The effect of the battery on the fuel savings is evaluated also. A case study vessel is used with a hybrid propulsion and hybrid power supply topology, namely, the Holland-class offshore patrol vessel (HCOPV), as shown in Figure 1.

The contribution of the research is twofold. First, a power load forecasting method is developed using recurrent neural networks (RNN) for varying operating profiles. The performance of the RNN is contrasted with the performance of the linear regression, moving average and ARIMA methods for power load forecasting. Second, a novel online optimization-based controller with a receding horizon principle leveraging predicted load demand is developed. The optimization-based controller is combined with an ECMS approach which assigns an equivalent consumption cost to the battery. The method is evaluated for operations with and without a battery.

1.3 Outline

This paper is organised as follows: section 2 gives the system description and information about the case study. section 3 describes the methodology applied for the load forecasting tools, the EMS methodology and the optimization problem. The results are shown in section 4, the discussion in section 5, and finally the conclusion is given in section 6.

2 System description

In this research a case study of the Holland-class offshore patrol vessel is used. The ship is a hybrid propulsion ship. In this study the benefit of adding a battery, to create a hybrid power supply system, is evaluated for the case study. The powertrain topology of the powertrain is shown in Figure 1.

The propulsion system is made up of two diesel engines and two electric motors. The diesel engines are 4-stroke diesel engines with a power of 5400 kW each, with a rated speed of 1000 rpm. The electric motors have a power of 400 kW each. The gears combine a diesel engine and a electric motor to drive a controllable pitch propeller on each of the two shafts. The vessel has 3 generator sets of 968 kW each and one emergency generator set of 255 kW, combining for a total of 4 [24]. The system has various hotel loads such as air-conditioning, lights, and water-cooling systems, these auxiliary loads are assumed to be constant. The size of the auxiliary loads are not described in the public domain, and will therefore not be states here. The selected battery has a capacity of 400 kWh, and allows 1c charging and discharging, therefore, the maximum power the battery can deliver is 400 kW. Due to limited space availability on the HCOPV, a larger battery size can not be accommodated by the vessel infrastructure.

3 Methods

An overview of the EMS structure is given in Figure 2. The information that is known at the start of an iteration

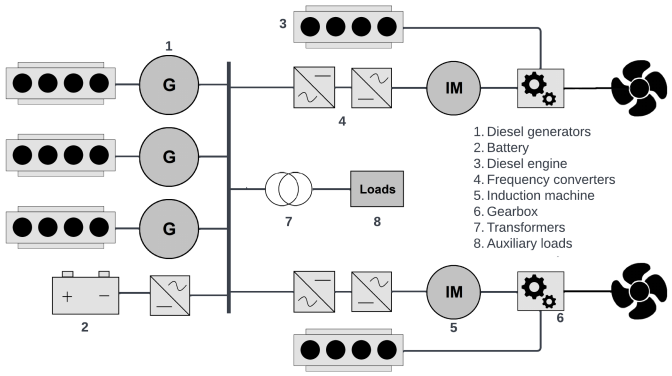

Figure 1: Powertrain of the Holland-class offshore patrol vessel, augmented with a battery.

is the operator setpoint for the shaft power, $P_{sh}(k)$. Based on the shaft power setpoint the operator setpoint for the vessel speed, $v_{set}(k)$, is assumed. It is assumed that the setpoints of shaft power and vessel speed are proportional. Based on the vessel speed setpoint the speed setpoints for the diesel engines, $n_{set}^{DE}(k)$, and induction machines, n_{set}^{IM}, are inferred.

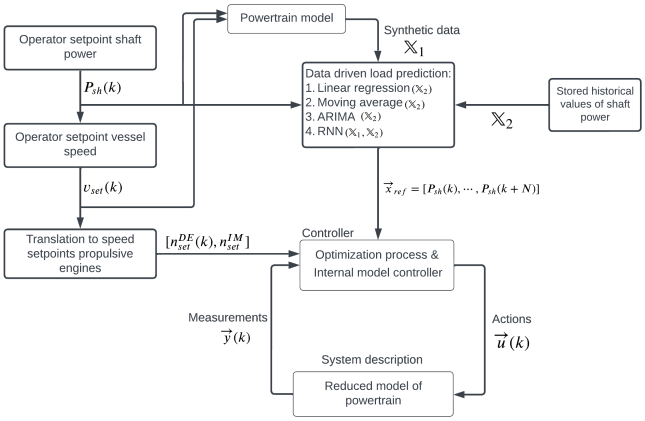

Figure 2: Overview of the energy management system structure.

The physical system is described by a powertrain model of the Holland-class offshore patrol vessel. This powertrain model is a mathematical representation that shows the dynamics of the components of the powertrain of the ship. The models chosen are selected based on availability, and accuracy. The models are made available in an adaptive pitch control framework, the framework is presented in [25, 6]. To operate this framework multiple controllers are required to maintain setpoints for the engines and motors and propeller pitch. It is outside the time limits and scope of this research to use this full model to evaluate the novel energy management strategy developed in this research as it would involve re-tuning multiple controllers. Instead, in this project the powertrain model is used in order generate synthetic data. The set of synthetic data features, $\mathbb{X}_1$, is used by the RNN load prediction method.

The controller is an optimization-based control tool. It uses reduced models of the powertrain as the internal model of the controller, in order to evaluate which set of decision variables will work best in order to minimize fuel consumption. The internal model of the controller has the purpose of modelling the relationship between power, torque and and specific fuel consumption of diesel engines, diesel generators and induction machines. Additionally, an artificial fuel consumption model is established for the battery. Based on the internal model of the controller, the optimizer is able to find a set point for the engines and battery. The speed setpoints for the induction machines and diesel engines, as well as the measurement variables, $\overrightarrow{y}(k)$, are used as input by the controller. The output is a set of decision variables , $\overrightarrow{u}(k)$, that minimizes fuel consumption of a prediction horizon with N steps. The internal model of the controller is described in subsection 3.1.

$\mathbb{X}_1$	Data description
x_1	Main engine shaft speed in [rpm]
x_2	Pitch ratio
x_3	Propeller torque M_p in [Nm]
x_4	Propeller thrust T_p in [N]
x_5	Vessel speed v_s in [knots]

Table 1: Generated synthetic data features.

To evaluate the output of the controller a reduced model of the powertrain model is used. In fact this model is the same as the internal model of the controller. The full powertrain model could not be used here, since in order to operate this full model multiple extra controllers for pitch control, engine control and induction machine control are required. Due to time constraints and the scope of the project, this is not possible to implement. Therefore, the reduced model is used to evaluate the output and recorded the measurement variables $\overrightarrow{y}(k)$.

Four data-driven load prediction tools are developed with four different methodologies. The focus in this research, however, is on the RNN. The RNN model is selected since it has proven to have excellent predictive capabilities in a multitude of fields. In the maritime domain the method is used for ship position estimations [26, 27], non-parametric modeling of ship maneuvering motion [28], as well as pitch, heave and roll motion predictions [29, 30]. The other three methods are univariate methods; Linear regression, moving average and ARIMA are used as a comparative measure for the RNN performance. Due to the shape of the operating profiles, as shown in Figure 4, and limited data availability of ship features, univariate prediction methods are used to predict the load demand. All four methods use historical data on the shaft power, $\mathbb{X}_2$, to predict future shaft power demand. The RNN also uses the set of synthetic data features, $\mathbb{X}_1$. The synthetic data features are shown in Table 1. The total input space for the RNN is $\mathbb{X} = \mathbb{X}_1 \cup \mathbb{X}_2$. The output to the prediction tools are reference values for the expected shaft power demand over a prediction horizon with N steps. The reference values are denoted by $\overrightarrow{x}_{ref}$. The reference values are used by the controller to make decisions over the prediction horizon. The input-output relationships for the RNN is shown in Figure 3, where P_{sh} is the shaft power demand. The input-output relationships of the univariate methods are the same, with the exclusion of the input space $\mathbb{X}_1$.

The univariate methods use a moving time window of data in $[t-\Delta^-, t-1]$ and estimate a linear regression model,

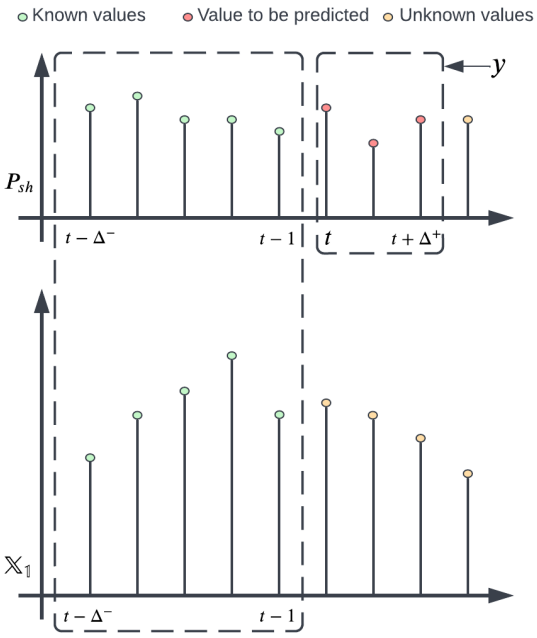

Figure 3: Input-output relationship for the Recurrent neural network.

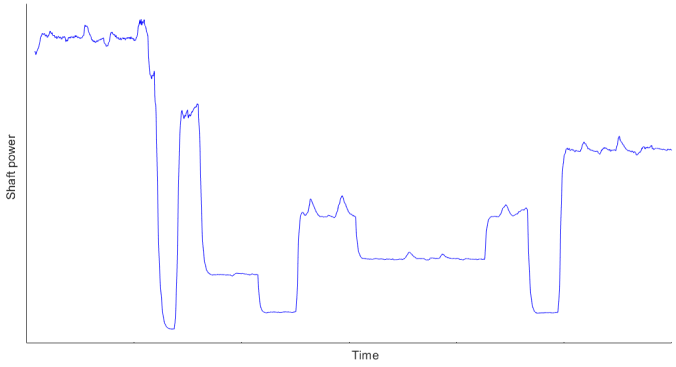

Figure 4: Operational profile of the Holland-class offshore patrol vessel.

moving average model and an ARIMA model, which is then used to compute Δ^+ seconds ahead, in time window $[t, t+\Delta^+]$. The RNN method trains a generalized model, the trained model is then used for all future load forecasting. Model selection parameters considered for the univariate methods are Δ^- and Δ^+. ARIMA also has the model selection parameters p,d, and q which signify the order of the auto-regressive, differencing and moving average parts of the model respectively. For the exact functions and implementation used for the forecasting methods, the interested reader is referred to [31] for the linear regression, ARIMA model and moving average, and [32] for the RNN. For the RNN model selection parameters considered are number of neurons, activation functions, optimizers, optimizer settings, number of epochs, batch size and Δ^- and Δ^+. Using 5-fold cross validation an optimal set of hyperparameters is found. A long-short term memory scheme is applied in conjunction with the RNN to solve the vanishing and exploding gradient problem while using large sequence of data.

As a point of comparison Figure 5 summarizes the performance of the four methods: Linear regression, moving average, ARIMA, and RNN. It shows the Mean absolute percentage error (MAPE) over an increasing prediction horizon. It highlights that the RNN outperforms the other methods, and is able to predict further in the future while maintaining a MAPE of under 5%. In Figure 6 the trend in time for the four methods is shown. It highlights that the ARIMA method has large outliers, and that the RNN method performs worse in cases of large variances in shaft power. Overall the RNN performs best, being able to predict 48 seconds in the future while maintaining a MAPE of less than 5%.

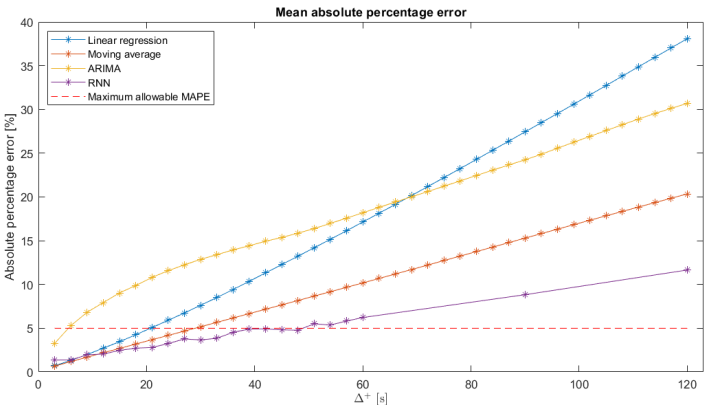

Figure 5: Mean absolute percentage error for the linear regression, moving average, ARIMA, and recurrent neural network.

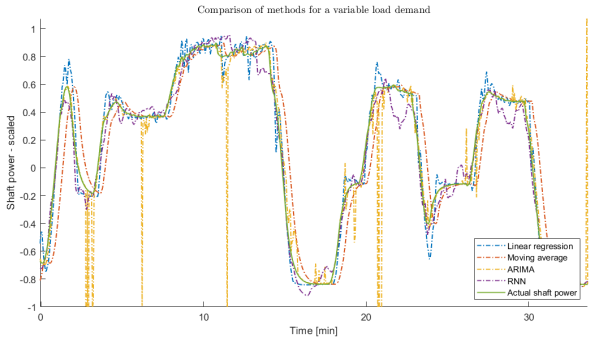

Figure 6: A section of the trend in time (actual versus predicted) shaft power for the linear regression, moving average, ARIMA, and recurrent neural network.

3.1 Energy Management System

The energy management strategy proposed in this paper determines the power split between the main engines and the induction machines (hybrid propulsion), and between the diesel generators and the battery (hybrid power supply). The speed setpoints for the propulsion machines are determined based on the operator vessel speed setpoint. The power setpoint for the main engines and induction machine is established by the controller through the decision variable $T_{IM,set}$, the torque setpoint of the induction machine. The setpoint for the main engine can be derived from this setpoint. The speed setpoint for the diesel generators is assumed to be fixed with the network electrical frequency at 60 Hz. The power setpoints for the battery and generators are established through individual decision variables for each diesel generator $P_{DG,i}$ $\forall i \in [1,3]$, and a current

setpoint for the frequency converter of the battery $I_{BAT,set}$. Thus, the set of decision variables, $\overrightarrow{u}(k)$, for a prediction horizon of N steps, is:

$$\overrightarrow{u}(k) = \begin{bmatrix} T_{IM,set}(k) \\ I_{BAT,set}(k) \\ P_{DG,i}(k) \\ ... \\ T_{IM,set}(k+N) \\ I_{BAT,set}(k+N) \\ P_{DG,i}(k+N) \end{bmatrix}.$$

The aim of the strategy is to minimise fuel consumption over a receding horizon. The objective function that achieves this is:

$$\underset{\overrightarrow{u}(k)}{min} \; J = \sum_{k=1}^{N} \dot{m}_f(k) \tag{1}$$

where $\dot{m}_f(k)$ is the total fuel consumption in timestep k. The fuel consumption is a function of the fuel consumption of the diesel engines $\dot{m}_{f,DE_i}(k)$, diesel generators $\dot{m}_{f,DG_i}(k)$ and the equivalent fuel consumption of the battery $\dot{m}_{f,BAT}(k)$. Mathematically, this is:

$$\dot{m}_f(k) = \sum_{i=1}^{2} \dot{m}_{f,DE_i}(k) + \sum_{i=1}^{3} \dot{m}_{f,DG_i}(k) + \dot{m}_{f,BAT}(k), \tag{2}$$

$$\dot{m}_{f,BAT}(k) = \frac{sfc_{BAT}(k) \cdot P_{BAT}(k) \cdot \Delta t}{(\eta_{BAT} \cdot \eta_{fc})^{sign(P_{bat})}}, \tag{3}$$

where, η_{BAT} and η_{fc} are the efficiencies of the battery and the frequency converter respectively. η_{BAT} is battery power dependant, whereas η_{fc} is assumed a constant.

$$\dot{m}_{f,DG_i}(k) = \frac{sfc_{DG_i} \cdot P_{DG_i,set} \cdot \Delta t}{3600} \text{ , } i \in [1,3] \tag{4}$$

$$\dot{m}_{f,DE_i}(k) = \frac{sfc_{DE_i} \cdot P_{DE_i} \cdot \Delta t}{3600} \text{ , } i \in [1,2] \tag{5}$$

The fuel consumption rate, $\dot{m}_{f,DE}$ in g/timestep, is calculated using the specific fuel consumption, sfc_{DE} in g/kWh, and engine power, P_{DE} in kW. Similarly, the fuel consumption rate, $\dot{m}_{f,DG}$ in g/timestep, is calculated using the specific fuel consumption, sfc_{DG} in g/kWh, and engine power, P_{DG} in kW.

The objective function is subject to system dynamics: Equation 2 until Equation 12, constraints: Equation 13 until Equation 18, and boundary conditions: Equation 21 until Equation 23. The objective function is also subject to the operating envelopes of the engines and battery, these are also constraints. They have been omitted in the description below.

$$\widetilde{P}_{sh,ref}(k) = P_{IM}(k) + P_{DE}(k) \tag{6}$$

$$P_{IM}(k) = 2\pi T_{IM,set}(k) \frac{n_{sh}(k)}{i_{GB}} \tag{7}$$

$$P_{DG,tot,s}(k) = \sum_{k=1}^{3} P_{DG_i} \text{ , } i \in [1,3]. \tag{8}$$

$$P_{DG,tot,d}(k) = -P_{BAT}(k) + P_{aux} + \frac{2P_{IM}(k)}{\eta_{IM}(k)} \tag{9}$$

$$P_{DG,tot,d}(k) = P_{DG,tot,s}(k) \tag{10}$$

$$P_{BAT}(k) = \sqrt{3} I_{BAT,set}(k) V_{line} f_p \tag{11}$$

$$SOC(k) = SOC(k-1) - \int_0^{\Delta t} \frac{I_{BAT}}{Q} \tag{12}$$

$$T_{IM,min}(k) \leq T_{IM,set}(k) \leq T_{IM,max}(k) \tag{13}$$

$$I_{BAT,min}(k) \leq I_{BAT,set}(k) \leq I_{BAT,max}(k) \tag{14}$$

$$P_{DG,min} \leq P_{DG,i}(k) \leq P_{DG,max} \tag{15}$$

...

$$T_{IM,min}(k+N) \leq T_{IM,set}(k+N) \leq T_{IM,max}(k+N) \tag{16}$$

$$I_{BAT,min}(k) \leq I_{BAT,set}(k+N) \leq I_{BAT,max}(k) \tag{17}$$

$$P_{DG,min} \leq P_{DG,i}(k+N) \leq P_{DG,max} \tag{18}$$

Operation of I_{BAT} between 0 and 0.5 indicates charging and between 0.5 and 1 indicates discharging of the battery.

$$I_{BAT,\min}(k) = \begin{cases} 0.5 & \text{if SOC}(k) \geq 0.8 \\ 0 & \text{if SOC}(k) < 0.8 \end{cases} \tag{19}$$

$$I_{BAT,\max}(k) = \begin{cases} 0.5 & \text{if SOC}(k) \leq 0.2 \\ 1 & \text{if SOC}(k) > 0.2 \end{cases} \tag{20}$$

$$\overrightarrow{x} \geq 0 \tag{21}$$

$$\overrightarrow{y} \geq 0 \tag{22}$$

$$\overrightarrow{u} \geq 0 \tag{23}$$

Note that the goal of reducing fuel consumption is enforced through the objective function, the reduction of CO2 emissions is assumed to occur through the reduction of fuel consumption as well. Propulsion availability is ensured through constraint described in Equation 10, which equates the demanded power with the supplied power. Finally, a secondary goal of the control formulation is to increase the battery lifetime by keeping state of charge of the battery between 20% and 80%, this is enforced through constraints on the battery current described in Equation 19 and Equation 20.

The optimisation problem can be classified as a non-linear programming problem (NLP). NLP have the characteristic that their solution time increases exponentially with the number of dimensions of the problem [33]. The optimization problem is tackled using a multi-start procedure. The multi-start procedure strategically samples the solution space. Each sample is used as a starting point for the solver to find a local, or preferred, global minimum. Then, the most optimal solution of the multiple starts is selected. The solver used for this research is the sequential quadratic programming (SQP). The interested reader is referred to [34], for a complete account of the SQP method. SQP was selected as it outperformed active-set and interior-point in some test cases on cost and computational time.

An equivalent fuel consumption (ESFC) curve was established for the battery. The curve is tuned in order to incentivize discharging and charging of the battery at the right times, in order to optimize fuel consumption reductions. For a specific 2 hour operating profile, various ESFC curves were compared and evaluated. More involved ESFC curves, which are SOC-dependant, estimated-time-of-arrival dependant, or power forecasting dependant were not considered due to time constraints of the project.

4 Results

Five comparative simulations have been run on the same operating profile of around 2 hours, namely:

- Optimization at every timestep for a control horizon of 3 seconds.
- Optimization at every timestep for a control horizon of 3 seconds, without a battery.
- Triggered optimization. The trigger activates for a change in shaft power or SOC of more than 5%.
- Optimization with 'perfect knowledge', control horizon of 48 seconds with 3 timesteps for t in range [t, t+24, t+48].
- Optimization with shaft power predictions using RNN, control horizon of 48 seconds with 3 timesteps for t in range [t, t+24, t+48].

The results for the five simulations are shown in Table 2. The table shows the total energy cost of the simulation. An equivalent cost of the battery is calculated with an assumed fuel cost, which is equal to the most optimal fuel setpoint of the diesel generators. Since simulation 3, 4, and 5 do not optimize at every timestep, not the exact correct amount of shaft power is delivered at each timestep, Table 3 highlights this.

Simulation	Total Fuel consumption [kg]			Energy battery		Total energy cost [GJ]
	Main engines	Diesel generator sets	Total	$SOC_{t_{end}}$	Equivalent cost [kg]	
1	1462.906	497.502	1960.408	0.200	63.198	87.015
2	1406.035	633.238	2039.273	1.000	0.000	87.689
3	1487.794	473.122	1960.916	0.186	64.346	87.086
4	1521.679	470.425	1992.104	0.344	51.856	87.890
5	1516.185	478.354	1994.540	0.382	48.790	87.863

Table 2: Simulation results: fuel and energy consumption.

Simulation	MAPE [%]	MPE [%]	Adjusted total energy cost [GJ]
1	0.00	0.00	87.015
2	0.00	0.00	87.689
3	1.08	-0.16	86.946
4	3.04	-0.62	87.345
5	5.65	-2.23	85.842

Table 3: Error values of the delivered versus requested total shaft power. Adjusted total energy cost based on the MPE.

5 Discussion

The results in Table 2 show that the total energy cost for the four sets of results are almost the same. This is not surprising as in all cases the exact same energy was demanded. So naturally, a very similar amount of energy is to be expended in order to deliver the required power. Two factors are contributing to the fact that there are no energy cost reductions for the EMS when using a prediction horizon. (1) The prediction horizon is short-term, in the order of seconds. It is easy to see that predictions of long-term trends in power demand, would allow the use of the battery to be far more efficient. In those cases the battery can be charged when it is expected that the battery is going to be needed in the future. Instead, battery charging and discharging for short-term load predictions is purely decided on short-term trends. Given the variance in the data of the shaft power, the charging and discharging in the short-term becomes quite random. Also, since the control horizon of the controller is not executed completely, but instead works with a receding horizon, sometimes sub-optimal setpoints are used as decision variable setpoints. (2) The capacity of the battery, which is 400 kW, is very small compared to the overall power demand. A larger battery capacity would allow more versatility in the use of the battery; it could take over the function of the diesel generator-sets, rather than take over 40% of one diesel generator-set. Fuel savings of 0.77% are achieved with a 400 kW battery compared to a no-battery situation.

The total energy cost, when adjusted for excess power delivered is shown in Table 3. The number merely indicates that had all the energy been delivered correctly at the right times, a lower amount of energy would have been needed. Of course this number does not say much, as the excess delivered energy was delivered at the wrong times. The effect of the limited control horizon, and excess power delivered by a control cycle that does not optimize every timestep, outdoes the potential fuel savings that might have been achieved in these simulations. Which is evident from the increased fuel consumption in these simulations, as shown in Table 2.

6 Conclusion

In this paper it is investigated how much fuel consumption reduction can be achieved by applying a causal, real-time ECMS to a hybrid propulsion and hybrid power supply plant with a power load forecasting scheme, for a case study vessel: The Holland-class offshore patrol vessel.

- The forecasting tools evaluated are Linear regression, moving average, ARIMA and RNN.
- The RNN outperformed the other methods and is able to predict the power demand for up to 48 seconds, while maintaining a MAPE of under 5%.
- The optimization-based controller is combined with an ECMS approach which assigns an equivalent consumption cost to the battery. The controller correctly identifies the power split for the hybrid propulsive system, and the power split for the hybrid power supply.
- A simulation proved that 0.77% fuel savings are achieved with a 400 kW battery, compared to a no-battery scenario.
- Fuel savings could not be proven for the EMS with a control horizon of 48 seconds.
- The limiting factors are the combination of the small control horizon, the limited battery capacity compared to the overall power demand and the limited tuning of the ESFC curve.

REFERENCES

[1] Yijie Zhang et al. "Two-level model predictive control energy management strategy for hybrid power ships with hybrid energy storage system". In: *Journal of Energy Storage* 52 (2022), p. 104763. ISSN: 2352-152X. DOI: https://doi.org/10.1016/j.est.2022.104763. URL: https://www.sciencedirect.com/science/article/pii/S2352152X22007733.

[2] Qiang Wang and Xue Yang. "Imbalance of carbon embodied in South-South trade: Evidence from China-India trade". In: *Science of The Total Environment* 707 (2020), p. 134473. ISSN: 0048-9697. DOI: https://doi.org/10.1016/j.scitotenv.2019.134473. URL: https://www.sciencedirect.com/science/article/pii/S004896971934464X.

[3] Hulda Winnes, Linda Styhre, and Erik Fridell. "Reducing GHG emissions from ships in port areas". In: *Research in Transportation Business & Management* 17 (2015). Energy Efficiency in Maritime Logistics Chains, pp. 73–82. ISSN: 2210-5395. DOI: https://doi.org/10.1016/j.rtbm.2015.10.008. URL: https://www.sciencedirect.com/science/article/pii/S2210539515000590.

[4] R.D. Geertsma et al. "Design and control of hybrid power and propulsion systems for smart ships: A review of developments". In: *Applied Energy* 194 (2017), pp. 30–54. ISSN: 0306-2619. DOI: https://doi.org/10.1016/j.apenergy.2017.02.060. URL: https://www.sciencedirect.com/science/article/pii/S0306261917301940.

[5] Jinyoung Ko et al. "Comparative investigation of NOx emission characteristics from a Euro 6-compliant diesel passenger car over the NEDC and WLTC at various ambient temperatures". In: *Applied Energy* 187 (2017), pp. 652–662. ISSN: 0306-2619. DOI: https://doi.org/10.1016/j.apenergy.2016.11.105. URL: https://www.sciencedirect.com/science/article/pii/S0306261916317366.

[6] M. Kalikatzarakis et al. "Ship energy management for hybrid propulsion and power supply with shore charging". In: *Control Engineering Practice* 76 (2018), pp. 133–154. ISSN: 0967-0661. DOI: https://doi.org/10.1016/j.conengprac.2018.04.009. URL: https://www.sciencedirect.com/science/article/pii/S096706611830090X.

[7] Omer Berkehan Inal, Jean-Frédéric Charpentier, and Cengiz Deniz. "Hybrid power and propulsion systems for ships: Current status and future challenges". In: *Renewable and Sustainable Energy Reviews* 156 (2022), p. 111965. ISSN: 1364-0321. DOI: https://doi.org/10.1016/j.rser.2021.111965. URL: https://www.sciencedirect.com/science/article/pii/S1364032121012302.

[8] K.E. Bailey, S.R. Cikanek, and N. Sureshbabu. "Parallel hybrid electric vehicle torque distribution method". In: *Proceedings of the 2002 American Control Conference (IEEE Cat. No.CH37301)*. Vol. 5. 2002, 3708–3712 vol.5. DOI: 10.1109/ACC.2002.1024504.

[9] P. Bowles, H. Peng, and X. Zhang. "Energy management in a parallel hybrid electric vehicle with a continuously variable transmission". In: *Proceedings of the 2000 American Control Conference. ACC (IEEE Cat. No.00CH36334)*. Vol. 1. 6. 2000, 55–59 vol.1. DOI: 10.1109/ACC.2000.878771.

[10] K.L. Butler, M. Ehsani, and P. Kamath. "A Matlab-based modeling and simulation package for electric and hybrid electric vehicle design". In: *IEEE Transactions on Vehicular Technology* 48.6 (1999), pp. 1770–1778. DOI: 10.1109/25.806769.

[11] Fabio Massimo Frattale Mascioli et al. "Optimization of Hybrid Electric Cars by Neuro-Fuzzy Networks". In: *Applications of Fuzzy Sets Theory*. Ed. by Francesco Masulli, Sushmita Mitra, and Gabriella Pasi. Berlin, Heidelberg: Springer Berlin Heidelberg, 2007, pp. 253–260. ISBN: 978-3-540-73400-0.

[12] Hyeoun-Dong Lee et al. "Torque control strategy for a parallel-hybrid vehicle using fuzzy logic". In: *IEEE Industry Applications Magazine* 6.6 (2000), pp. 33–38. DOI: 10.1109/2943.877838.

[13] Niels J Schouten, Mutasim A Salman, and Naim A Kheir. "Energy management strategies for parallel hybrid vehicles using fuzzy logic". In: *Control Engineering Practice* 11.2 (2003). Automotive Systems, pp. 171–177. ISSN: 0967-0661. DOI: https://doi.org/10.1016/S0967-0661(02)00072-2. URL: https://www.sciencedirect.com/science/article/pii/S0967066102000722.

[14] E.A. Sciberras and R.A. Norman. "Multi-objective design of a hybrid propulsion system for marine vessels". In: *IET Electr Syst Transp* 2 (July 2012), pp. 148–157. DOI: 10.1049/iet-est.2011.0011.

[15] Lino Guzzella and Antonio Sciarretta. *Vehicle Propulsion Systems*. Springer Berlin Heidelberg, 2013. DOI: 10.1007/978-3-642-35913-2. URL: http://dx.doi.org/10.1007/978-3-642-35913-2.

[16] G-Q Ao et al. "Fuel economy and NOisubx/sub/i emission potential investigation and trade-off of a hybrid electric vehicle based on dynamic programming". In: *Proceedings of the Institution of Mechanical Engineers, Part D: Journal of Automobile Engineering* 222.10 (Oct. 2008), pp. 1851–1864. DOI: 10.1243/09544070jauto644. URL: https://doi.org/10.1243/09544070jauto644.

[17] Olivier Grondin et al. "Energy management strategy for Diesel hybrid electric vehicle". In: Oct. 2011, pp. 1–8. DOI: 10.1109/VPPC.2011.6043132.

[18] A. Sciarretta et al. "A control benchmark on the energy management of a plug-in hybrid electric vehicle". In: *Control Engineering Practice* 29 (2014), pp. 287–298. ISSN: 0967-0661. DOI: https://doi.org/10.1016/j.conengprac.2013.11.020. URL: https://www.sciencedirect.com/science/article/pii/S0967066113002323.

[19] A. Sciarretta et al. "A control benchmark on the energy management of a plug-in hybrid electric vehicle". In: *Control Engineering Practice* 29 (2014), pp. 287–298. ISSN: 0967-0661. DOI: https://doi.org/10.1016/j.conengprac.2013.11.020. URL: https://www.sciencedirect.com/science/article/pii/S0967066113002323.

[20] Amam EE Breijs A. "Energy management – adapt your engine to every mission." In: *Proceedings of the 13th international naval engineering conference* 2 (2016), pp. 1–8.

[21] Yijie Zhang et al. "Two-level model predictive control energy management strategy for hybrid power ships with hybrid energy storage system". In: *Journal of Energy Storage* 52 (2022), p. 104763. ISSN: 2352-152X. DOI: https://doi.org/10.1016/j.est.2022.104763. URL: https://www.sciencedirect.com/science/article/pii/S2352152X22007733.

[22] Ali Haseltalab, Rudy R. Negenborn, and Gabriel Lodewijks. "Multi-Level Predictive Control for Energy Management of Hybrid Ships in the Presence of Uncertainty and Environmental Disturbances**This research is supported by the project ShipDrive: A Novel Methodology for Integrated Modelling, Control, and Optimization of Hybrid Ship Systems (project 13276) of the Dutch Technology Foundation STW." In: *IFAC-PapersOnLine* 49.3 (2016). 14th IFAC Symposium on Control in Transportation SystemsCTS 2016, pp. 90–95. ISSN: 2405-8963. DOI: https://doi.org/10.1016/j.ifacol.2016.07.016. URL: https://www.sciencedirect.com/science/article/pii/S2405896316302129.

[23] Thanh Long Vu et al. "Power Management for Electric Tugboats Through Operating Load Estimation". In: *IEEE Transactions on Control Systems Technology* 23.6 (2015), pp. 2375–2382. DOI: 10.1109/TCST.2015.2399440.

[24] *Damen*. URL: https://products.damen.com/en/ranges/opv-holland-class/holland-class-ocean-going-patrol-vessel-3750/deliveries/opv-3750-friesland.

[25] R.D. Geertsma et al. "Pitch control for ships with diesel mechanical and hybrid propulsion: Modelling, validation and performance quantification". In: *Applied Energy* 206 (2017), pp. 1609–1631. ISSN: 0306-2619. DOI: https://doi.org/10.1016/j.apenergy.2017.09.103. URL: https://www.sciencedirect.com/science/article/pii/S0306261917313855.

[26] D.G. Lainiotis and Konstantinos Plataniotis. "Neural network estimators: application to ship position estimation". In: Jan. 1994, 4710–4717 vol.7. ISBN: 0-7803-1901-X. DOI: 10.1109/ICNN.1994.375037.

[27] D.G. Lainiotis et al. "Neural network application to ship position estimation". In: Nov. 1993, I384–I389 vol.1. ISBN: 0-7803-1385-2. DOI: 10.1109/OCEANS.1993.325979.

[28] Lizhu Hao et al. "Recurrent neural networks for non-parametric modeling of ship maneuvering motion". In: *International Journal of Naval Architecture and Ocean Engineering* 14 (2022), p. 100436. ISSN: 2092-6782. DOI: https://doi.org/10.1016/j.ijnaoe.2022.100436. URL: https://www.sciencedirect.com/science/article/pii/S2092678222000024.

[29] José del Águila Ferrandis et al. *Learning functionals via LSTM neural networks for predicting vessel dynamics in extreme sea states*. Dec. 2019.

[30] Yuchao Wang et al. "Multi-dimensional prediction method based on Bi-LSTMC for ship roll". In: *Ocean Engineering* 242 (2021), p. 110106. ISSN: 0029-8018. DOI: https://doi.org/10.1016/j.oceaneng.2021.110106. URL: https://www.sciencedirect.com/science/article/pii/S002980182101430X.

[31] Robin John Hyndman and George Athanasopoulos. *Forecasting: Principles and Practice*. English. 2nd. Australia: OTexts, 2018.

[32] Ian Goodfellow, Yoshua Bengio, and Aaron Courville. *Deep Learning*. http://www.deeplearningbook.org. MIT Press, 2016.

[33] Frederick S. Hillier. *Introduction to operations research*. McGraw-Hill Education, 2021.

[34] Jorge Nocedal and Stephen J. Wright. *Numerical optimization*. Springer, 2006.